

Alma Mater Studiorum – Università di Bologna

---

DOTTORATO DI RICERCA IN ONCOLOGIA E PATOLOGIA SPERIMENTALE  
PROGETTO 2 “PATOLOGIA SPERIMENTALE”

Ciclo XXV

Settore Concorsuale di afferenza: 06/A2

Settore Scientifico disciplinare: MED 04

# PATHOGENESIS OF CELL TOXICITY BY PLANT TOXINS

Presentata da: **Dott.ssa Manuela Pedrazzi**

Coordinatore Dottorato  
**Chiar.mo Prof. Sandro Grilli**

Relatore  
**Chiar.mo Prof. Andrea Bolognesi**

**DIPARTIMENTO DI MEDICINA SPECIALISTICA, DIAGNOSTICA E SPERIMENTALE -DIMES**

---

**Esame finale anno 2013**

*I love dedicated this thesis to Riccardo and Lucrezia*

---

<b>Chapter 1: INTRODUCTION</b>	<b>1</b>
<b>RIBOSOME INACTIVATING PROTEINS: generality and historical note</b>	<b>2</b>
<b>1.1 General properties</b>	<b>3</b>
1.1.1 Definition and Subdivision of RIPs	3
1.1.2 Distribution	6
1.1.3 Molecular Evolution	10
<b>1.2 Biological activities</b>	<b>10</b>
1.2.1 The enzymatic activity	10
1.2.2 Interaction of RIPs with cell: uptake and routing	12
1.2.3 Effects on laboratory animals and humans	14
1.2.4 Antiviral activity	15
<b>1.3 Possible use in experimental and clinical medicine</b>	<b>16</b>
1.3.1 Immunotoxins	16
1.3.2 Anti-tumor therapy	17
1.3.3 Immune disorders	18
<b>Chapter 2: MATERIALS AND METHODS</b>	<b>19</b>
<b>2.1 Materials</b>	<b>20</b>
<b>2.2 Methods</b>	<b>23</b>
2.2.1 Sequencing of stenodactylin	23
2.2.2 Cell culture	25
2.2.3 Cell protein Inhibition	25
2.2.4 Cell viability assay	26
2.2.5 Cell and nuclear morphology	27
2.2.6 Assessment of apoptosis	27
2.2.7 Caspase -3/7, -8,-9,-2 activities	28
2.2.8 Measurement of mitochondrial membrane potential loss	29
2.2.9 Assessment of oxidative stress	29
2.2.10 Native PAGE	30
2.2.11 Immunofluorescence using anti-stenodactylin antibodies	30
2.2.12 Western Blot analysis	30
2.2.13 Real-time PCR Analysis	31
<b>Chapter 3: AMINO ACID SEQUENCE OF STENODACTYLIN</b>	<b>33</b>
<b>BACKGROUND: Primary and tertiary structure of RIPs</b>	<b>34</b>
<b>AIM OF THE PROJECT</b>	<b>36</b>
<b>RESULTS AND DISCUSSION</b>	<b>39</b>
<b>3.1 Stenodactylin amino acid sequence</b>	<b>39</b>
3.1.1 Amplification and cloning of the stenodactylin gene	39
<b>3.2 Sequence analysis</b>	<b>40</b>
<b>3.3 Sequence comparison between stenodactylin and other RIPs</b>	<b>46</b>
3.3.1 Sequence comparison with type 2 RIPs	46
3.3.2 Sequence comparison with type 1 RIPs	48
3.3.3 Phylogenetic analysis	50

---

<b><u>Chapter 4: CELL DEATH MECHANISMS INDUCED BY STENODACTYLIN</u></b> .....	<b>52</b>
<b>BACKGROUND: RIPs and cell death mechanisms</b> .....	<b>53</b>
<b>AIM OF THE WORK</b> .....	<b>59</b>
<b>RESULTS AND DISCUSSION</b> .....	<b>60</b>
<b>4.1 Cell viability and protein synthesis inhibition assays</b> .....	<b>60</b>
<b>4.2 Evaluation of the cytotoxic effect of stenodactylin at the IC<sub>100</sub> concentration</b> .....	<b>62</b>
4.2.1 Assessment of apoptosis.....	62
4.2.2 Necroptosis.....	68
4.2.3 Evaluation of oxidative stress.....	71
4.2.4 Assessment of autophagy.....	78
<b>4.3 The cytotoxic effect of RIPs at IC<sub>50</sub> concentration</b> .....	<b>81</b>
4.3.1 Inhibition of protein synthesis and activation of caspases 3/7.....	81
4.3.2 Evaluation of apoptotic cell death.....	83
<b><u>Chapter 5: EFFECTS OF EBULIN I AND NIGRIN b ON NB100 CELLS</u></b> .....	<b>90</b>
<b>BACKGROUND: Ribosome inactivating proteins from Sambucus</b> .....	<b>91</b>
<b>AIM OF THE PROJECT</b> .....	<b>93</b>
<b>RESULTS AND DISCUSSION</b> .....	<b>94</b>
<b>5.1 The cytotoxic effects of Ebulin I and Nigrin b</b> .....	<b>94</b>
5.1.1 Inhibition of protein synthesis <i>in vitro</i> .....	94
5.1.2 Cell viability.....	95
5.1.3 Evaluation of cell death.....	97
<b><u>Chapter 6: CONCLUSIONS</u></b> .....	<b>102</b>
<b><u>Chapter 7: BIBLIOGRAPHY</u></b> .....	<b>105</b>

## ABSTRACT

Ribosome inactivating proteins (RIPs) are a family of plant proteins that depurinate the major rRNA, thus arresting protein synthesis. RIPs are divided into type 1, single chain proteins with enzymatic activity, and type 2 RIPs (toxic and non-toxic), which contain the enzymatic chain linked by a disulfide bridge to the binding chain. RIPs have been used alone or as toxic component of immunotoxins for experimental therapy of many diseases. Still today many unanswered questions remain about the cell death mechanisms induced by RIP. The knowledge of cell death pathway(s) induced by RIPs could be useful for clarifying the mechanisms induced by RIPs and for designing specific immunotherapy.

The purpose of the current study was to (i) determine the amino acid sequence of toxic type 2 RIP stenodactylin and compare with the sequence of other RIPs (ii) study the cell death mechanisms induced by stenodactylin in human neuroblastoma cells (NB100) and (iii) study the cell death pathway induced by the non-toxic type 2 RIPs ebulin 1 and nigrin b, and compare the results with the ones obtained with other RIPs.

Stenodactylin is the most toxic type 2 RIP. Comparison between stenodactylin and other RIPs, reveals that the amino acid residues that are involved for the enzymatic activity of RIPs were conserved within the sequence of the A chain of stenodactylin. The B chain of stenodactylin showed a positive charge in the sugar binding site 2 $\gamma$ . Phylogenetic trees showed that the A chain of stenodactylin is related to ricin and other toxic RIPs, whereas the B chain is more related to the non-toxic type 2 RIPs.

The pathogenesis of cell intoxication induced by stenodactylin was investigated using NB100 cells, which showed to be very sensitive to RIPs. High doses of stenodactylin (IC<sub>100</sub>) can activate the effector caspases (perhaps through the DNA damage and/or intrinsic/extrinsic pathways) and also causes ROS generation.

To elucidate the temporal dynamic of events caused by stenodactylin, the cells were intoxicated with toxin at its IC<sub>50</sub>. The results showed that the RIP caused a caspase-dependent apoptosis, mainly via extrinsic pathway. Moreover, the activation of caspases precedes the inhibition of protein synthesis.

Ebulin 1 and nigrin b show high enzymatic activity in a cell-free system, but they lack high cytotoxicity. Both toxins showed 10<sup>6</sup>-10<sup>5</sup> times less toxic in NB100 cells than stenodactylin and ricin, and 10<sup>3</sup> times than saporin. Preliminary studies demonstrated that the cell death mechanism induced by the two non-toxic RIPs was partially caspase-dependent apoptosis, but other cell death mechanisms seem to be involved.

*Chapter 1*

# Introduction

## **Ribosome Inactivating Proteins: generality and historical note**

Ribosome inactivating proteins (RIPs) are rRNA N-glycosidases present in some species of plants and bacteria that depurinate the major subunit of rRNA, thus arresting protein synthesis. Since ancient time, the biological effects of RIPs are known, for example the abortifacient activity of some medical plants such as *Trichosanthes kirilowii* and *Mormordica charantia*, and the poisonousness of the seeds of castor bean (*Ricinus communis*) and jequirity bean (*Abrus precatorius*).

The scientific history of RIPs started in 1888 when Stillmark linked the toxicity of castor bean to the property of agglutinating erythrocytes. Soon after, different ricin-like toxic proteins have been identified, i.e., in the seeds of *Abrus precatorius* (abrin) and in the 1920s in the roots of *Adenia digitata* (modeccin). Following, Lin and co-workers demonstrated that RIPs were more toxic to tumor than to normal cells (Lin *et al.*, 1970). Later, it has been discovered the two chain structure of the toxins with carbohydrate binding/lectin activity and inhibitory activity on protein synthesis. These enzymes have been called type-2 RIPs to distinguish them from RIPs that possess a single chain structure, which have been denominated type-1 RIPs. Structural and genetic studies have indicated that type 1 and type 2 RIPs evolved from a common ancestor gene (Ready *et al.*, 1984). RIPs inhibit irreversibly the protein synthesis by preventing the ribosome from binding elongation factor 2 (EF-2) in eukaryotes and factor G (EF-G) in prokaryotes. The mechanism was resolved by Endo and co-workers (Endo *et al.*, 1987). The authors discovered that the enzymatic activity of RIPs is based on the N-glycosidation cleavage of the specific adenine corresponding to the residue A<sub>4324</sub> of 28S rRNA in the 60S subunit of rat ribosomes. This adenine is located in the  $\alpha$ -sarcin-ricin loop and is conserved in large rRNAs from bacteria to humans (Mehta and Boston, 1998).

During the last decades a lots of RIPs have been isolated, characterized and cloned, for their application in human therapy.

## 1.1 General properties

### 1.1.1 Definition and Subdivision of RIPs

The term RIPs was introduced by Stirpe to define plant proteins that inactivate animal ribosomes when the enzymatic activity and the structure were unknown (Stirpe *et al.*, 1982). The designation RIP can be associated with their enzymatic activity, namely RNA N-glycosylase activity. All proteins that catalyze the endohydrolysis of the N-glycosidic bond at one specific adenine of the large ribosomal RNA are considered rRNA N-glycosylases (EC 3.2.2.22). Other proteins can inactivate or damage ribosomes by different mechanisms (e.g., RNases or proteases) but are not called RIPs; it is thus important to associate the term RIP with proteins that exhibit this N-glycosylase activity. Subsequently, it has been found that some RIPs remove more than one adenine residue per ribosome (Barbieri *et al.*, 1994). Based on the observation that some RIPs remove adenine residues from DNA and other polynucleotides (Barbieri *et al.*, 1997), the term adenine polynucleotide glycosylase was proposed for these proteins (Barbieri *et al.*, 2001).

Currently, the term RIP is reserved for proteins containing an RNA N-glycosidase domain that is structurally related to the classical RIPs.

RIPs are classified into three groups based on their physical properties and the absence or presence of a lectin-like chain. A schematic representation of the most characteristic RIP structures is presented in Figure 1.1

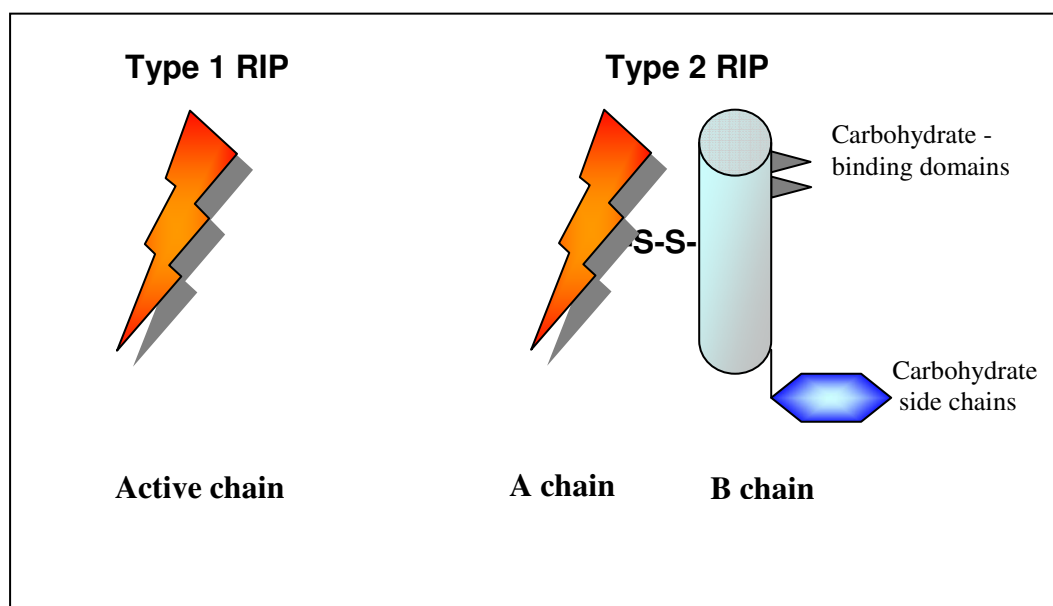


**Fig. 1.1** A schematic representation of type 1 and type 2 RIPs.

#### 1.1.1.1 Type 1 RIPs

This group of RIPs contains i.e., pokeweed antiviral protein (PAP), saporin (from *Saponaria officinalis* L.), dianthin (*Dianthus caryophyllus*) and momordin (*Momordica charantia*). Type 1 RIPs are monomeric enzymes of approximately 30 kDa. They are basic proteins (usually with a  $pI \geq 9.5$ ) that share a number of highly conserved active cleft residues and secondary structures within the active site despite showing differences in overall sequence homology and post-translational modifications (Nielsen and Boston, 2001). Different studies on protein and DNA sequence have shown that most type 1 RIPs are synthesized as pre-proteins composed of a signal peptide, the mature protein and a C-terminal extension (Chow *et al.*, 1990). Detailed localization studies have demonstrated that these cytotoxic proteins are located in vacuoles or other extracytoplasmic compartments. For example, PAPs are observed in the cell wall matrix and in some vacuoles (Ready *et al.*, 1986), and saporin is present in the intercellular spaces and in the paramural region between the primary wall and plasmalemma and within the vacuole (Carzaniga *et al.*, 1994). Type 1 RIPs are divided into three sub-groups (Van Damme *et al.*, 2001). The first sub-group is composed of “classical” type 1 RIPs, which are found in several dicotyledons; these enzymes are synthesized in the ER and then follow the secretory pathway to their final subcellular destination. The second sub-group of RIPs belongs to the *Poaceae* family (monocotyledons), and these enzymes are synthesized without a signal peptide. The third sub-group of RIPs is present in *Z. mays* and related (*Panicoideae*) species. These enzymes consist of two different polypeptides and are thus called “two chain” type 1 RIPs. These two chains are synthesized as inactive precursors.

#### 1.1.1.2 Type 2 RIPs

Type 2 RIPs are divided into two groups: toxic (e.g., ricin, abrin, modeccin, viscumin, volkensin and stenodactylin) and non-toxic (e.g., ebulin and nigrin), based on differences in their cytotoxicity.

These enzymes can be heterodimeric or tetrameric, with a molecular mass of 60 kDa or 120 kDa, respectively. The polypeptide, with enzymatic activity (the A chain) is linked to a galactose-binding lectin (B chain) through a disulfide bond. The union of two heterodimers by another disulfide bond between the two B chains yields the tetrameric protein. The group of heterodimeric RIPs includes abrin, ebulin 1, modeccin, ricin, volkensin, nigrin b and stenodactylin, while the tetrameric structure is typical of the *Ricinus* agglutinin (RCA). RCA consists of two identical heterodimers, is very similar to ricin, and is not linked by covalent bonds (Olsens *et al.*, 1978). RCA was the first non-toxic type 2 RIPs to be identified. A

number of non-toxic type 2 RIPs have been found in some species of the genus *Sambucus*. The most representative and studied members are nigrin b, extracted from the bark of the common (black) elder *Sambucus nigra* (Girbes *et al.*, 1993a), and ebulin 1, purified from the leaves of the dwarf elder *Sambucus ebulus* 1 (Girbes *et al.*, 1993b). Although the non-toxic type 2 RIPs show strong anti-ribosomal molecular activity *in vitro*, similar to ricin, they lack the high toxicity in cultured animals cells and *in vivo* rodents ( $10^3$ - $10^5$  less toxic than ricin) (Ferrerias *et al.*, 2011). The lectin chain can bind to galactosyl moieties of glycoproteins and /or glycolipids that are present on the surface of eukaryotic cells and allow the translocation of the A chain into the cytosol. The non-toxic type 2 RIPs present individual changes in the high-affinity sugar binding sites of the B chains, which alter their intracellular trafficking can explain their different toxicity (Girbes *et al.*, 2003).

The type 2 RIPs derive from a pre-proprotein formed by a single precursor that consists of a signal peptide and two different domains separated by a linker peptide. The current understanding of the biosynthesis of RIPs is based on studies on ricin and RCA. The preproricin is co-translationally translocated into the endoplasmic reticulum (ER) lumen. During this process, the signal peptide is cleaved, four asparagines residues are N-glycosylated, and five disulfide bridges are formed to obtain the proricin. The proricin is transported via the ER and the Golgi complex into protein storage vacuoles. During this transport, the glycosylate chains are converted into complex type N-glycan. In the protein bodies, the short peptide is cleaved from the N-terminus, and the excision of the linker yields the mature ricin, in which the A and B chains are linked by a disulfide bond (Lord *et al.*, 1994). Mature ricin is present only inside the protein bodies and is thus sequestered from the ribosome, preventing ricin from entering the cytoplasm and killing the cells. Nearly all type 2 RIPs are synthesized and processed similarly.

#### 1.1.1.3 Type 3 RIP

Type 3 RIP has an N-terminal domain that resembles type 1 RIPs, but the N-terminal domain is linked to an unrelated carboxyl-terminal domain with unknown function (Reinbothe *et al.*, 1994). This protein is expressed at lower levels than other RIPs and was identified in barley (where it is called JP60). Its gene does not contain a putative signal peptide, indicating that it is synthesized on free polysomes in the cytoplasm. Localization studies demonstrated that this protein is located in the nucleus and sometimes in the cytoplasm (Gorschen *et al.*, 1997). This protein is synthesized in stress conditions and may correspond to an inducible suicide mechanism.

### 1.1.2 Distribution

RIPs are widespread and almost ubiquitous in the plant kingdom, but not all the plants contain RIPs. For example, in the complete genome of *Arabidopsis thaliana*, no sequence that encodes a putative RIP has been found. RIPs have been detected in *Angiospermae*, both mono- and dicotyledons. Type 1 RIPs appeared to be more prevalent than type 2 RIPs, including some plants that are eaten raw and are in phylogenetically distant families such as: *Asparagaceae*, *Caryophyllaceae*, *Cucurbitaceae*, *Euphorbiaceae*, *Nyctaginaceae*, *Phytolaccaceae* and *Poaceae* (Table 1.1). Toxic type 2 RIPs have only been identified in six plants, which are members of *Euphorbiaceae*, *Fabaceae*, *Passifloraceae*, and *Viscaceae*, while non-toxic type 2 RIPs have been discovered in *Euphorbiaceae*, *Sambucaceae*, *Lauraceae*, *Ranunculaceae*, *Liliaceae* and *Iridaceae* (Table 1.2). The expression level of RIPs in plant tissues is highly variable, ranging from traces to hundreds of milligrams per 100 g, and they can be present in a single tissue or in all tissues of a plant (i.e., roots, leaves, fruits, seeds). Sometimes, several forms of RIPs were observed in the same tissue; for example, isoforms of saporin were discovered in the seeds, leaves and root of soapwort (Ferrerias *et al.*, 1993), and several non-toxic RIPs have been identified in various tissues of *Sambucus* species (Girbes *et al.*, 2003). In some plants, both toxic and non-toxic RIPs may exist (e.g., ricin and RCA in castor beans).

The expression of RIPs in plants enhances during senescence, and unfavorable conditions, such as different stresses (Stirpe *et al.*, 1996) and in virally infected cells (Barbieri *et al.*, 2001).

RIPs are not limited to the plant kingdom. The type 1 RIPs stx 1 and stx 2 were isolated from *Escherichia coli* and Shiga toxin from *Shigella dysenteriae* (Reisbig *et al.*, 1981; Obrig, 1997). Other RIPs have been detected in the alga *Laminaria japonica* (Liu *et al.*, 2002) and in mushrooms (Lam and Ng, 2001).

Table 1.1: some type 1 RIPs

<b>TYPE 1 RIPs</b>			
<b>MAGNOLIIDAE</b>			
<b>Lauraceae</b>	<i>Cinnamomun camphora</i>	seeds	Camphorin
<b>CARYOPHYLLIDAE</b>			
<b>Aizoaceae</b>	<i>Mesembryanthemum crystallinum</i>	leaves	<i>Mesembryanthemum crystallinum</i> RIP1
<b>Amaranthaceae</b>	<i>Amaranthus viridis</i>	leaves	Amaranthin
	<i>Celosia cristata</i>	leaves	CCP 25
<b>Caryophyllaceae</b>	<i>Agrostemma githago</i>	seeds	Agrostin 2,5 e 6
	<i>Dianthus barbathus</i>	leaves	Dianthin 29
	<i>Dianthus caryophyllus</i>	leaves	Dianthin 30 e 32
	<i>Dianthus sinensis</i>	leaves	RIP 1,2,3
	<i>Lychnis chalcedonica</i>	seeds	Lychnin
	<i>Saponaria ocymoides</i>	seeds	Ocymoidine
	<i>Saponaria officinalis</i>	seeds	Saporin S5, S6, S8, S9
		leaves	Saporin L1, L2
		roots	Saporin R1, R2, R3
	<i>Stellaria aquatica</i>	leaves	Stellarin
<i>Vaccaria pyramidata</i>	seeds	Pyramidatine	
<b>Chenopodiaceae</b>	<i>Beta vulgaris</i>	leaves	Beetins 27
	<i>Chenopodium album</i>	plants	CAP30B
	<i>Spinacia oleracea</i>	roots	SOP
<b>Nyctaginaceae</b>	<i>Bougainvillea spectabilis Willd</i>	leaves	Bouganin
	<i>Mirabilis expansa R&amp;P</i>	roots	ME1 and ME2
		seeds	MAP-S
<b>Phytolaccaceae</b>	<i>Phytolacca americana</i>	leaves	PAP I, PAP II
		seeds	PAP-S1 e S2
		roots	PAP-R
	<i>Phytolacca dioica</i>	seeds	PD-S1, S2, S3
		leaves	PD-L1, L2, L3, L4
	<i>Phytolacca dodecera</i>	leaves	Dodecandrin
	<i>Phytolacca acinosa</i>		PAP
	<i>Phytolacca insularis</i>	leaves	PIP
cdna		PIP 2	
<b>ASTERIDAE</b>			
<b>Lamiaceae</b>	<i>Clerodendrum aculeatum</i>	leaves	Protein CA-SRI
	<i>Clerodendrum inerme Gaerth</i>	leaves	CIP-29 and CIP-34
<b>ROSIDAE</b>			
	<i>Benincasa hispida</i> var. <i>chieh-qua</i>	seeds	hyspidin
		leaves	Bryodin-L
	<i>Bryonia dioica</i>	roots	Bryodin 1 e 2

<b>Cucurbitaceae</b>	<i>Luffa acutangula</i>	seeds	Luffaculin
	<i>Luffa aegyptiaca</i>	seeds	LRIP (Luffin c)
	<i>Luffa cykubdruca</i>	seeds	Luffin a e b
	<i>Luffa cylindrica</i>	seeds	Luffin S
		seeds	Luffacilina
	<i>Marah oreganus</i>	seeds	Mor I e II
	<i>Momordica balsamina</i>		Momordin II
	<i>Momordica charantia</i>	seeds	Momordin I
		seeds	$\alpha$ , $\beta$ MMC
		seeds	Charantin
	<i>Momordica cochinchinensis</i>	seeds	Momorcochin S
		roots	Momorcochin R
	<i>Trichosanthes cucumerina</i> <i>var. anguina</i>	seeds	Trichoanguin
	<i>Trichosanthes cucumeroides</i>	roots	B trichosanthin
<i>Trichosanthes kirilowii</i> <i>Maximowicz</i> <i>Trichosanthes kirilowii</i>	seeds	Trichokirin $\alpha$ , $\beta$ kirilowina	
<i>Trichosanthes kirilowii</i>	seeds	S-Trichokirin	
	roots	Trichosanthin TAP29 TCS $\alpha$ , $\beta$ , $\gamma$	
<b>Euphorbiaceae</b>	<i>Croton tiglium</i>	seeds	Crotin I e II (2, 3)
	<i>Gelonium multiflorum</i>	seeds	Gelonin (GAP)
	<i>Jatropha curcas</i>	seeds	Curcin 2
	<i>Manihot palmat</i>	seeds	Mapalmin
	<i>Manihot utulissima</i>	seeds	Manutin 1 e 2
<b>Fabaceae</b>	<i>Pisum sativum</i> var. <i>arvense</i> <i>Poir</i>	seeds	Pisavin $\alpha$ , $\beta$
	<i>Pisum sativum</i> var. <i>macrocarpon</i>	legums	Sativin
<b>ASTERIDAE</b>			
<b>Sambucaceae</b>	<i>Sambucus ebulus</i>	leaves	Ebulitin $\alpha$ , $\beta$ , $\gamma$
	<i>Sambucus nigra</i>	fruits	Nigritin f1 e f2
<b>LILIIDAE</b>			
<b>Agavaceae</b>	<i>Yucca recurvifolia</i>	leaves	YLP
<b>Asparagaceae</b>	<i>Asparagus officinalis</i>	seeds	Asparin 1, 2
<b>Liliaceae</b>	<i>Muscari armeniacum</i> L. e <i>Miller</i>	bulbs	Musarmin 1, 2, 3
<b>Iridaceae</b>	<i>Iris holleica</i> var. <i>Prof.</i> <i>Blaauw</i>	bulbs	IRIP 1, 2, 3
<b>Poaceae</b>	<i>Hordeum vulgare</i>	seeds	Barley RIP, JIP60
	<i>Secale cereale</i>	seeds	RPSI
	<i>Triticum aestivum</i>	germ	Tritin
		leaves	Tritin L
		seeds	Tritin S
<i>Zea mays</i>	seeds	Mais RIP1, b-32	

Table 1.2: some type 2 RIPs toxic and non-toxic.

<b>TOXIC TYPE 2 RIPs</b>			
<b>ROSIDAE</b>			
<b>Euphorbiaceae</b>	<i>Ricinus communis</i>	seeds	Ricin (D, E)
<b>Fabaceae</b>	<i>Abrus precatorius</i>	seeds	Abrin a, b, c, d
<b>Viscaceae</b>	<i>Phoradendron californicum</i>	leaves	PCL, <i>Phoradendron californicum lectin</i>
	<i>Viscum album</i>	leaves	MLI (viscumin), II, III
<b>DILENIIDAE</b>			
<b>Passifloraceae</b>	<i>Adenia volkensis</i>	roots	Volkensin
	<i>Adenia lanceolata</i>	caudex	Lanceolin
	<i>Adenia stenodactyla</i>	caudex	stenodactylin
	<i>Adenia digitata</i>	roots	Modeccin 4B and 6B
<b>NON-TOXIC TYPE 2 RIPs</b>			
<b>MAGNOLIIDAE</b>			
<b>Lauraceae</b>	<i>Cinnamomum, camphora</i>	seeds	cinnamomin
	<i>Cinnamomum porrectum</i>	seeds	porrectin
<b>Ranunculaceae</b>	<i>Eranthis hyemalis</i>	bulbs	EHL, <i>Eranthis hyemalis lectin</i>
<b>ROSIDAE</b>			
<b>Euphorbiaceae</b>	<i>Ricinus communis</i>	seeds	RCA ( <i>Ricinus communis agglutinin</i> )
<b>Fabaceae</b>	<i>Abrus pulchellus</i>	seeds	Pulchellins
<b>ASTERIDAE</b>			
<b>Sambucaceae</b>	<i>Sambucus ebulus</i>	leaves	Ebulin l
		rizhome	Ebulin r1 e r2
		fruits	Ebulin f
	<i>Sambucus nigra</i>	fruits	Nigrin f, SNA-If
		barks	Nigrin b, SNAI, SNAI' Basic Nigrin b, SNLRP1 2
		leaves	Nigrin 11 e 12, SNAld
		seeds	Nigrin s, SNAIII
		<i>Sambucus racemosa</i>	barks
<i>Sambucus sieboldiana</i>	barks	Sieboldin b and SSA	
<b>LILIIDAE</b>			
<b>Liliaceae</b>	<i>Poligonatum multiflorum</i>	leaves	PMRIPm e PMRIPt
<b>Iridaceae</b>	<i>Iris holleica var. Prof Blaauw</i>	bulbs	IRA-b e IRA-r

### 1.1.3 Molecular Evolution

Several aspects of the evolution of RIPs are known, but many questions remain unanswered. A contribution for the compression of RIP evolution comes from genome studies.

The RNA N-glycosidase domain derives from a common ancestor gene presents for over 300 millions years. From this domain derived: the type 1 and the type 2 RIPs after a fusion of RNA N-glycosidase domain with a sugar binding domain. The latter seems to be acquired by later transfer from bacterium. This hypothesis is supported by (i) the B chain shows a high similarity with carbohydrate-binding part of a  $\beta$ -glycosidase-like glycosyl hydrolase and an  $\alpha$ -L-arabinofuranosidase B family protein from the *Actinomyces bacterium C.acidiphila*, and (ii) the cysteins important for the disulfide bond are present in the bacterial sequences (Peumans and Van Damme, 2010).

Type 2 RIPs group is formed by three sub-groups: the classical type 2 RIPs, the truncated type 2 RIPs (called also secondary type 1 RIPs) and B lectin group. Although the truncated type 2 RIPs are formed only by A chain, they are not related with type 1 RIP. Indeed, they arose from type 2 RIP, that belong to *Cucurbitaceae*, *Euphorbiaceae* and *Iridaceae* families, which lost the lectin domain by three independent evolutionary events (Van Damme *et al.*, 2001). The type B lectin RIPs have been isolated from cucumber (*C. sativus*) roots (Masuda *et al.*, 1999) and from several *Sambucus* species. The type B protein SNAII is formed by the A chain deletion of the genuine type 2 RIP (SNA-V) (Van Damme *et al.* 1997; Girbès *et al.*, 2004).

## 1.2 Biological activities

### 1.2.1 The enzymatic activity

Early studies found that ricin inhibits protein synthesis both in cells and in a cell-free system, by preventing the ribosome from binding elongation factor 2 (Montanaro *et al.*, 1973; 1975). The mechanism underlying the ribosomal damage was discovered by Endo and co-workers. Based on ricin studies, they found that ricin recognizes a specific and highly conserved region in the large subunit of rRNA and then cleaves the N-C glycosidic bond between a specific adenine and the nucleotide on the rRNA. Using the rat liver ribosome, the authors demonstrated that the specific adenine removed (A<sub>4324</sub>) is inside a GAGA sequence that is present in an universally conserved loop (the sarcin/ricin domain) and is located at the top of a stem in 28S rRNA (Endo *et al.*, 1987) (Fig. 1.2). This observation was extended to other RIPs, which are officially classified as rRNA N-glycosidases (EC 3.2.2.22) (Stirpe *et al.*,

1988). However, there are marked differences in substrate specificity. For example, PAP deadenylates ribosomes from bacteria, plants and yeast, while ricin shows a strong activation on mammalian and yeast ribosomes, but not on plants or *E. coli* ribosomes. Type 1 and type 2 RIPs have a different substrate specificity, and type 1 RIPs have a broader spectrum of activity than type 2. Because the GAGA loop presents 14 nucleotides that are highly conserved from *E. coli* to humans, the different sensitivity may be due to ribosomal proteins that allow or prevent access of the RIPs to the sarcin/ricin loop (Vater *et al.*, 1995). The different RIP structures may also cause the diverse ribosome substrate specificity.

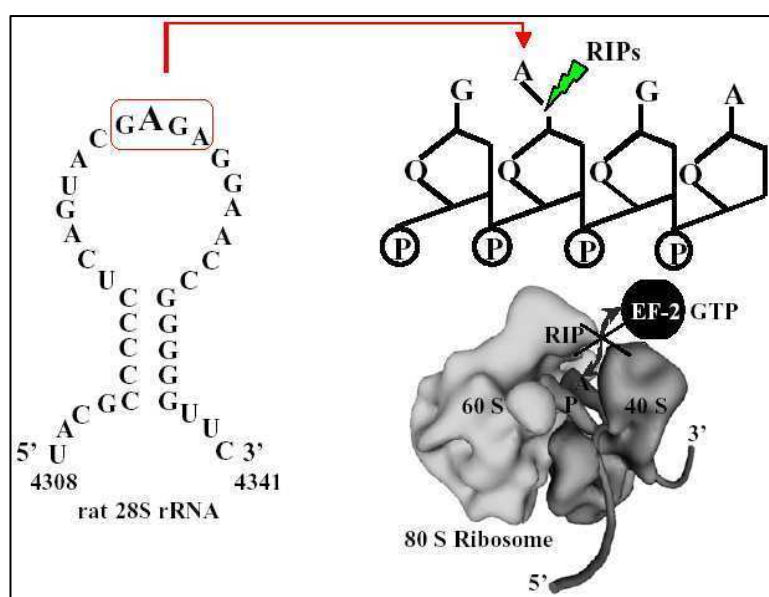


**Fig. 1.2.** Enzymatic mechanism of ribosome inactivating proteins.

Through the development of fluorescence-based HPLC-methods (Zamboni *et al.*, 1989), RIPs were shown to act on other substrates. For example, most RIPs show an effect on herring sperm DNA and poly(A), and one-third of the RIPs also act on RNA from tobacco mosaic virus (TMV) (Barbieri *et al.*, 1997). Based on the observation that RIPs can deadenylate a range of polynucleotides, the term polynucleotide: adenosine glycosidases and then adenine polynucleotide glycosylase was proposed (Barbieri *et al.*, 2001). Some RIPs also exhibit a guanosine glycosidase activity, and can remove guanine residues from both eukaryotic and prokaryotic rRNA (Endo *et al.*, 1987 and Rajamohan *et al.*, 1999). This a guanosine glycosidase activity activity has only been observed in two RIPs, i.e., PAP and ricin, and is undetectable in gelonin, momordin, PAP-s and saporin-S6, which only remove adenine

(Barbieri *et al.*, 2000). Hudak and co-workers found that PAP depurinates capped mRNA. This activity may contribute to the antiviral activity of RIPs (Hudak *et al.*, 2002).

### 1.2.2 Interaction of RIPs with cell: uptake and routing

The cell-RIP interaction shows that protein synthesis is inhibited at least 30 min after the RIP is introduced. Only a few molecules reach their target (Sandvig *et al.*, 1976), but one molecule is sufficient to induce cell death (Eiklid *et al.*, 1980).

Type 1 RIPs show lower toxicity compared with type 2 RIPs. This difference is related to the different interactions of these proteins with cells, which appear to depend on the protein structure. In particular, the presence of lectin-containing B chains allows the RIP to bind to the cell membrane and enter the cell. The low cytotoxicity of type 1 RIPs is explained by the absence of lectin chain, which reduces entry to the cells (Barbieri *et al.*, 1993).

Studies on type 2 RIPs have identified different mechanisms through which the RIPs bind to the cell surface. The B chain has galactose-specific lectin activity, which allows the protein to interact with the galactose-containing glycoproteins and glycolipids that are present on the surface of every cell type. An alternative mechanism involves the interaction of mannose cell receptors with the carbohydrate side chains that are present in the toxin.

Studies on ricin demonstrated that after interaction with the receptor, the toxin enters into the cytosol through the endocytic pathway. Ricin and possibly other RIPs can reach the endosomal compartment through two distinct mechanisms: the clathrin-dependent or clathrin-independent pathways (Sandvig and van Deurs, 1996).

Once inside the cells, RIPs follow an intracellular pathway through which the RIP molecules have three different destinations: (i) some RIPs translocate to the Golgi apparatus, then to the ER and finally to the cytoplasm; (ii) a certain fraction of RIPs are degraded after lysosomal internalization; and (iii) some RIPs are expelled from the cells (Sandvig and van Deurs, 2005) (Fig. 1.3). The altered destination and processes could cause different cytotoxicity. Indeed, the non-toxic type 2 RIP nigrin b enters cells, equally as ricin, but nigrin b is more rapidly and extensively degraded and excreted from cells (Battelli *et al.*, 1997). The number of lysines is also important. Although volkensin is excreted by cells faster than ricin, it shows higher toxicity. One possible reason is that volkensin, similar to ricin and abrin, has few lysines, which make it resistant to proteolysis. As a consequence, the non-degraded form is excreted by cells and is available for further entry into the cells (Battelli *et al.*, 2004; Chambery *et al.*, 2004). Stenodactylin and lanceolin, the most toxic type 2 RIPs that have been discovered, have the same intracellular routing observed for ricin. After binding to a receptor, they are

internalized by clathrin-independent endocytosis and reach the Golgi apparatus. Their high cytotoxicity seems to be related to their high affinity to receptors, greater uptake and lower proteolysis, which allows the re-uptake of non-degraded RIPs (Battelli *et al.*, 2010).

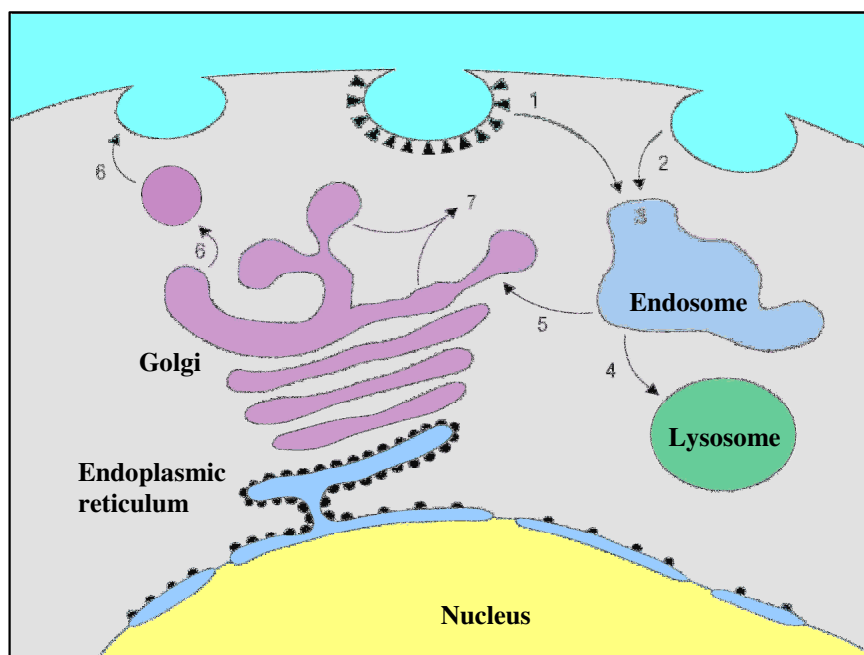


**Fig. 1.3.** Endocytosis of the ricin A chain. Endocytosis by the clathrin-dependent pathway (1) and clathrin-independent pathway (2), inclusion within the endosome (3), lysosomal internalization for degradation (4), transportation of the A chain to the Golgi apparatus (5), and finally expulsion outside the cells (6) or into the cytoplasm (7).

The endocytic mechanism of type 1 RIPs is still not well understood. Two mechanisms have been proposed: (i) endocytosis after binding to either the galactosyl residues or the mannose receptor on the cell membrane and (ii) the passive “fluid phase” endocytosis (pinocytosis), which allows the internalization of the toxin without receptor binding (Madan and Ghosh, 1992). Saporin-S-6 enters into cells through the binding of the  $\alpha 2$ -macroglobulin receptor (Cavallaro and Soria, 1995). In some cells, however, there was no correlation between the level of this receptor and the sensitivity to saporin S-6, indicating a  $\alpha 2$ -macroglobulin receptor-independent mechanism (Bagga *et al.*, 2003a). Studies on the intracellular routes that are followed by type 1 RIPs show diversity within this group. Saporin, which enters into cells by via receptor-mediated endocytosis, has a Golgi-independent pathway (a different intracellular movement compared with ricin) (Vago *et al.*, 2005) and recently it has been observed a nuclear localisation of saporin (Bolognesi *et al.*, 2012). In contrast, PAP presents a retro-translocation from the ER into the cytosol, similar to the mechanism utilized by type 2 RIPs (Parikh *et al.*, 2005). This observation suggests that type 1 RIPs may also be able to follow the cellular route for misfolded proteins without being degraded by the proteasome.

### 1.2.3 Effects on laboratory animals and humans

#### 1.2.3.1 Toxicity and lesions

The effect of type 2 RIPs on humans have long been after many people were poisoned with ricin. Low doses of ricin cause digestive tract convulsions, while higher doses produce gastrointestinal symptoms, with subsequent haemorrhaging in the stomach and intestine; degenerative changes in the heart, liver and kidney; and then death. When small particles are inhaled, severe respiratory symptoms followed by acute respiratory failure and death are observed (Balint, 1974). Little information is known about the effect of type 1 RIPs in humans. Type 1 RIPs have been reported to produce fever and rashes when trichosanthin was used to induce abortion (Lu and Jin, 1989) or administered to AIDS patients (Byers *et al.*, 1990).

All RIPs are strongly immunogenic, and their administration to animals induces the formation of antibodies, with cross-reaction among RIPs of the same family (Strocchi *et al.*, 1992). However, recently it has been observed that the type 2 RIP lanceolin cross reacts with sera against type 1 RIPs, momordin I and PAP R (Stirpe *et al.*, 2007). Many type 1 RIPs, as well as ricin, are allergenic and induce the formation of IgE (Zheng *et al.*, 1991). Allergenicity has also been observed in laboratory personnel working with RIPs, as in our laboratory. These toxins are present even in eaten raw, and their allergenic properties could be the cause of allergies induced by some vegetables (Stipe and Battelli, 2006).

RIPs also display immunosuppressive activity both on the humoral- and cell-mediated response by interfering with an early step in the immune response (Spreafico *et al.*, 1983).

These toxins also have abortifacient activity. In China, trichosanthin is used to induce early and mid-term abortion, with over 95% success and minimal effects. It causes the death of the fetus by inducing necrosis of the syncytiotrophoblast cells and fragmentation of placenta villi when administered intra-amniotically (Stirpe and Battelli, 2006).

The effects of RIPs have predominantly been studied in rats, and severe damage has been observed in the liver, kidney and spleen.

An electron microscopy study showed that in ricin-poisoned rats, Kupffer and sinusoidal cells appear to be damaged first, with subsequent necrosis of the hepatocytes. Moreover, necrosis of the macrophage-rich red pulp of the spleen was also observed (Derenzini *et al.*, 1976). In addition, treatment with modeccin causes lesions in the liver and in hepatocytes (Sperti *et al.*, 1979). In contrast, abrin does not cause lesion formation in the liver or hepatocytes but instead induces necrosis of the acinar pancreatic cells (Barbieri *et al.*, 1979). Subsequently, increase of apoptotic changes in lymphoid tissues in rats treated with abrin and ricin were

detected (Griffiths *et al.*, 1987). In addition, high doses of type 1 RIPs in mice damages the liver, kidney and spleen, and necrosis and fatty changes were also observed in these mice (Battelli *et al.*, 1990). In mice, high doses of nigrin b (a non-toxic type 2 RIP) cause gut derangement, especially of the small intestine (Girbés *et al.*, 2003). Because all RIPs have the same enzymatic activity, the differences observed may be due to the different entry mechanisms into cells. The damage induced by RIPs, such as massive necrotic lesions and apoptosis, are different from the damage caused by other protein synthesis inhibitors. This difference suggests that RIPs have other effects beyond the inhibition of protein synthesis. Ricin (Licastro *et al.*, 1993), viscumin (Hajto *et al.*, 1990) and modeccin (Yamasaki *et al.*, 2004) induce the production of tumor necrosis factor (TNF) and interleukins by human mononuclear cells, which could explain the fever and general inflammation that are observed in animals poisoned with these toxins.

#### 1.2.3.2 Axonal transport and the effect on the nervous system

Ricin, abrin, modeccin and viscumin are retrogradely transported along the axon to the neurons when injected into peripheral nerves. When injected in the central nervous system, only modeccin and volkensin are retrogradely transported to the peripheral nervous system. This specific transportation could be caused by their B chain, which allows their retrograde transport to other areas through the projecting neurons. Because these RIPs can be retrogradely transported, they were used to study the central nervous system by producing selective lesions (Wiley and Lappi, 1994). The retrograde transport of ricin along nerves which are relevant to the injected area, was observed when RIPs were injected outside nerves in several tissues, such as the anterior eye chamber (Dumas *et al.*, 1979), the submandibular gland (Harper *et al.*, 1980), the dental pulp (Henry *et al.*, 1987), the superior lip (Hino *et al.*, 1988) and the lateral rectus muscle (de la Cruz *et al.*, 1991). Recently, two potent type 2 RIPs, i.e., lanceolin and stenodactylin, were found to be retrogradely transported through axons to central nervous system, and even low doses of these toxins are highly neurotoxic, especially for microglia. These results all suggest that these toxins can be used to selectively lesion neuronal populations (Monti *et al.*, 2007).

#### **1.2.4 Antiviral activity**

All type 1 RIPs and few type 2 RIPs show to possess antiviral activity against plants, fungal and animal viruses.

Pokeweed antiviral protein (PAP) was the first to be discovered with this antiviral activity and is one of the most potent. It was found that the extracts from the leaves of pokeweed inhibited

the plant viral infection, such as tobacco mosaic virus (Grasso and Shepherd, 1978) cucumber mosaic virus (Tomlinson *et al.*, 1974), and many others. When small amount of extract, which contained PAP and virus were mixed and rubbed on the surface of plants were able to block viral infection (Duggar and Armstrong, 1925). The mechanism of this activity is still not completely understood. Viral infection changes the permeability of cell membrane and allows RIPs (normally located in protein bodies, such as ricin, or in cell wall matrix or vacuole, as PAP, or in intracellular space, as saporin) to come into contact with plant ribosome of infected cells. The ribosome would be inactivated with subsequent cell death and block of viral replication (Fernández-Puentes and Carrasco, 1980). However, through recombinant techniques, it was found that ribosome inactivation is not necessary for the antiviral activity. Mutants of PAP, which lack their enzymatic activity, are not toxic when expressed in transgenic tobacco plants, but there are able to protect the tobacco plants against potato virus X (Tumer *et al.*, 1997) and also fungal pathogen (Zoubenko *et al.*, 1997). This suggested the idea that RIPs are able to damage directly the virus by their effect on DNA.

RIPs showed to inhibit also animal viruses, for example blocking the viral replication of influenza virus (Tomlinson *et al.*, 1974), polio virus, herpes simplex virus (Foà-Tomasi *et al.*, 1982) and HIV virus (Zarling *et al.*, 1990). Studies on effects on HIV-1 infection by type 1 RIPs confirmed the idea that their enzymatic activity and antiviral property are two distinct functions. For example, trichosanthin inhibits HIV RNA and protein accumulation without effecting host-cell gene expression (McGrath *et al.*, 1990).

### **1.3 Possible use in experimental and clinical medicine**

The role of RIPs in nature is still not clear. Their wide distribution and conservation throughout evolution suggest that one possible role of these proteins is to confer an advantage to plants, perhaps against pathogens and predators. Though many questions about their specific function in plants remain unanswered, RIPs have been used in medicine for several purposes, such as creating immunotoxins, anti-tumor therapy and immune disorders.

#### **1.3.1 Immunotoxins**

RIPs present a high cytotoxic effect, but they lack the selectivity needed for therapeutic use. To increase their specificity against undesired or harmful cells, RIPs have been combined with carriers that recognize select antigens or receptors that are expressed on the membrane surface of the targeted cells. Carriers that can be used include hormones, growth factors, receptors, lectins, antigens, and vitamin-binding proteins, but the most powerful and

frequently utilized carriers are monoclonal and polyclonal antibodies. When a RIP is chemically linked to an antibody or antibody fragment, it is called an immunotoxin (IT), in contrast, if the RIP and antibody are synthesized using DNA recombinant techniques, the resulting product is defined a recombinant immunotoxin. In the latter, the gene for the Fab or Fv fragment of an antibody is fused with the gene encoding a truncated toxin; the plasmid vector expressing the recombinant IT is then transfected into bacteria or yeast to produce the single-chain fusion protein.

Both type 1 and of type 2 RIPs have been used for immunotoxins. Ricin is the most commonly used type 2 RIP, but the whole toxin is not required for this purpose because the B chain would allow non-specific binding to any cell. To avoid this non-specific binding, different strategies have been utilized: (i) the B chain can be blocked or modified; (ii) the deglycosylated A chain of ricin; and (iii) a non-toxic type 2 RIPs (e.g., ebulin I and nigrin b) have been utilized as the toxic part of immunotoxins (Stirpe, 2004). The type 1 RIPs that are most commonly used for immunotoxins are PAP, saporin and gelonin; when compared with the A chain of ricin, they are less dangerous, more stable and easy to prepare. Moreover, saporin-6 is more efficient than the A chain of ricin (Siena *et al.*, 1988).

Most immunotoxins have been prepared for use against cancer cells, the endothelial cells of tumor vasculatures, immunocompetent cells or cells infected by viruses.

### **1.3.2 Anti-tumor therapy**

Several studies has been conducted with tumor transplanted in animals, and the results showed that the efficacy of the therapy appeared to be related to tumor size. ITs were more effective in preventing the development of neoplastic masses when the treatment was started soon after the inoculum of tumors (Pasqualucci *et al.*, 1995).

ITs have been used to cancer patients in phase I or I/II clinical trials against both solid and haematological tumors. Better results were obtained against hematologic malignancies, especially for lymphoma treatments (Frankel *et al.*, 2003). Ricin A chain or blocked ricin were used in patients with B and T-cell leukemia and lymphomas (Bolognesi and Polito, 2004) and ITs containing saporin and an anti-CD30 or CD22 monoclonal antibody were given to patients with Hodgkin's and non Hodgkin's lymphoma respectively (Polito *et al.*, 2011). ITs have been used also against solid tumor but the results were modest, probably because hematological neoplastic cells are easier to access and target *in vivo* compared to solid tumor cells. However, the use of immunotoxins in cancer therapy has not completely fulfilled the hope. Indeed, immunotoxins present some problems: formation of antibodies against carrier

and the RIP, capillary leak syndrome, hepatotoxicity and recurrence of the disease. The latter is probably caused by the advance state of the tumor in which the trial were performed. The immune response against the antibody could be overcome using humanized antibodies, whereas therapy with a rotation of different toxin could avoid the immune response against the RIP.

### **1.3.3 Immune disorders**

ITs have been used also for autoimmune diseases. One approach was to conjugate saporin S-6 with anti-idiotypic antibodies, while another was to construct ITs with the antigens responsible for the disease. This antigen-toxin could combine with and kill the immunocompetent cells. IT composed of antiidiotypic antibody and saporin was utilized in the treatment of guinea pig B lymphocytic leukemia and as result the immunoglobulin-secreting leukemic cells were selectively eliminated (Glennie *et al.*, 1987). Antigen-toxin IT has two main advantages: the carrier molecule is a human molecule, and their determinants are very small. Good results were obtained with ricin-tetanus toxoid conjugates which were able to selectively eliminate the specific antibody-producing B cell clones, without affecting the remainder of the B cell repertoire (Volkman *et al.*, 1982). The A chain of ricin was conjugate to human thyroglobulin for the cure of patients with Hashimoto disease (Rennie *et al.*, 1983). Specific suppression of immune response to acetylcholine receptor was obtained *in vitro* with IT containing antibody against the nicotinic acetylcholine receptor and RIP, for the treatment of focal muscle spam (Hott *et al.*, 1998), of strabismus by destroying oculomotor muscle (Christiansen *et al.*, 2002) and for the therapy of myasthenia gravis (Hossann *et al.*, 2006).

RIPs have been also utilized for the prevention and treatment of graft versus host disease (GVHD). The first clinical applications of IT, made with toxic subunit of ricin, were the purging of the bone marrow of T cells to avoid GVHD both in allogeneic and autologous transplantation (Filipovich *et al.*, 1984; Colombatti *et al.*, 1984). Even saporin-S6, which is one of the most stable and active type-1 ribosome-inactivating proteins, has been used for this purpose (Tazzari *et al.*, 2001; Polito *et al.*, 2009b).

*Chapter 2*

# Materials and Methods

## 2.1 Materials

### RIPs

Stenodactylin was purified from the caudex of *Adenia stenodactyla* as described by Stripe *et al.*, 2007. Saporin was purified from the seeds of *Saponaria officinalis* as described by Barbieri *et al.*, 1987. Ricin was purified from the seeds of *Ricinus communis* as described by Nicolson *et al.*, 1974. Ebulin I was purified from the leaves of *Sambucus ebulus* as described by Girbés *et al.*, 1993b. Nigrin b was purified from the bark of *Sambucus nigra* as described by Girbés *et al.*, 1993a.

*Adenia* plants were purchased from Exotica Botanical Rarities, Erkelenz-golkrath, Germany and, if not used immediately on arrival, were kept in the greenhouse of the Botanical Garden of the University of Bologna.

### Cell cultures

The cell lines used were NB100 derived from human neuroblastoma, and COLO 320 derived from human colon carcinoma. RPMI 1640, fetal calf serum, L-glutamine, antibiotics, were purchased from Sigma-Aldrich (St.Louis, MO, USA). Trypan blue, and trypsin/EDTA were obtained from BioWhittaker (Vervies, Belgium).

Cytotoxicity was evaluated using L-[4,5-<sup>3</sup>H] leucine purchased by GE Healthcare (Buckingham shire, UK). Flasks and plates were from Falcon (Franklin Lakes, NJ, USA).

### Antibodies

Mouse anti-PARP, anti-R.I.P1, anti-BAD, anti-BAX antibodies were obtained from BD transduction Laboratories (Heidelberg, Germany). The horseradish peroxidase-conjugated anti-mouse or anti-rabbit IgG, rabbit anti-LC3, anti-rabbit TRITC were purchased from Sigma Aldrich. Rabbit anti-stenodactylin polyclonal antibodies were obtained as described by Strocchi *et al.*, 1992.

### Kits

The apoptosis was evaluated using the luminescent kit Caspase-Glo<sup>™</sup> 3/7 Assay, Caspase-Glo<sup>™</sup> 2 Assay, Caspase-Glo<sup>™</sup> 8 Assay, Caspase-Glo 9<sup>™</sup> Assay (Promega Corporation, Wisconsin, USA) and the Annexin V-EGFP/PI detection kit (Biovision, Mt. View, CA).

The viability was measured using the colorimetric CellTiter 96<sup>®</sup> Aqueous One Solution Cell Proliferation Assay (Promega). The CellTiter 96<sup>®</sup> Aqueous One Solution Reagent contains a novel tetrazolium compound [3-(4,5-dimethylthiazol-2-yl)-5-(3-carboxymethoxyphenyl)-2-

(4-sulfophenyl)-2H-tetrazolium, MTS] and an electron coupling reagent (phenazine ethosulfate; PES).

The mitochondrial potential changes were detected using the Mitochondria Staining Kit (Sigma Aldrich).

The oxidative stress was assayed by Total ROS/Superoxide Detection Kit (Enzo Life Science, Farmingdale, NY, USA).

For RT-PCR analysis the GenElute Mammalian Total RNA Kit and the primers were purchased from Sigma-Aldrich.

For stenodactylin sequence the total RNA was isolated using the RNeasy Minikit, whereas the plasmids were purified by QIAfilter plasmid purification kit, both purchased from QIAGEN (Valencia CA, USA). The PCR products were purified using the High Pure PCR Product Purification kit obtained from Roche Applied Science (Mannheim, Germany). The reverse transcriptase MuLV, the dNTPs were obtained from GeneAmp RNA PCR kit (Applied Biosystem, Roche, New Jersey, USA). The chemically competent *E.coli* INVαF' and the pCR® II cloning vector were purchased from Invitrogen (Life technology-Carlsbad-CA, USA).

## **Reactives**

The liquid scintillation was Ready-Gel (Beckman Instrument, Fullerton, USA). The reagents and the molecular weight standard were purchased from GE Healthcare.

DAPI-Antifade was from Resnova SRL, Genzano di Roma, Italy.

The pan-caspase inhibitor Z-Vad-fmk (carbobenzoxy-valyl-alanyl-aspartyl-[O-methyl]-fluoromethylketone) was supplied by Vinci-Biochem (Florence, Italy). The inhibitor of necroptosis necrostatin-1, catalase, superoxide dismutase and sodium pyruvate were obtained from Sigma-Aldrich.

The Immobilon Western detection Reagent and the PVDF membrane were purchased from Millipore (Milford, MA, USA).

For native-PAGE it was used the gel precasted and the buffer strips obtained from GE-Healthcare.

The iScript cDNA synthesis Kit and the SsoFast™ EvaGreen® Supermix were obtained from Bio-Rad (Hercules, CA, USA).

Other reagents used were from Merck (Darmstadt, Germany), Carlo Erba, Milano, Italy and Sigma.

## **Instruments**

Cells were maintained at 37°C in humidified atmosphere at 5% CO<sub>2</sub> in the HeraCell Haereus incubator (Hanau, Germany).

Cell-incorporated radioactivity was measured by a β-counter (Beckman Coulter, Fullerton, CA, USA).

Morphological cell analysis was carried out with a digital camera from Motic Microscopes, (Xiamen,China). Fluorescence microscopy was performed with a Nikon Eclipse E600 fluorescence microscope (Nikon instruments, Cadenzano, Firenze).

Absorbance at 492nm was measured by a microtiter plate reader Multiskan EX, ThermoLabsystem, (Helsinki, Finland).

Flow cytometry analysis, was done using the FACSAria BD analyzer (Franklin Lakes, New Jersey, USA).

The luminescence was read using the Fluoroskan Ascent FL (Labsystem, Finland).

Protein concentration was determined by UVICON 860 Spectrophotometer (Kontron Instruments, Milano, Italy). The DNA content was determined by Beckman DU 640 spectrophotometer The protein were separated on SDS-PAGE and then blotting using the Mini Protean 3 Cell electro-blotting apparatus (Bio-Rad).

The native PAGE analysis was conducted using the the PhastSystem (GE-Healthcare).

RT-PCR was performed using the CFX96 Real-Time PCR System (Bio-Rad).

PCR was conducted using the thermal cycler PCR system 2400 (Perkin Elmer).

## **Statistical analysis**

Statistical analyses were conducted using the XLSTAT-Pro software, version 6.1.9 (Addinsoft 2003). Result are given as means ±SD of three different experiments. Data were analyzed by ANOVA, followed by a comparison with Dunnett's test.

## **DNA sequencing Softwares**

A search for sequence similarity was performed with the BLAST program available on-line (<http://www.ncbi.nlm.nih.gov/BLAST>). Multiple sequence alignment program ClustalW (<http://npsa-pbil.ibcp.fr>) was used to detect the extent of sequence conservation and the secondary structure prediction was carried out using PSIPRED (<http://bioinf.cs.ucl.ac.uk>).

The tertiary structure was predict using SWISS-MODEL (<http://swissmodel.expasy.org>).

Phylogenetic tree was made in MEGA 5 using neighbor-joining analysis (Saitou and Nei, 1987).

## 2.2 Methods

### 2.2.1 Sequencing of stenodactylin

#### 2.2.1.1 Synthesis of cDNA

The caudex of *A. Stenodactyla* was disrupted using mortar and pestle and grinded to a fine powder under liquid nitrogen. Approximately 100 mg of total RNA was isolated using the RNeasy Minikit (Qiagen) according to the manufacturer's instruction. Poly(A)-rich RNA was reverse transcribed using the synthetic oligonucleotide J1 (5' CGTCTAGAGTCGACTAGTGC(T)<sub>20</sub> 3'). Approximately 2 µg of total RNA and 1µl of RNase inhibitor were incubated at 65°C in a thermal cycler for 5 min. It was later cooled on ice for 1 minutes and it was added 15 µl of reaction mixture containing: 1×PCR Buffer PEII, 5 mM of MgCl<sub>2</sub>, 1 mM of each dNTP, 10 µM of J1, and 100 U/µl of MuLV reverse transcriptase (Roche). The reaction mixture was incubated 20 min at 23°C, then for 20 min at 42°C, and finally 5 min at 99°C.

#### 2.2.1.2. Reverse transcription

The cDNA specific primers for full-length of stenodactylin were designed and synthesized based on the volkensin sequences. Three couple of primers were used to detect the full length amino acid sequence of stenodactylin (STA2-STB1R for A-chain; STA2-STB3R for A-chain and a piece of B-chain; STB1-STB5R for B-chain). The primer sequences are reported in Table 2.1.

**Table 2.1.** Primer sequence

STA2	5' GCCACGGTAGAGAGRTACACT 3'
STB1R	5' AAGTCGTCTCCCCGGAAGGGC 3'
STB3R	5' GGC GGGGTTGATGGTTCC3'
STB1	5' TGCCCTCCGGGGAGACGACT3'
STB5R	5' TAGGAACCATTGCTGGTTGGA3'

For cDNA amplification 2 µl of the above-synthesize cDNA were used and 16 µl of master mix and 0.5 µM of each primers were added. A typical reaction master mix included: 1×PCR buffer/Mg<sup>2+</sup>, 0.25 mM dNTPs Mix, 2.5 U Taq Polymerase (Biotools, Madrid, Spain). PCR amplification was done with PCR conditions reported in Table 2.2.

**Table 2.2.** PCR condition

Stage	Step	Temperature °C	Duration	N°. of cycles
I	Initial denaturation	94	5 min	1
II	Denaturation	94	30 sec	} 35
	Annealing	55/54	30 sec-45 sec	
	Extension	72	2 min	
III	Final extension	72	10 min	1
	Hold	4		

About 5 µl of amplified products from each tube along with 3 µl of loading dye were separated on 0.8% agaroses gel using 1X TAE buffer along with *HindIII* / *EcoRI* double digest as DNA molecular weight marker.

### 2.2.1.3 cDNA cloning

The PCR product was purified using the High Pure PCR product Purification Kit (Roche) according to the manufacturer's instruction.

The purified PCR product was ligated into the pCR<sup>®</sup>II cloning vector (Invitrogen). For ligation, optimal molar ratio is 1:3 of vector: insert. The components of ligation mixture was mixed into a 0.5 ml microcentrifuge tube and incubated at 14°C overnight in a thermal cycler. The vector contains genes for ampicillin and kanamycin resistance that make it possible to select for transformed bacteria.

The ligation mixtures were used to transform the Chemically Competent *E. Coli* INVαF' (Invitrogen). *E. coli* INVαF' cells were provided as frozen 50 µl aliquots with the TA Cloning<sup>®</sup> kit. The required number of tubes was thawed on ice. 5 µl of the ligation mixture was gently pipetted into the thawed competent cells and mixed gently. The tubes were incubated on ice for 30 min and then heat shocked for 30 sec in 42 °C water bath and then placed on ice for 2 min. SOC medium provided with the kit was prewarmed to room temperature. 250 µl of prewarmed SOC medium was added onto each sample after the heat shock. The samples were incubated at 37 °C shaking horizontally at 225 rpm for 1 hr. 50 and 100 µl of each sample was spreaded onto a prewarmed LB/amp plate with 40 µl of XGal from the 20 mg/ml stock. After 15 min, the plates were inverted and incubated at 37°C overnight, and the following day

the plates with colonies were stored at 4°C. The transformants colonies were analyzed. The white colonies (transformants clones) were screened by PCR using the appropriate couple of primers. Using a yellow tip the colony was dipped into a PCR tube and then streaked it onto a fresh agar plate using a numbered template. The PCR mix included: 0.25 mM dNTPs, 1× PCR Buffer, 1µM of each primers, 0.125 U Taq Polymerase (Biotools), PCR program was done as reported in Table 2.2.

#### 2.2.1.4 Isolation of the plasmids

The positive white colonies from the agar plates were transferred to a Falcon tube each, containing 10ml LB-medium with 100 µg/ml ampicillin, and incubated overnight at 37°C at 225 rpm. The cells were collected by centrifugation (2800 rpm for 10 min) and then purified using plasmid purification kit (Qiagen) following the manufacturer's instructions.

The DNA content or copy number of the plasmids was determined by measuring their absorbance at 260 nm where an absorbance of 1 is equivalent to 50 µg DNA/ml.

Plasmid quality and the presence of sequence fragment was checked by running the precipitated samples on a 1% agarose gel by digestion with *EcoRI*. This gives information on conformation and structural integrity of isolated plasmid DNA.

#### 2.2.1.5 DNA sequence

DNA sequencing was carried out on the CENIT Support system (Villamayor-Salamnca, Spain). The sequence reactions were performed using pCRII plasmid and the M13 and M13R universal primers, according to the manufacturer's recommendations.

### **2.2.2 Cell culture**

NB100 and COLO320 cells were maintained in the logarithmic phase of growth in RPMI 1640 medium containing 10% heat-inactivated foetal bovin serum, 2 mM L-glutamine, 100U/ml penicillin and 100 µg/ml streptomycin (hereafter named complete medium), in humidified air with 5% CO<sub>2</sub> at 37°C. Cells were checked for the absence of Mycoplasma infection.

### **2.2.3 Cell protein inhibition**

#### 2.2.3.1 Cells

NB100 cells ( $2 \times 10^4$ /well) were seeded in 24-well microtiter plates in 250 µl of complete medium in the absence (control cultures) or in the presence of stenodactylin, ricin, saporin at concentrations ranging from  $10^{-7}$  to  $10^{-14}$  M in complete medium. After 48 h, cells were

incubated at 37°C for further 4 h with L-[4,5-<sup>3</sup>H] leucine (0.125µCi/well) (GE Healthcare) in serum and leucine-free medium. Protein synthesis was arrested with 20% trichloroacetic acid (TCA) for 30 min at 4°C. After three washes with 5% TCA, 200 µl/well of KOH 1N were added and incubation for 10 min at 37°C was performed. Cell-incorporated radioactivity was measured by a β-counter with Ready-Gel scintillation liquid containing 0.7% acetic acid.

The IC<sub>50</sub> and IC<sub>100</sub> (concentration of RIP required to inhibit cell protein synthesis by 50% and 100%, respectively), were calculated by regression analysis.

#### 2.2.3.2 Cell-free system

Cell-free protein synthesis for ebulin 1 and nigrin b was determined with a coupled transcription-translation *in vitro* assay using the rabbit reticulocyte lysate system. The reaction mixture was composed of 4 µl rabbit reticulocyte lysate, 1.2 U/µl RNase inhibitor (Amersham Biosciences Inc., GE), 2.8 U/µl T7 RNA polymerase (Takara-Bio, Shiga, Japan), 0.24 mg luciferase T7 plasmid (Promega), and nuclease-free water to a final volume of 8 µl. The reaction tubes were incubated at 30°C for 10min and chilled on ice. Then 1,6 µl of either water or dilutions of the respective RIP with increasing concentrations was added to the test tubes and the samples were incubated at 30°C for 30 min. At this time 20 µl of water at room temperature were added to the sample and 28 µl of room temperature luciferase assay reagent in a luminometer tube. The relative luciferase activities of the samples were determined in a Luminova 1254 luminometer (BIO ORBIT) for 10 sec with an initial delay of 2 sec. The inhibitory effects of proteins were represented as the IC<sub>50</sub> value which is defined as the amount of inhibitory protein that gives a 50% of inhibition of protein synthesis.

#### **2.2.4 Cell viability assay**

Cell viability was evaluated with the colorimetric assay CellTiter 96<sup>®</sup> Aqueous One Solution Cell Proliferation. This colorimetric kit allows to determine the number of viable cells.

The MTS tetrazolium compound is bio-reduced by cells into a colored formazan product that is soluble in RPMI medium. This conversion is presumably accomplished by NADPH or NADH produced by dehydrogenase enzymes in metabolically active cells. The quantity of formazan product is measured by the absorbance at 490nm.

Cells (3×10<sup>3</sup>/well) were seeded in 96-well microtiter plates in 100 µl RPMI complete medium. After 24 h, cells were incubated in the absence (control culture) or in the presence of stenodactylin, ricin, saporin, ebulin 1, nigrin b at scalar concentrations (from 10<sup>-6</sup> to 10<sup>-14</sup> M) in complete medium. After the indicated times the medium was removed and 100 µl/well plus

20 µl/well of colorimetric kit solution were added. After 1 h of incubation at 37°C the absorbance at 492 nm was measured.

#### 2.2.4.1 Viability in the presence of inhibitors and/or scavengers

The RIP cytotoxicity was also evaluated on NB100 cells pretreated with 100 µM of the pan-caspase inhibitor Z-Vad-fmk, 100 µM of the necroptosis inhibitor necrostatin-1, 10 U/ml catalase, 10 U/ml heat inactivated catalase (65 °C for 30 min), 100 U/ml superoxide dismutase or 1 mM Sodium pyruvate. The reagents were added to NB100 cells 3 h before RIPs and they were re-added to cultures every 24 h. In cells treated with  $10^{-12}$  M stenodactylin, the incubation with the RIP was only for 2 h. The 2h treatment was performed to evaluate the early effects of stenodactylin.

#### **2.2.5 Cell and nuclear morphology**

NB100 cells ( $2 \times 10^4$  /500 µl complete RPMI medium) were incubate with stenodactylin  $10^{-12}$  M in 24-well microtiter plates for 24, 48, 72, 96 h at 37°C. Morphology was assessed by phase contrast microscopy.

For nuclear analysis, the NB100 cells ( $2 \times 10^4$  /500 µl complete RPMI medium) were seeded directly on a coverslips in 35 mm dishes for 48 h. After treatment with stenodactylin ( $10^{-12}$  M) for 24 h, the cells were washed with PBS and fixed with 2% p-formaldehyde (freshly prepared) for 30 min. After washing with PBS, the cells were incubated with 7 µl DAPI/antifade (4',6-diamidino-2-phenylindole) and visualized under Nikon Eclipse E600W fluorescence microscope.

#### **2.2.6 Assessment of apoptosis**

Apoptotic cell death was examined by flow cytometry and by fluorescence microscope using Annexin V-EGFP/PI detection kit and by luminometer measuring caspase activation.

The scavengers or the inhibitors were added 3 h before the RIPs were added and cells treated with  $10^{-12}$  M stenodactylin, the incubation with the RIPs was for 2 h.

##### 2.2.6.1 Quantification by flow cytometry

Cells ( $2 \times 10^5$ /3 ml complete RPMI) were seeded in 25 cm<sup>2</sup> flasks, and after 24 h, the cells were treated with stenodactylin ( $10^{-12}$  M), ebulin 1 ( $10^{-7}$  M) and nigrin b ( $10^{-7}$  M). After the indicating times the cells were centrifuged at 400×g for 5 min, washed in 2 ml fresh medium, centrifuged again and resuspended in 294 µl binding buffer provided in the kit. Annexin V-EGFP (3 µl) and propidium iodide (3 µl) were added. Tubes were incubated for 10 min in the

dark at room temperature. Cells were analyzed by flow cytometry within 30 min, using the FACS Aria BD analyzer.

#### 2.2.6.2 Detection by fluorescence microscopy

Cells ( $1.5 \times 10^4/500 \mu\text{l}$ ) were seeded directly on a coverslips in 35 mm dishes 48 h prior the experiments. After the indicating time from the treatments, 198  $\mu\text{l}$  binding buffer, 1  $\mu\text{l}$  of Annexin V-EGFP and 1  $\mu\text{l}$  of PI were added. Following incubation at room temperature for 10 min in the dark, the coverslips were inverted on glass slide and the cells were observed under a Nikon Eclipse E600W fluorescence microscope equipped with a 60X objective (Nikon, Melville, NY). Image merge was obtained by Image J 1.42q software.

#### **2.2.7 Caspase -3/7, -8,-9,-2 activities**

The caspase -3/7,-8, -9, -2 were assessed by the luminescent assay Caspase-Glo™, specific for each caspase. Each kit provides a luminogenic caspase substrate, which contains the tetrapeptide sequence specific for each caspase (DEVD, VDVAD, LEHD, LETD for caspase 3/7, -2, -9,-8, respectively). The caspase cleavages its substrate generating a luminescent signal, produced by luciferase. Luminescence is proportional to the amount of caspase activity present.

Cells ( $4 \times 10^3/\text{well}$ ) were seeded in 96-well microtiter plates in 100  $\mu\text{l}$  RPMI complete medium. After 24 h, the RPMI was removed and the cells were treated with 100  $\mu\text{l}$  RPMI containing RIP (stenodactylin  $10^{-12}$  M and  $10^{-14}$  M; ricin  $10^{-13}$  M; saporin  $10^{-11}$  M; ebulin I  $10^{-7}$  M and nigrin b  $10^{-7}$  M). After incubation at the indicating times, the medium was removed and 50  $\mu\text{l}/\text{well}$  of RPMI and 50  $\mu\text{l}/\text{well}$  of Caspase-Glo™ 2, Caspase-Glo™ 8, Caspase-Glo™ 3/7 I were added. For caspase 9, 80  $\mu\text{l}/\text{well}$  of RPMI and 20  $\mu\text{l}/\text{well}$  of Caspase-Glo™ 9 were added. Plates were shaken at 420 rpm for 1 min and then incubated for 20 min at room temperature in the dark. The luminescence was measured by Fluoroskan Ascent FL (integration time 10 sec) and the values were normalized for the viability.

Caspase 8 inhibitor Z-IETD-fmk (z-Ile-Glu(OMe)-Thr-Asp(OMe) fluoromethyl ketone, Sigma-Aldrich) was added to the cell 3 h before RIPs, at the concentration of 25  $\mu\text{M}$ .

For the experiments with inhibitors or scavengers and stenodactylin ( $10^{-12}$  M), the RIP was added 3 h after the inhibitors and left in contact with cells for 2 h. The scavengers and the inhibitors were added every 24 h.

### **2.2.8 Measurement of mitochondrial membrane potential loss**

The change in mitochondrial membrane potential ( $\Delta\psi_m$ ) was measured using the cationic, lipophilic dye, JC-1 (5,5',6,6'-tetrachloro-1,1',3,3'-tetraethylbenzimidazolocarbo-cyanine iodide) purchased from Mitochondria Staining Kit (Sigma). In health cells, due to the electrochemical potential gradient, the dye concentrates in the mitochondrial matrix, where it forms red fluorescent aggregates (J-aggregates). Any event that dissipates the mitochondrial membrane potential prevents the accumulation of the JC-1 dye in the mitochondria and thus, the dye is dispersed throughout the entire cell leading to a shift from red (J-aggregates) to green fluorescence (JC-1 monomers).

Cells ( $2 \times 10^4$ /500  $\mu$ l) were seeded directly on a coverslips in 35 mm dishes 48 h prior the experiments. After the RPMI was removed and stenodactylin was added for 24 h ( $10^{-12}$  M) or for 16 h ( $10^{-14}$  M). At the end of the treatments, the cells were stained with 500  $\mu$ l of JC-1 dye (1:100 in RPMI) and incubated at room temperature for 10 min in dark. The cells were then washed three times with Staining buffer purchased from the kit. The coverslips were inverted on glass slide and the cells were observed under a Nikon Eclipse E600W fluorescence microscope equipped with a 60X objective.

### **2.2.9 Assessment of oxidative stress**

The oxidative stress was detected by using the Total ROS/superoxide Detection Kit, which through the combination of two specific fluorescent probes, it is enable to measure the global level of reactive oxygen species (ROS) and specifically superoxide in living cells. The total ROS detection dye (green) reacts directly with a wide range of reactive species, (e.g., hydrogen peroxide, peroxy-nitrite), while the superoxide detection dye (Red) is a cell-permeable probe that reacts specifically with superoxide.

#### 2.2.9.1 Quantification by flow cytometry

Cells ( $4 \times 10^5$ /3ml complete RPMI) were seeded in 25 cm<sup>2</sup> flasks, and after 24 h, the cells were treated with stenodactylin ( $10^{-12}$  M) for 8 h. Then the media was removed and the cells were washed twice with 1 $\times$  Wash buffer purchased form the Kit. After trypsinization, the cells were centrifuged at 400 $\times$ g for 5 min, and washed with the Wash buffer and collected in flow cytometry tubes. The cells were centrifuged at 400 $\times$ g for 5 min and the cell pellet was resuspended in 500  $\mu$ l of Superoxide Detection Mix, according to the manufacturer's instruction. Cells were analyzed by flow cytometry within 30 min, using the FACSaria BD analyzer.

### 2.2.9.2 Detection by fluorescence microscopy

Cells ( $1.5 \times 10^4/500\mu\text{l}$ ) were seeded directly on a coverslips in 35 mm dishes 48 h prior the experiment. After, the medium was removed and 1 ml of RPMI containing stenodactylin ( $10^{-12}$  M) was added for 8 h. Subsequently the medium was removed and was added 600  $\mu\text{l}$  of ROS/Superoxide Detection Mix, according to the manufacturer's instruction. Following incubation at  $37^\circ\text{C}$  for 1 h in the dark, the coverslips were inverted on glass slide and the cells were observed under a Nikon Eclipse E600W fluorescence microscope equipped with a 60X objective (Nikon, Melville, NY). Image merge were obtained by Image J 1.42q software.

### **2.2.10 Native PAGE**

Stenodactylin and catalase were analyzed by polyacrylamide electrophoresis gels in native condition. The two proteins were incubated in Native Sample Buffer (40 mM Tris-HCl pH 6.8, 0.005% bromophenol blue) for 20 min at  $37^\circ\text{C}$ . Then the samples were analyzed on the PahstGel 8-25 gradient using the PhastSystem instrument. The gel was stained with Coomassie Brilliant Blue G250 0.1% (w/v) in 50% methanol and 10% acetic acid.

### **2.2.11 Immunofluorescence using anti-stenodactylin antibodies**

Cells ( $2.5 \times 10^4/1\text{ml}$ ) were seeded directly on a coverslips in 35 mm dishes 72 h prior the experiments. Then, the cells were cold-treated with stenodactylin ( $10^{-12}$  M), catalase (10 U/ml) or in the combination of both. After 30 min at  $4^\circ\text{C}$  the cell were fixed with 1% p-formaldehyde (freshly prepared). After 30 min at  $37^\circ\text{C}$ , the cells were washed three times with PBS and the 1% of BSA in PBS was added. After 1 h at  $37^\circ\text{C}$ , the cells were washed three times with PBS and was added anti-stenodactylin antibodies (1:1000 in 1% BSA). After 2 h at  $37^\circ\text{C}$  and three washes, the anti-rabbit TRITC antibody (1:500) was added. After 1 h at  $37^\circ\text{C}$  and three washes the coverslips were inverted on glass slide and the cells were observed under the fluorescence microscope.

### **2.2.12 Western Blot analysis**

Cells ( $1 \times 10^6/20$  ml RPMI complete) were seeded in 75  $\text{cm}^2$  flasks and, after 24 h, medium was removed and the stenodactylin ( $10^{-14}$  M or  $10^{-12}$  M) was added. At different times of incubation, ranging from 8 to 24 h, cells were harvested with a cell scraper, collected by centrifugation at  $500 \times g$  for 5 min a room temperature. Cell pellets were lysed by adding 100  $\mu\text{l}$  of Cell Lytic-M (Sigma-Aldrich) supplemented with Protease inhibitor Cocktail (1:100), Phosphatase inhibitor cocktail 1 (1:100) and sodium-orthovanadate (1:500). After 45 min at

0°C, vortexing every 5 min, insoluble material (nuclear pellet plus membranes) was removed by centrifugation at 12,000×g for 25 min at 4°C. Protein supernatant (cell lysate) was collected and stored at -20°C. Protein content was quantified by spectrophotometer using the Kalb and Bernlohr formula (Kalb and Bernlohr, 1977). The protein (50 µg/lane) were separated by SDS-PAGE (10% gel) and blotted for 45 min at 100 V to Immobilon (polyvinylidene difluoride, PVDF) membrane (Millipore). Non-specific antibody binding sites were blocked by incubation with blocking buffer (TRIS buffered saline, 0.1% Tween 20 (TBS/T)) with 5% casein, for 1 h at room temperature. After 5 washes with TBS/T, membranes were incubated overnight at 4°C with various primary antibodies: anti-PARP antibody at 1: 2000 directed against uncleaved (116 kDa) and the cleaved form of PARP (85 kDa), anti-BAD 1:5000, anti-BAX 1:1000, anti-LC3 1:5000 direct against LC3I (18 kDa) and LC3II (16 kDa), anti R.I.P1 1:2000, monoclonal anti-β-actin which detects β-actin (42 kDa) was used as protein loading control. All antibodies were diluted in TBS/T with 5% bovine serum albumin. After 5 washes with TBS/T, membranes were incubated for 1 h at room temperature with horseradish peroxidase-conjugated anti-mouse or anti-rabbit antibody or goat anti-rabbit secondary antibody used at 1:10000, diluted in blocking buffer with 5% casein. After further 5 washes, proteins were detected by incubating the membrane with Immobilon Western detection Reagent (Millipore) according to manufacturer's protocol and the image was taken on Kodak® BioMax light Film. The level of expression of different proteins was analysed by using the public domain software Image J.

### **2.2.13 Real-time PCR Analysis**

Cells ( $2 \times 10^5$ /well) were seeded in 6-well culture plates in complete medium. After 24 h the cells were treated with stenodactylin ( $10^{-14}$  M) for the indicating times. Total RNA from NB100 cells was isolated using the GenElute Mammalian Total RNA Kit (Sigma). RNA quantity was determined spectrophotometrically according to optical densities at 260 and 280 nm, whereas its integrity checked by a standard electrophoresis in agarose gel. cDNA was synthesized from 800 ng of the total RNA and the cDNA synthesis was performed using the iScript cDNA Synthesis kit (Bio-Rad) following the manufacturer's direction, applying 4 µl of 5×iScript Mix, 1 µl of iScript reverse, the sample and Nuclease free water to the total volume of 20 µl. The reaction mix was incubate for 5 min 25°C, followed by 30 min incubation at 42°C, then 15 min 48°C, followed by 5 min at 85°C and then store the cDNA product at -20°C. The resulting cDNA was used in the real time PCR reaction.

Real-time PCR was performed in 20  $\mu$ l of reaction mixture consisting of 10  $\mu$ l of 2 $\times$ EvaGreen Supermix (Bio-Rad), 1  $\mu$ l of each primer (final concentration of 0.4  $\mu$ M) (Table 2.3), 3  $\mu$ l of template and 6  $\mu$ l of Nuclease free water.

RT-PCR was performed using the CFX96 Bio-Rad Real-Time System and the following cycling program: enzyme activation for 30 sec at 98°C, 44 cycles of denaturation for 3 sec at 98°C and annealing/extension for 8 sec at 60°C, and melt curve for 5 sec/step at 65°C-95°C (in 0.5°C increments). Triplicates of each sample were loaded in a 96 well plate.

The threshold cycle (Ct) value for each gene was normalized to the Ct value of GAPDH. Relative mRNA expression was calculated by the following formula:  $2^{-\Delta\Delta Ct}$  where  $\Delta Ct = Ct^{\text{target gene}} - Ct^{\text{reference gene}}$  and  $\Delta\Delta Ct = \Delta Ct^{\text{treated}} - \Delta Ct^{\text{control}}$ .

**Table 2.3.** Primer sequences for RT-PCR

<b>Gene</b>	<b>Primer sequence</b>
<b>BAD</b>	F-GAGTGACGAGTTTGTGGAG R-CACCAGGACTGGAAGACT
<b>BAX</b>	F-AGCTGACATGTTTTCTGACG R-GCCTTGAGCACCAGTTTG
<b>GADPH</b>	F-CCCTTCATTGACCTCAACTACATG R-TGGGATTTCCATTGATGACAAGC

*Chapter 3*

**Amino acid sequence of  
Stenodactylin**

## **BACKGROUND: Primary and tertiary structure of RIPs**

The amino acid sequence and three-dimensional structure of many type 1 (e.g., saporin and dianthin) and type 2 (e.g., ricin, abrin and ebulin) RIPs are known and have been reported in the literature and the GenBank database.

A comparison of these sequences shows the similarity between the type 1 and the A chains of type 2 RIPs and among the B chains of type 2 RIPs. However, the complete primary structure sequence homologies vary from 17 to 80%. Although highly variable, several amino acid residues seem to be important for the catalytic activity, and they are conserved in type 1 and in the A chain of type 2 RIPs. Based on the ricin A chain sequence, the conserved residues are Tyr<sup>80</sup>, Tyr<sup>123</sup>, Glu<sup>177</sup>, Arg<sup>180</sup> and Trp<sup>211</sup>. The adenine-binding site can also hold guanine (in PAP and trichosanthin) or pteric acid (in ricin and PAP) (Yan *et al.*, 1997; Kurinov *et al.*, 1999; Gu and Xia, 2000). This result suggests that N-glycosylase activity is not directed only to adenine but may also be directed toward other purine derivatives; however, this hypothesis is controversial. Near the active site, six other amino acids are important and conserved in both mono and bi-chain RIPs (with the exception of the type 1 RIPs from irises). These residues (Asn<sup>78</sup>, Arg<sup>134</sup>, Gln<sup>173</sup>, Ala<sup>178</sup>, Glu<sup>208</sup> in ricin) are not involved in the depurination mechanism, but they help maintain the catalytic conformation (Katzin *et al.*, 1991; Hao *et al.*, 2001). Site-directed mutagenesis studies have shown that mutating of amino acid important for the catalytic activity causes a substantial reduction in activity. Frankel and co-workers, found that a positive charge at position 180 is essential for solubility and enzyme activity; indeed, the conversion of Arg<sup>180</sup> to His reduces the enzymatic activity almost 1000-fold (Frankel *et al.*, 1990). Conversion of Glu<sup>177</sup> to Gln reduces enzyme activity of 200-fold (Ready *et al.*, 1991). In type 2 RIPs, the A and B chains are linked by a disulfide bridge between two cysteines. In ricin, the two cysteines that are involved are Cys<sup>259</sup> of the A chain and Cys<sup>4</sup> of the B chain (Katzin *et al.*, 1991).

X-ray diffraction analysis indicates that the three-dimensional structures are well conserved between RIPs, with the only differences in the C-terminal region and the surface loop structure. Ricin was the first RIP analyzed by X-ray diffraction, and its structure was published 1987 (Montfort *et al.*, 1987). The X-ray diffraction data demonstrated that the A chain is a globular protein that is folded into three domains that largely exhibits  $\alpha$ -helical and  $\beta$ -strand structures. The A chain includes two N-glycosylation sites (Asn<sup>10</sup>-Phe<sup>11</sup>-Thr<sup>12</sup> and Asn<sup>236</sup>-Gly<sup>237</sup>-Ser<sup>238</sup>), but these sites do not appear to be important for proper folding (Mlsna *et al.*, 1993). The B chain folds into two topologically similar domains, and they are stabilized

by four disulfide bridges. Each fold is formed by 12 antiparallel  $\beta$ -strands that are connected by  $\beta$ -turns and  $\Omega$  loops. Each fold is composed of three subdomains ( $1\alpha$ ,  $1\beta$  and  $1\gamma$  for domain 1 and  $2\alpha$ ,  $2\beta$  and  $2\gamma$  for domain 2). Only two of these subdomains,  $1\alpha$  and  $2\gamma$ , demonstrate galactoside-binding activity through a network of hydrogen bonds. Despite creating one more hydrogen bond, subdomain 1 presents with lower affinity for lactose than domain 2 (Hatakeyama *et al.*, 1986). Moreover, domain 2 can bind the N-acetylgalactosamine (GalNAc), while this binding cannot occur in domain 1 due to steric hindrance (Rutenber and Robertus, 1991). Although the three-dimensional structures of the B chains are very similar, the main differences are observed in the amino acid residues that are present in the binding site, especially Tyr<sup>248</sup> in  $2\gamma$  of domain 2. The presence of a positive charge in this domain causes a loss of functionality because the hydrophobic interaction between the pyranose ring of galactose and the aromatic ring of Tyr is lost (Van Damme *et al.*, 2000). X-ray crystallography studies of ebulin 1 (a non-toxic type 2 RIP) revealed changes in key amino acids within the sugar-binding  $2\gamma$  subdomain. These changes reduce the affinity of ebulin 1 for galactosides and, therefore, for galactose-containing glycoproteins or glycolipids of the plasma membrane surface, thus reducing the cytotoxicity of the molecule (Ferrerias *et al.*, 2010). Based on these studies, the carbohydrate-binding properties play an important role in the cytotoxicity of double chain RIPs.

## AIM OF THE PROJECT

Among all plant toxins, the most potent is a type 2 RIP purified from the caudex of the Passifloraceae *Adenia stenodactyla*, (stenodactylin). This RIP has a high enzymatic activity toward ribosomes and hsDNA substrates and a median lethal dose (LD<sub>50</sub>) for mice of 2.76 µg/kg at 48 h (Stirpe *et al.*, 2007). Moreover, similar to modeccin and volkensin (Wiley and Kline, 2000), stenodactylin is retrogradely transported when injected into the central nervous system (Monti *et al.*, 2007).

Currently, little is known about stenodactylin at the protein sequence level. Only the first 22 and 21 amino acid residues of the A and B chains have been determined using direct Edman degradation. A protein sequence alignment between stenodactylin, modeccin (*A. digitata*), lanceolin A1, lanceolin A2 (*A. lanceolata*) and volkensin (*A. volkensii*) showed that the A chain of stenodactylin shares 21/21 identity with lanceolin A2 and 15/21 with volkensin (Fig. 3.1). The identity among the B chains is also very high, except for the first three N-terminal residues; the sequence DPV is present only in the stenodactylin and volkensin B chains (Stirpe *et al.*, 2007).

Alignment:		
Lanceolin A1	-FPKVILDCTRATVERYTQFI	20
Lanceolin A2	VFPKVI <del>F</del> DCTRATVERYTQFI	21
Stenodactylin A chain	VFPKVI <del>F</del> DCTRATVERYTQFIM	22
Modeccin A chain	-FPKVTLDDTRATVESYTT	
Volkensin A chain	VFPKVPFDVPKATVESYTRFIR	22
	**** : ..**** **:**	
Lanceolin B1	D--CPFGETTAYIVGRDXXCV	19
Lanceolin B2	D--CPSGETTAYIVGRDXXCV	19
Stenodactylin B chain	DPVCPSGETTAYIVGRDXXXV	21
Modeccin B chain	EMICPSGETTAYIVGRXGXXV	
Volkensin B chain	DPVCPSGETTAFIVGRDGRCV	21
	** *****:****	

**Fig. 3.1.** Amino acid alignment of the N-termini of lanceolin, stenodactylin, modeccin and volkensin subunits. The single letter code has been used for amino acids. Identical residues (\*), conserved substitutions (:), and semi-conserved (.) substitutions are reported. X, unassigned amino acid positions.

Through a collaboration between our laboratory and Falini and co-workers, stenodactylin was crystallized, and crystal was tested using X-ray diffraction experiments. Figure 3.2 shows the crystal and the typical diffraction pattern of stenodactylin (Tosi *et al.*, 2009).

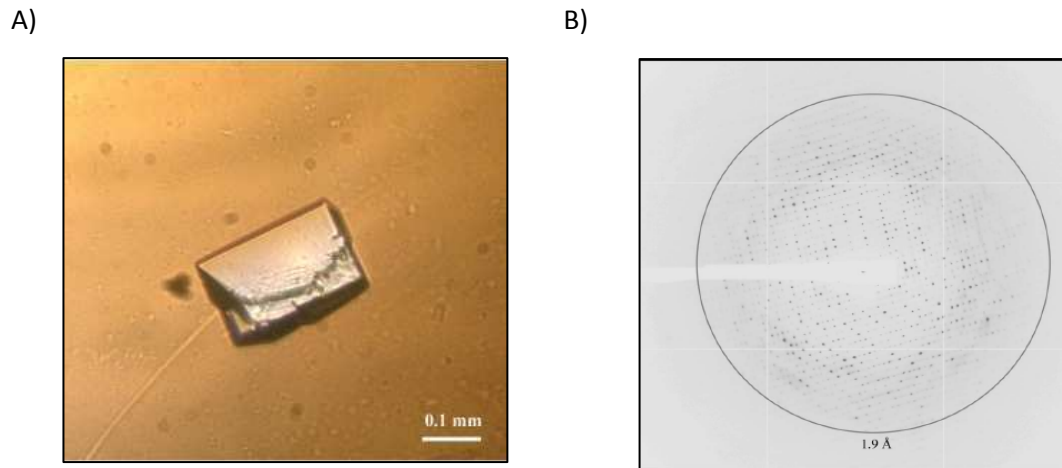


**Fig. 3.2.** Crystal of stenodactylin (A) and X-ray diffraction (B) (Tosi *et al.*, 2009).

The purpose of this project was to determine the complete amino acid sequence of stenodactylin. The DNA sequence was determined using three different primer pairs that were designed based on the first 20 amino acids known for the A and B chains and the volkensin sequence. The volkensin sequence was chosen because both RIPs derive from plants belonging to the same genus and because the two RIPs show high sequence identity in the first 20 amino acids, as previously reported (Stirpe *et al.*, 2007).

The sequence of stenodactylin was aligned and compared with the sequences of other RIPs, including both type 2 (toxic and non-toxic) and type 1.

The alignment and comparison is important (i) to identify both conserved and non-conserved amino acids, (ii) to understand the degree of evolutionary change and (iii) to detect amino acids that are important for their enzymatic activity. Stenodactylin is the most toxic RIP, and comparing its sequence with that of others less toxic RIPs (e.g., ricin) could provide useful information about which amino acids are directly or indirectly involved in their toxicity. The correlation between amino acids and cytotoxicity can be further studied through site-directed mutagenesis.

The one-dimensional amino acid sequence of stenodactylin, together with the already published crystallographic analysis, will be used to determine the three-dimensional structure.

The three-dimensional structure is essential in understanding the protein function and the relationship between structure and cytotoxicity. Particularly, the structure appears to be important for some chemical-physical characteristics, such as the hydrophobic profile and the distribution of electrostatic charges particularly in domains that are near the catalytic site. Changes in these domains or in the catalytic site could explain the different biological

behavior of RIPs. Analyzing the tertiary structures can indicate the orientation and the position of amino acids that are involved in binding sugar. The ability of RIPs to bind to glycoprotein receptors seems to correlate with their cytotoxic properties. Binding occurs prior to internalization and intracellular transport; thus, reduced binding ability or binding to distinct receptors could lead to distinct intracellular pathways, which could cause different cytotoxic effects.

RIPs are used to construct immunotoxins, which have been utilized for several clinical applications (mainly in hematological neoplasias). However, their application is currently limited because immunotoxins present several problems: formation of antibodies against the carrier and the RIP, capillary leak syndrome and hepatotoxicity. The ability to manipulate the protein structure and function is crucial to design more specific and less immunogenic immunotoxins.

## RESULTS AND DISCUSSION

### 3.1 *Stenodactylin* amino acid sequence

#### 3.1.1 Amplification and cloning of the *stenodactylin* gene

Based on of the N-terminal amino acid sequences of the A and B chains of *stenodactylin* obtained in our laboratory by Edman degradation and based on the amino acid sequence of *volkensin*, primers were designed for the PCR amplification of *A. stenodactyla* genomic DNA. Using the *volkensin* sequence information available in GenBank (CAD61022), five specific primers were designed for the *stenodactylin* sequence.

##### 3.1.1.1 Isolation of the Amplicons

The three primer pairs were used to amplify the A chain, the A chain with part of the B chain and the B chain of *stenodactylin*. As reported in Figure 3.3, the amplicons of expected size (~ 0.85 kb for the A and B chains alone and ~ 1.1kb for the combined A and small segment of B chains) were obtained, and the PCR products were purified as described in the materials and methods.

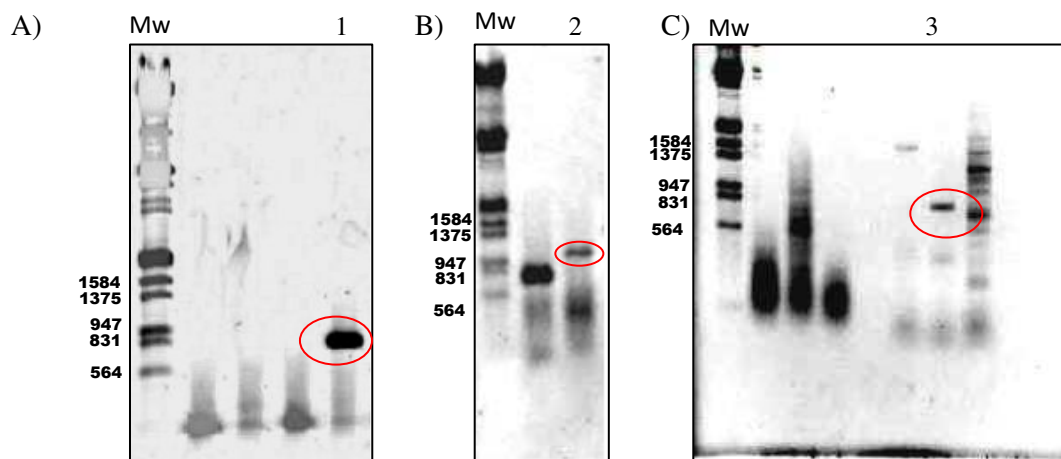


**Fig. 3.3.** Amplification of *stenodactylin* A-chain (A, lane 1), A-chain and a part of B-chain (B, lane 2), B-chain (C, lane 3). MW:  $\lambda$  Hind III/EcoRI double digest DNA marker. The red circles are to indicate the amplicate.

##### 3.1.1.2 Ligation and confirmation of recombinants

The three purified fragments were ligated into the pCR<sup>®</sup> II vector and then transferred into *E.coli* INV $\alpha$ F'. Because the vector contained genes for ampicillin-resistance, only bacteria with the vector grew on agar plates containing ampicillin.

The transformed white colonies were picked for plasmid isolation and restriction analysis. The fraction of the transformants that were positive for the presence of the fragment of the A chain, the combined A and small segment of B chains, and the B chain were 8/8, 2/12 and 4/16, respectively. Two clones for each fragment were purified and sequenced using M13 primers.

### 3.2 Sequence analysis

The fragments corresponding to the *stenodactylin* gene ends presented a homologous overlapping region. The sequence information was analyzed using the algorithms available at <http://expasy.org>. The full-length caudex cDNA sequence analysis revealed that *stenodactylin* is encoded by a 1572-bp open reading frame (ORF) that encoded a polypeptide of 524 amino acids (Fig. 3.4). Only the first 11 amino acids were obtained only by Edman degradation.

The gene contains 753 bp that encode the A chain (251 amino acid residues with a calculated  $M_r$  of 28,420.38) and 771 bp that encode the B chain (267 amino acid residues with a calculated  $M_r$  of 28,468.32) separated by an internal linker sequence of 45 bp (between the amino acids 252 and 266). The probable C-terminal end of the A chain and the linker sequence were estimated based on the homology with the *volkensin* gene. *Stenodactylin* contains a total of 13 cysteine residues. The A chain includes Cys<sup>9</sup>, Cys<sup>157</sup> and the C-terminal Cys<sup>246</sup>, which is involved in the intermolecular disulfide bond. The B chain includes 12 cysteines (Cys<sup>270</sup>, Cys<sup>286</sup>, Cys<sup>305</sup>, Cys<sup>329</sup>, Cys<sup>344</sup>, Cys<sup>415</sup>, Cys<sup>428</sup>, Cys<sup>454</sup>, Cys<sup>472</sup>, Cys<sup>457</sup>, Cys<sup>461</sup>), eight of which (Cys<sup>286</sup>-Cys<sup>305</sup>, Cys<sup>329</sup>-Cys<sup>344</sup>, Cys<sup>415</sup>-Cys<sup>428</sup>, and Cys<sup>454</sup>-Cys<sup>472</sup>) form conserved intramolecular disulfide bridges; one cysteine (270) at the N-terminal binds to the A chain. The amino acid residues that are important for the enzymatic activity of RIPs were conserved within the sequence of the A chain of *stenodactylin* (Tyr<sup>74</sup>, Tyr<sup>113</sup>, Glu<sup>163</sup>, Arg<sup>166</sup>, and Trp<sup>200</sup>). In addition, based on the online program NetNGlyc1.0, two possible glycosylation sites were detected at position Asn<sup>359</sup>-Gly<sup>360</sup>-Thr<sup>361</sup> and Asn<sup>399</sup>-Val<sup>400</sup>-Thr<sup>401</sup>. The sugar presence could explain the difference between the molecular weight of the B chain based on the amino acid sequence (28 kDa) and the molecular weight observed by electrophoretic mobility (32 kDa). As reported for other type 2 RIPs, the A chain of *stenodactylin* contains only two lysines (of the 251 amino acids that comprise the A chain). Lysine residues are potential ubiquitination sites, and the small number of lysines is important to avoid ubiquitination and subsequent degradation (Deeks, *et al.*, 2002).





B)

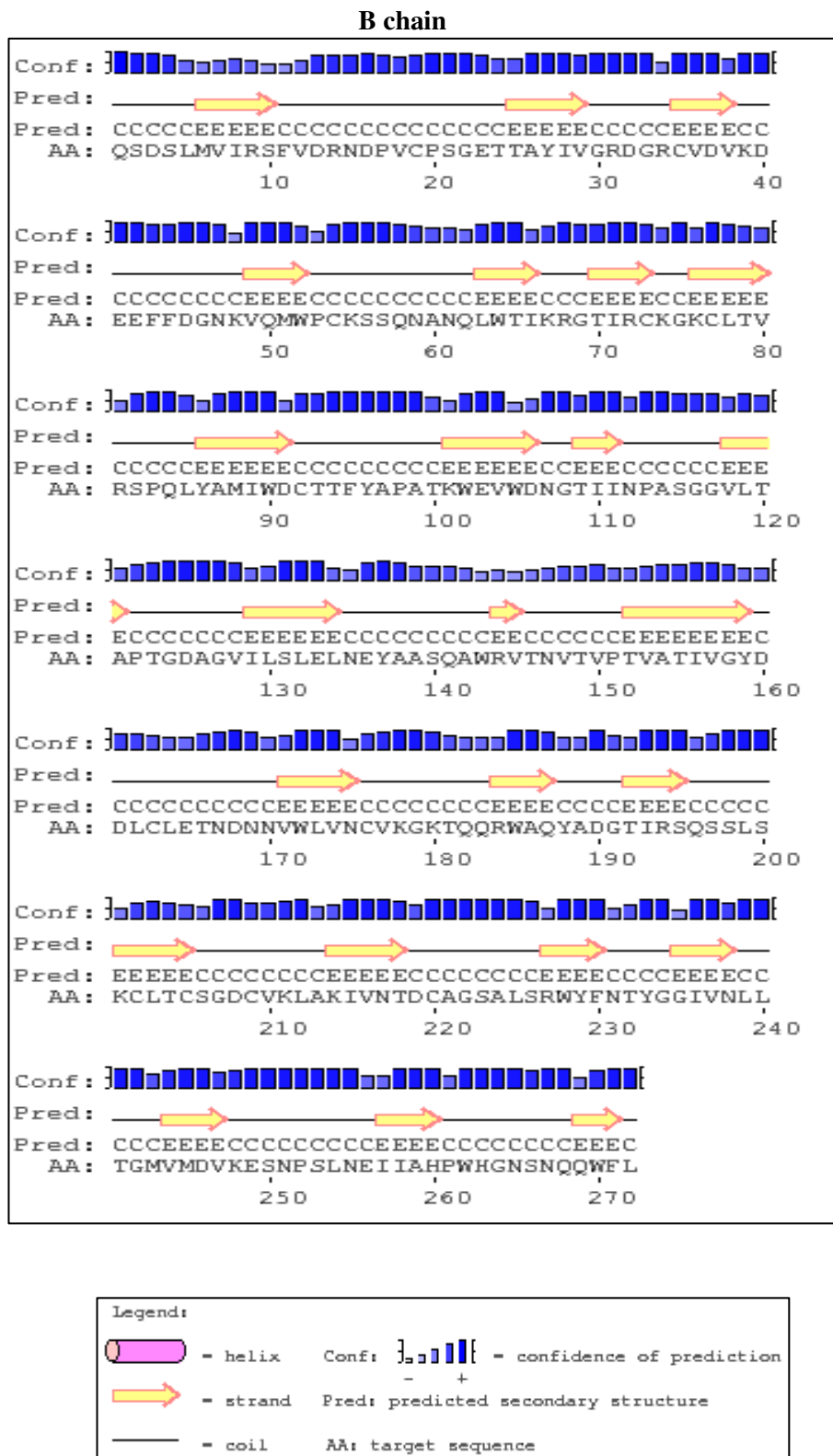


**Fig. 3.5.** Secondary structure analysis of *stenodactylin* A chain (A) and B chain (B). The secondary structure motifs was predicted using the PSIPRED Protein Structure Prediction Server. The predicted -helix and -sheet structure elements and randomly structured coil regions of the target sequences are displayed according to the symbols shown in the legend. The confidence levels of the prediction are reported in the figure.

The stenodactylin polypeptide sequence was aligned with volkensin using the Clustal W software. A comparison of the amino acid sequence of stenodactylin with volkensin showed 86.1% amino acid identity (Fig. 3.6). This homology was not surprising because these two RIPs were purified from plants belonging to the same genus (*Adenia*). The results show higher identity between the B chains (90.3%) than between the A chains (81.7%). In addition, the A chain of stenodactylin contains one more cysteine at position 9 compared with volkensin. The same additional cysteine was observed in lanceolin, but its role remains unclear (Stirpe, *et al.*, 2007). The B chains of both stenodactylin and volkensin contain 12 cysteine residues. The catalytic key residues that are involved in the enzymatic mechanism and the 12 amino acids that are involved in the active center of the A chain (amino acids from 158 to 174 in stenodactylin) are almost conserved, except for Ala<sup>165</sup> in stenodactylin, which is replaced with Ser<sup>164</sup> in volkensin.

VOLKENSIN	VFPKVPFDVPKATVESYTRFIRVLRDELAGGVSPQGIRRLRNPAEIQPSQGFILIQLTGY	60
STENODACTYLIN	VFPKVFID <sup>C</sup> TRATVERYTQFIMLLRNELAGDVSPQGIRRLRNPAEQPTQRFILIQLN <sup>G</sup> F	60
	***** * :**** * : * : * : * : * : * : * : * : * : * : * : * : * : * : * : *	
VOLKENSIN	VGSVTLIMDVRNAYLLGYLSHNVLYHFNDVSASSIASVFPDAQRRQLPFGGGYPSMRNYA	120
STENODACTYLIN	VSSVTLIMDVSNAYLLGYESRNFVYHFNDVSTSSIADVFPDVQRQLPFE <sup>G</sup> GGYPSMRHYA	120
	* . ***** ***** * : . * : ***** : ***** . ***** . * : ***** ***** . **	
VOLKENSIN	PERDQIDHGIVELAYAVDRLYYSQ-NNNQIALGLVICAGMVAEASRF <sup>R</sup> FRYIEGLVRQ <sup>S</sup> IVG	179
STENODACTYLIN	PERDQIDHGFIELAYAVDTLYYSSQGYEQIARSLVLCAGMVAE <sup>E</sup> AARFRYIEGLVRQ <sup>S</sup> IVG	180
	***** : ***** ***** . : * * . * : * : ***** : ***** *****	
VOLKENSIN	PGDYRTRFPDALMYSIVTQWQTLSE <sup>R</sup> IQGSFN <sup>G</sup> AFQPVQLGYASDPFYWDNVAQAITRLS	239
STENODACTYLIN	PGDYGTFRPDALMYSVVTAWQTLSE <sup>R</sup> IQGSFDGAFQPVQLGYASDPFYWDNVAQAITRLS	240
	*** ***** : * ***** ***** : ***** ***** ***** *****	
VOLKENSIN	LMLFVCSQPPRQSDSPLVIRSFVDRNDPVCPSGETTAFIVGRDGR <sup>C</sup> VDVKVEE <sup>F</sup> FDGNKV	299
STENODACTYLIN	LMLFCAKPPRQSDSLMVIRSFVDRNDPVCPSGETTAYIVGRDGR <sup>C</sup> VDVKDEE <sup>F</sup> FDGNKV	300
	*** . * : ***** : ***** ***** ***** : ***** ***** ***** *****	
VOLKENSIN	QMWPCKSSQNANQLWTLKRDGTIR <sup>C</sup> Q <sup>G</sup> KCLTVRSPQLYAMIWDCTTFYAPATKWEVWDNG	359
STENODACTYLIN	QMWPCKSSQNANQLWTIKRDGTIR <sup>C</sup> K <sup>G</sup> KCLTVRSPQLYAMIWDCTTFYAPATKWEVWDNG	360
	***** ***** : ***** : ***** ***** ***** ***** ***** ***** *****	
VOLKENSIN	TIINPASGRVLTAPTGEAGVTLNLQFNEYAASQAWRVNTVPTVTTIVGYDDL <sup>C</sup> LETNG	419
STENODACTYLIN	TIINPASGGVLTAPTGDAGVILSLELNEYAASQAWRVNTVPTVATIVGYDDL <sup>C</sup> LETND	420
	***** ***** : * * . * : ***** ***** ***** : ***** ***** *****	
VOLKENSIN	NGVWLANCVK <sup>G</sup> KAQQRWTLYADG <sup>T</sup> IRSQSTLSK <sup>C</sup> LACSGSCV <sup>K</sup> LAKIVNTDCAGSANSRW	479
STENODACTYLIN	NNVWLVNCV <sup>K</sup> GKTQQRWAQYADG <sup>T</sup> IRSQSSLSK <sup>C</sup> LTCSGDCV <sup>K</sup> LAKIVNTDCAGSALS <sup>R</sup> W	480
	* * * . ***** : ***** : ***** ***** : ***** : * * . ***** ***** ***** *	
VOLKENSIN	YFDNYGGIVNLRITGMVMDVKESNPSLNEIIAHPWHGNSNQWFL	523
STENODACTYLIN	YFN <sup>T</sup> YGGIVNLLTGMVMDVKESNPSLNEIIAHPWHGNSNQWFL	524
	* * : ***** ***** ***** ***** ***** ***** ***** ***** *****	

**Fig. 3.6.** Alignment between stenodactylin and volkensin (GenBank CAD61022). Identical residues (\*), conserved substitutions (:), and semiconserved substitutions (.) are reported. The A and B chains are presented in black; the sequence of the linker peptides is presented in gray. The amino acids that are involved in the catalytically active center of the A chain are underlined, while the ones involved in the enzymatic mechanism are high-lighted in gray. Cysteine residues are high-lighted in yellow. The dash indicates a gap introduced into the sequences to maximize alignments.

Figure 3.7 shows a 3D model of stenodactylin (A) and volkensin (B). The three-dimensional structures were predicted using the 3D structure template of cinnamomin (isoform III) using the online Swiss model program. Both structures are similar, and the B chain of stenodactylin is composed of two subdomains that contain short strands of  $\beta$ -sheets and turns and loops, as found in other type 2 RIPs.

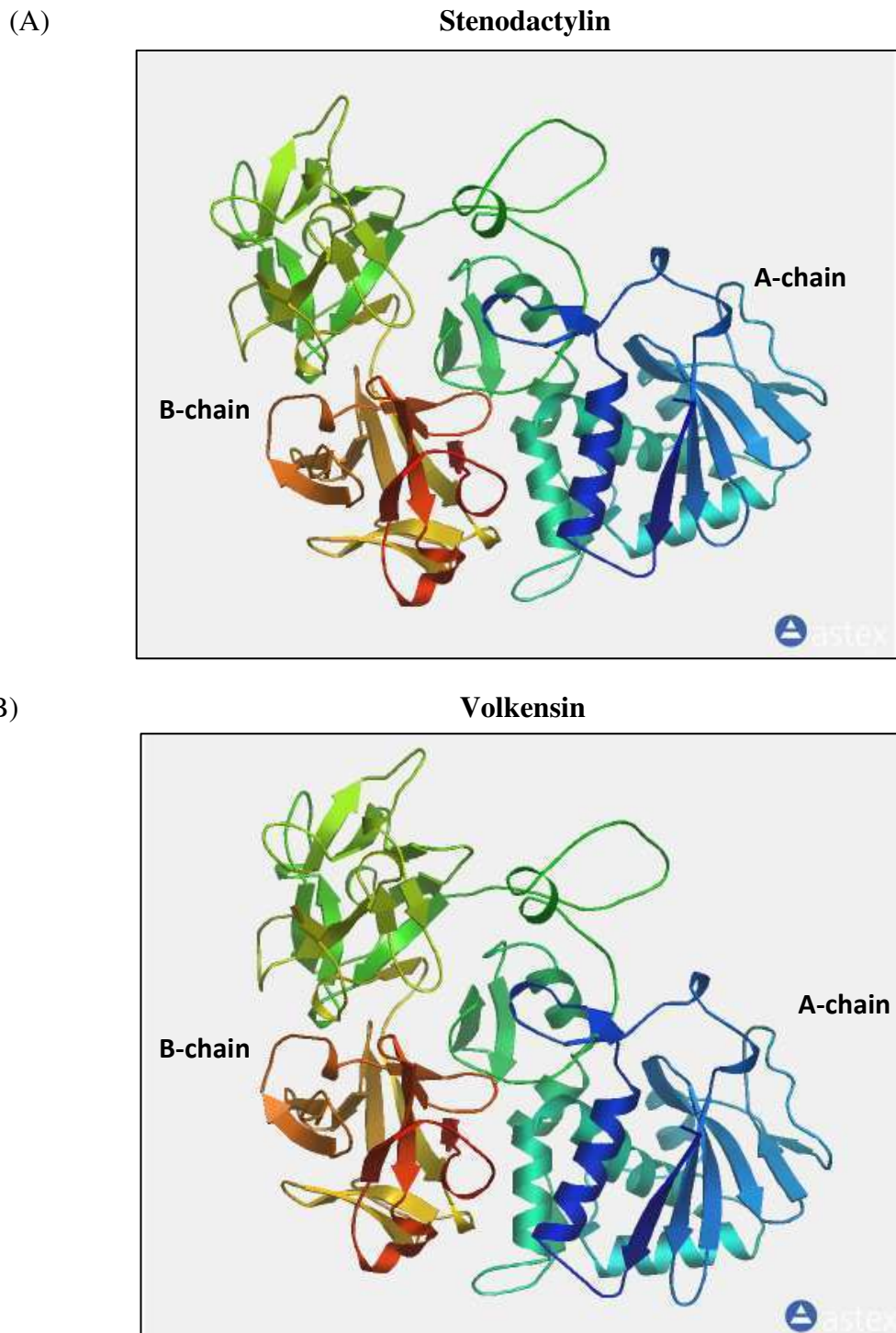


**Fig. 3.7.** 3D model of stenodactylin (A) and volkensin (B) predicted by Swiss-model protein structure prediction server. The A chain is presented in blue, and the B chain is presented in green and orange.

### 3.3 Sequence comparison between stenodactylin and other RIPs

#### 3.3.1 Sequence comparison with type 2 RIPs

The amino acid sequence of stenodactylin was aligned with the amino acid sequences of toxic type 2 RIPs (e.g., volkensin, ricin, abrin, viscumin, riproximin) and non-toxic (e.g., cinnamomin, ebulin I and nigrin b) that have been reported in GenBank (Fig. 3.8). The multiple alignment analysis showed that in all RIP B chains contain eight cysteine residues that are involved in four conserved intramolecular disulfide bridges and the B chain N-terminal cysteine that forms the intermolecular disulfide bridge between the A and B chains. Furthermore, the catalytic key residues (Tyr<sup>74</sup>, Tyr<sup>113</sup>, Glu<sup>163</sup>, Arg<sup>166</sup>, Trp<sup>200</sup> in stenodactylin) that are involved in the enzymatic mechanism are conserved in all A chains of the RIPs.

Crystallographic studies of ricin showed that the B chain folds into two similar globular domains. Each of these domains is composed of three subdomains (1 $\alpha$ , 1 $\beta$  and 1 $\gamma$  for domain 1 and 2 $\alpha$ , 2 $\beta$  and 2 $\gamma$  for domain 2). Only two of these subdomains, 1 $\alpha$  and 2 $\gamma$ , bind to galactoside. The amino acids involved in the 1 $\alpha$  binding site of ricin are Asp<sup>337</sup>, Gln<sup>350</sup>, Trp<sup>352</sup>, Asn<sup>361</sup> and Gln<sup>362</sup>, while the ones constituting the 2 $\gamma$  binding site are Asp<sup>549</sup>, Ile<sup>561</sup>, Tyr<sup>563</sup>, Asn<sup>570</sup>, Gln<sup>571</sup> (Rutenber and Robertus., 1991). Analysis of stenodactylin and all the other considered RIPs showed that all the amino acids that are involved in the first binding site of ricin are fully conserved, although Gln<sup>350</sup> is replaced by Ile<sup>302</sup> in abrin. In the 2 $\gamma$  binding site of stenodactylin, only one amino acid is changed compared with ricin; Tyr<sup>563</sup> is replaced with His<sup>512</sup> in stenodactylin. The same substitution was observed in volkensin (Chambery *et al.*, 2004), *R. communis* agglutinin (RCA) (Roberts *et al.*, 1985) and *P. multiflorum* (PMRIPm) (Van Damme *et al.*, 2000). Site-directed mutagenesis studies on the ricin B chain demonstrated that the replacement of Tyr<sup>248</sup> with His<sup>248</sup> reduced its binding activity (Lehar *et al.*, 1994).

The presence of a positive charge within the 2 $\gamma$  binding site prevents the hydrophobic interaction between the pyranose ring of galactose and the aromatic ring of Tyr; this substitution reduced functionality (Van Damme *et al.*, 2000). Cinnamomin contains two substitutions in the 2 $\gamma$  binding site compared with ricin (Trp<sup>537</sup> for Tyr<sup>537</sup> and His<sup>543</sup> for Gln<sup>535</sup>). While the first substitution was between two aromatic amino acids, the second one introduces a positive charge.

Because the lectin activity requires strictly conserved amino acids in both the 1 $\alpha$  and 2 $\gamma$  domains, their change may explain the reduced cytotoxicity of cinnamomin (Wang *et al.*, 2006). In addition, Tyr<sup>537</sup> in ricin is replaced with Phe<sup>522</sup> in ebulin I. This substitution

indicates to alters the binding of galactosides and may reduce the cytotoxicity of ebulin 1 (Pascal *et al.*, 2001).

All these data suggest that the 2 $\gamma$  binding site is important for the toxicity of RIPs, and any changes in this site could affect RIP binding. However, this hypothesis does not correlate with the results obtained with stenodactylin. In contrast, stenodactylin, which showed a change in this subdomain, is one of the most toxic RIPs.

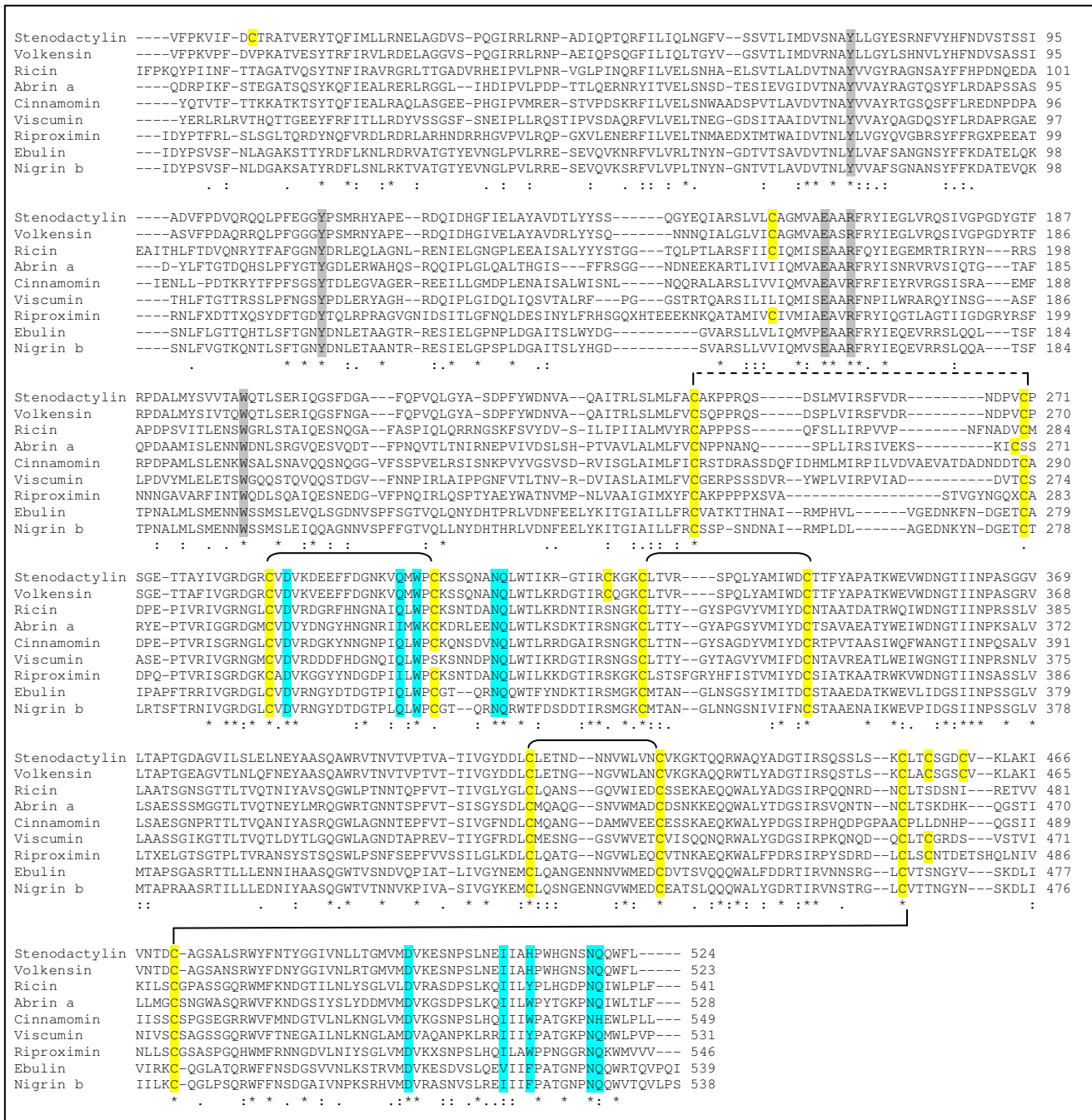


**Fig. 3.8.** Protein sequence alignment of stenodactylin with volkensin (acc.no CAD61022), ricin (acc.no P02879), abrin a (acc.no P11140), cinnamomum (acc.no AAF68978), viscumin (acc.no P81446), riproximin (acc.no CAJ38823), ebulin 1 (acc.no CAC33178), nigrin b (acc.no P33183). Identical residues (:), conserved substitutions (.) and semiconserved substitutions (.) are reported. Cysteine residues are high-lighted in yellow. The catalytic key residues are high-lighted in gray. The amino acid residues formed the carbohydrate-binding

site are high-lighted in light blue. The position of the intramolecular and intermolecular disulfide bonds are indicated by solid and dashed lines. Dashes denote gaps introduced to obtain maximal homology.

Table 3.1 demonstrates the identity between stenodactylin with toxic and non-toxic type 2 RIPs. The results show that there is a high percentage of identity between the A chains of stenodactylin and volkensin. All other identities were lower, ranging from 27.7 to 31.4%.

As reported in the literature (Barbieri *et al.*, 1993), a high degree of identity was detected when the B chain was compared with other B chains (90.3% with volkensin and ranging from 42.1 to 47.7% with the other RIPs). These data support the hypothesis that the B chain is a product of a gene duplication event (Villafranca and Robertus, 1981).

**Table 3.1.** Identity of eight type 2 RIP A-chains, B-chains and whole RIP with stenodactylin.

	<b>Identity (%)</b> (stenodactylin) A chain	<b>Identity (%)</b> (stenodactylin) B chain	<b>Identity (%)</b> (stenodactylin) whole
<b>Volkensin</b>	81.7	90.3	86.1
<b>Ricin</b>	31.4	47.7	40.3
<b>Viscumin</b>	31.0	46.0	38.1
<b>Abrin a</b>	31.2	44.6	37.9
<b>Riproximin</b>	27.7	43.3	35.8
<b>Cinnamomin</b>	33.0	42.1	37.3
<b>Ebulin</b>	28.7	44.2	36.5
<b>Nigrin b</b>	29.0	43.9	36.5

### 3.3.2 Sequence comparison with type 1 RIPs

The sequence of stenodactylin was aligned with saporin, dianthin and momordin using Clustal W software and the type 1 RIP amino acid sequences reported in GenBank (Fig. 3.9). The amino acid residues that are important in the active site of the RIPs (Tyr<sup>74</sup>, Tyr<sup>113</sup>, Glu<sup>163</sup>, Arg<sup>166</sup> and Trp<sup>200</sup> in stenodactylin) were conserved in all the four RIPs, while a strong difference was observed in the lysine residues. Stenodactylin only has two lysine residues, while saporin, dianthin and momordin contain 22, 19 and 10 lysine residues, respectively. Savino and co-workers reported that the saporin-6 sequence contains three lysines (220, 226, and 234) that are protected and are either conserved or replaced by positively charged or polar residues in other RIPs (Savino *et al.*, 2000). These authors deduced that the region containing these lysine residues is important for the interaction with the ribosome. Moreover, in saporin

and dianthin, the length of the loop containing the lysines is relatively short, thus providing better accessibility to the ribosome for both RIPs. In stenodactylin, these three lysines are replaced with Phe<sup>210</sup>, Ala<sup>223</sup> and Asn<sup>231</sup>. Because Phe and Ala are nonpolar amino acids, we hypothesize that the molecular recognition of the ribosome involves other residues in stenodactylin. The comparison of the stenodactylin A chain sequence with type 1 RIPs showed a very low level of identity (Table 3.2). As above reported, the stenodactylin A chain showed a low degree of identity when compared with other type 2 RIPs A chains, with the exception of volkensin. Moreover, the identity of the A chains was lower than the identity of the B chains. The homology between the type 1 RIPs and the stenodactylin A chain was even lower than the identity calculated between the stenodactylin A chain and other type 2 RIPs A chains.

Stenodactylin	VFPKVFDC	TRATVERY	TQFIMLLR	NELAGDVS	PQGIRRLR	NPADIQPT	QRFILIQ	LNGF	60	
Momordin	--DVSFRL	SGADPRS	YGMFIKDL	RNALPFRE	KVYNIP	LLL--PSV	SAGRYLL	MHLFNY	55	
Saporin	-VTSITL	DLVNPTA	GQYSSFD	KIRNNVK	DPNLKYG	GTDAVIG	PPSK-EK	FLRINFQ	58	
Dianthin	-ATAYTL	NLANP	SASQYSS	FLDQIRNN	VRDTS	LIYGGTD	VAVIGAP	STDKFLR	59	
	:	*	*	:	**	:	.	:::	:::	
Stenodactylin	VS-SVTL	IMDVSN	AYLLG	YESR----	NFVYHF	NDVSTSS	SIAD-V	FDPV--	QRQ-QL	110
Momordin	DGKTIT	VALDVT	NVYIM	GYLAD----	TTSYF	FNEPAAE	LASQYV	FRDA--	RRKITL	108
Saporin	RG-TVSL	GLKRD	NLYVV	AYLAM	DNTNVN	RAYFKSE	ITSAEL	TALFPE	ATTANQ	117
Dianthin	RG-TVSL	GLRREN	LYVV	AYLAM	DNANVN	RAYFKN	QITSAE	LALFPE	VVAVAN	118
	:::	:	*	*	:::	*	.	*	:::	*
Stenodactylin	GGYF	PSMRHYA	-----	PE-RD	QIDHGF	IELAY	AVDTLY	YSSQGYE	QIARSL	164
Momordin	GNYERL	QIAA----	GKPREK	IPIGL	PALDSA	ISTLLH	YDS--	TAAAG	ALLVLI	161
Saporin	EDYQS	IEKNAQ	ITQGDK	SRKELG	LIDLLT	FMEAVN	KKARV	VKNEAR	FLLIAT	177
Dianthin	EDYQA	IEKNAK	ITTGDS	RKELGL	GINLLI	TMIDG	VNKKV	RVVVK	DEARFL	178
	*	:	*	*	:::	*	:	:	*	:::
Stenodactylin	ARFRYI	EGLV	RQSI	VGP	GDYGT	FRPDAL	MYSV	VTAWQ	TLSE	220
Momordin	ARFKYI	EQIQ	ERA----	YRDE	VPSLA	TISLE	NSWS	GLSKQI	QLAQ	216
Saporin	ARFRYI	QNLV	TKNF----	PNKF	DSDNK	VIQFE	VSWRK	I	STAI	224
Dianthin	ARFRYI	QNLV	TKNF----	PNKF	DSENK	VIQF	VSWSK	I	STAI	225
	**:	**:	:	:	.	..	:	*	*	:
Stenodactylin	GYASD	PFYWD	NVAQA	ITRL	SLML	FACAK	PPR			251
Momordin	DNKGN	RVQIT	NVTSK	VVTS	NIQLL	LNTR	NI-			246
Saporin	-NKDY	DFGFG	KVRQ	VKDL	QMGLL	MYL	GPK-			253
Dianthin	-NKDY	DFGFG	KVRQ	AKDL	QMGLL	KYL	GRPKS			255
	:	*	.	:	:	*	:			

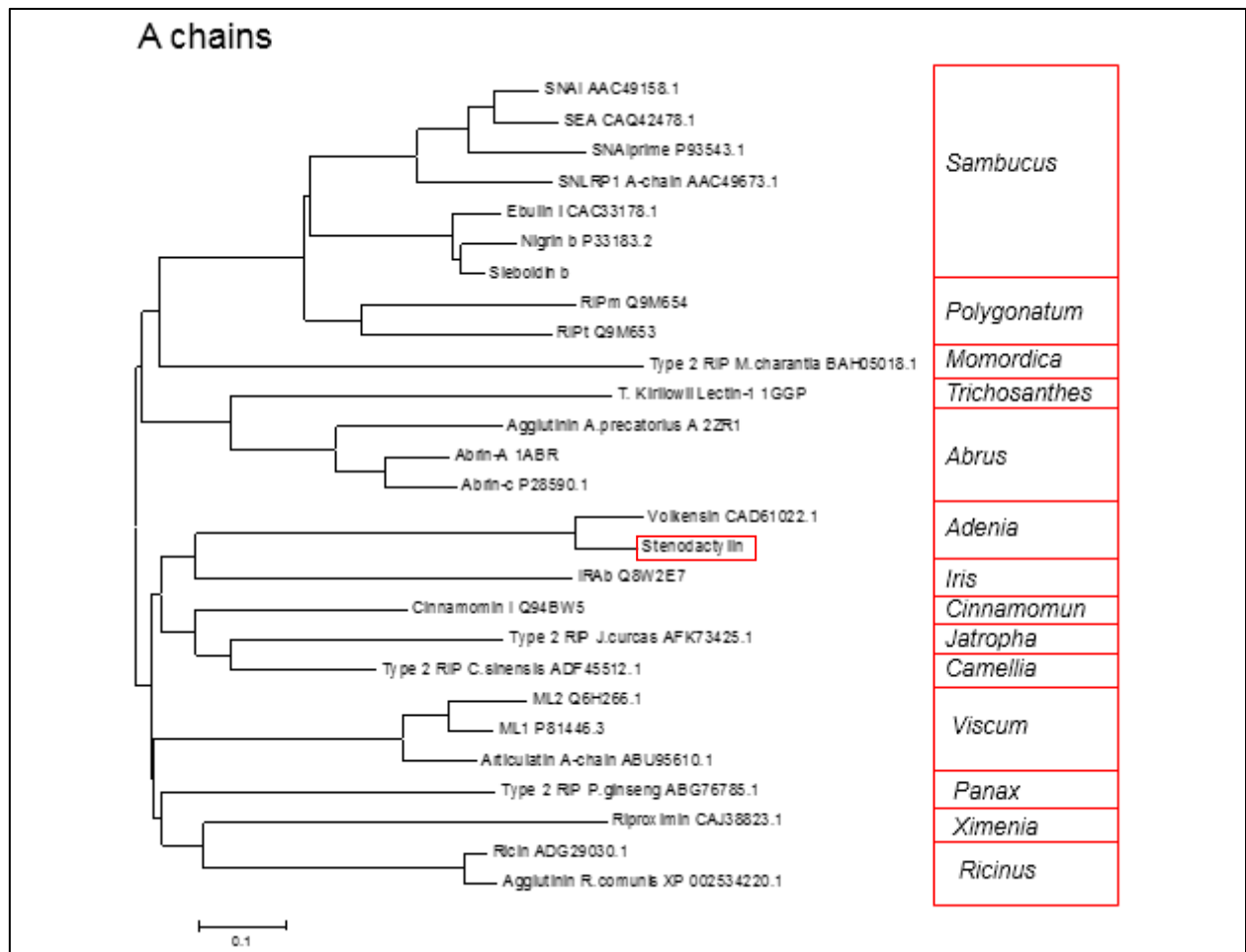
**Fig. 3.9.** Protein sequence alignment of stenodactylin with saporin (acc.no CAA41948,1), dianthin 30 (acc.no CAA41953,1), and momordin (P16094.2). Identical residues (\*), conserved substitutions (:), and semiconserved substitutions (.) are reported. The dashes indicate gaps introduced into the sequences to maximise alignments. The catalytic key residues are high-lighted in gray. The saporin-6 lysines (220, 226 and 234) and the corresponding residues of other RIPs are high-lighted in yellow.

**Table 3.2.** Identity of t type 1 RIP with A-chain stenodactylin.

	<b>Identity (%)</b> (Stenodactylin) A chain
<b>Saporin</b>	18.9
<b>Dianthin</b>	18.1
<b>Momordin</b>	24.0

### 3.3.3 Phylogenetic analysis

To understand the relationship between stenodactylin and other type 2 RIPs (both toxic and non-toxic), phylogenetic trees were constructed based on the amino acid sequences of the A and the B chains of 11 families (*Sambucaceae*, *Liliaceae*, *Cucurbitaceae*, *Fabaceae*, *Passifloraceae*, *Iridaceae*, *Laureceae*, *Euphorbiaceae*, *Viscaceae*, *Araliaceae* and *Olacaceae*). In the evolutionary tree, all the 27 RIPs segregated into two major clusters for each chain. Interestingly, the A chain of stenodactylin is in the same cluster as the A chains of ricin and viscum, while the B chain of stenodactylin is in the same side branch as the B chains of the non-toxic type 2 RIPs (Fig. 3.10).



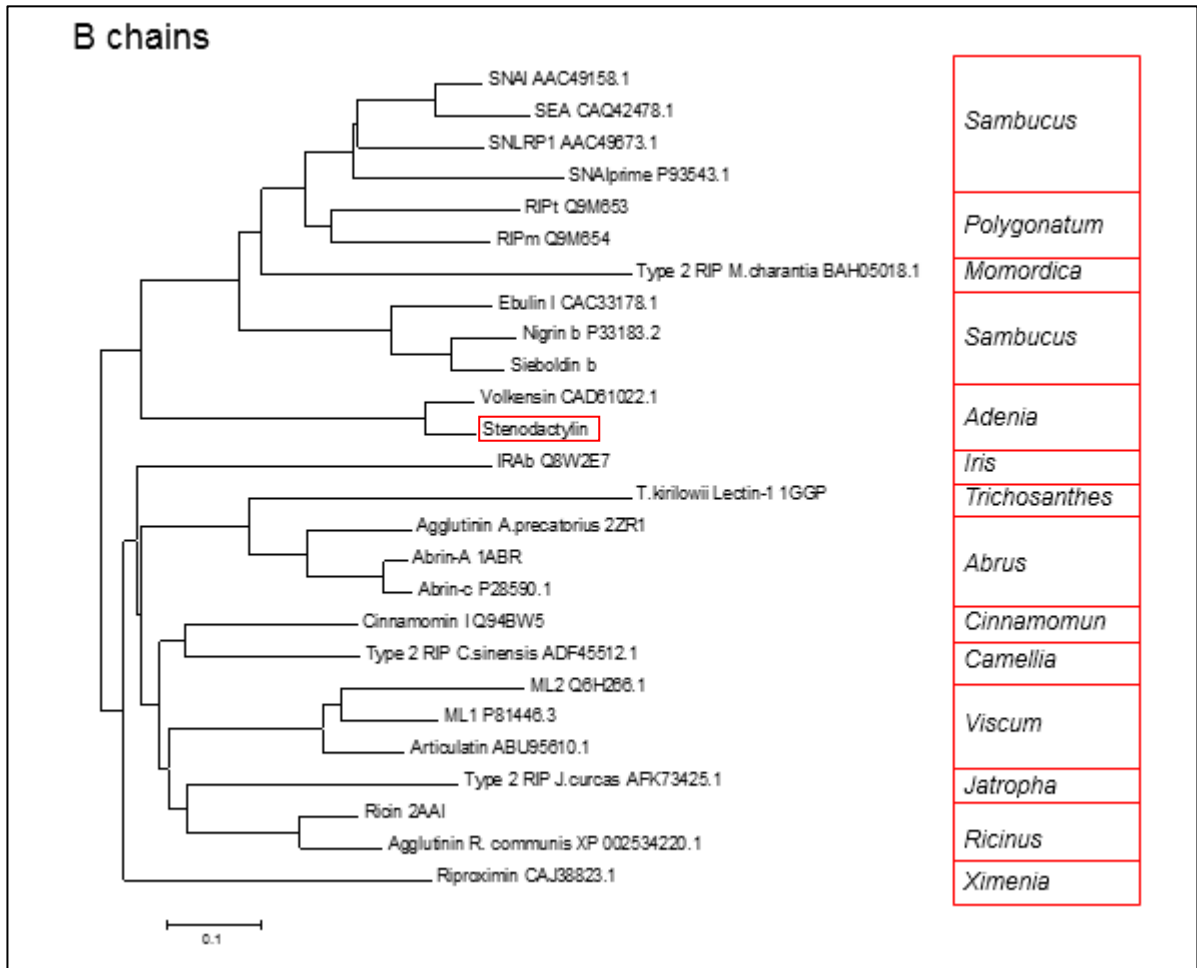


**Fig. 3.10.** Phylogenetic tree of type 2 RIPs (A chain and B chain) belonging to different plant species.

*Chapter 4*

Cell death mechanisms induced  
by  
Stenodactylin

## **BACKGROUND: RIPs and cell death mechanisms**

In the past, RIP cytotoxicity was commonly attributed to protein synthesis inhibition resulting from ribosomal damage, and this inhibition would be followed by necrosis. However, this view changed when Griffiths and co-workers observed morphological changes that are typical of apoptosis in cells in which ricin and abrin were concentrated after intramuscular injection into rats (Griffiths *et al.*, 1987). Abrin- and ricin-treated cells exhibit condensation and breakdown of nuclear DNA into discrete fragments in bovine pulmonary endothelial cells (Hughes *et al.*, 1996) and the human macrophage U937 cell line (Kochi and Collier, 1993). In addition to ricin and abrin, several other RIPs also induce apoptosis, such as viscumin (Bussing *et al.*, 1996), saporin (Bergamaschi *et al.*, 1996; Bolognesi *et al.*, 1996), pokeweed anti-viral protein from seeds (PAP-S), momordin (Bolognesi *et al.*, 1996) and trichosantin (Zhang *et al.*, 2001; Li *et al.*, 2007).

Many studies have been conducted to understand the relationship between RIP N-glycosidase activity and the triggering of the apoptotic events. However, many questions have remained opened.

Kochi and Collier proposed that apoptotic events become visible only when protein synthesis is inhibited by about 90% (Kochi and Collier, 1993). However, studies on rhabdomyosarcoma cells showed that  $\alpha$ -sarcin induces DNA fragmentation, activation of caspase 3 and cleavage of PARP even at concentration slightly below its IC<sub>50</sub> (the value representing the protein concentration required to kill 50% of the cells). In contrast, another inhibitor of protein synthesis, cycloheximide (CHX), did not induce any apoptotic effects even at concentrations that almost abolished protein synthesis (Olmo *et al.*, 2001). The same authors demonstrated by indirect studies that the pan caspase inhibitor Z-Vad-fmk did not reduced  $\alpha$ -sarcin-inhibited protein synthesis activity, and they proposed that caspase activation was a downstream effect of the inhibition of protein synthesis. Moreover, they observed that even in the presence of the caspase inhibitor, a percentage of cells continued to die, suggesting the presence of both caspase-dependent and -independent cell death mechanisms. The same hypothesis that apoptosis and enzymatic activity on ribosomes are correlated was confirmed by results obtained when studying recombinant mistletoe lectin A chain (rMLA) mutants. The mutant form of mistletoe lectin showed greatly reduced activity in a cell-free system and this reduced activity was associated with very low cytotoxicity (Langer *et al.*, 1999).

Contrary to previous reports, many other studies have demonstrated that either the RIP activity was not sufficient to induce apoptosis or that the programmed cell death occurred

independent of translation inhibition. Studies with PAP mutants (Hur *et al.*, 1995), ricin mutants (which are non toxic to yeast cells) (Li *et al.*, 2007) and Shiga toxin (Di *et al.*, 2011) demonstrated that the N-glycosidase activity of RIPs was not the only mechanism to induce apoptosis. In all these three cases, the ribosome-depurinating ability of the mutated RIPs was not altered, while their cytotoxic effects decreased. Particularly in ricin-treated cells, the hallmarks of apoptosis were not present.

Other groups hypothesized that the translation inhibition was independent from apoptosis. These hypotheses were based on the results from temporal/dose studies or from mutant RIPs. In ricin-treated cells, morphological changes and the loss of mitochondrial membrane potential were observed before translation was completely inhibited (Soler-Rodríguez *et al.*, 1993). Abrin mutant and saporin mutant that lacked translation inhibition activity induced apoptosis in HeLa and U937 cells, respectively (Shih *et al.*, 2001; Sikriwal *et al.*, 2008). Moreover, low doses of RIPs, such as ricin, volkensin and riproximin, promote both the translation of unfolded protein response (UPR) genes and the activation of the apoptotic pathway (cleavage of PARP and caspase 7 activation). Therefore, the authors suggested that the apoptotic pathway is not induced by protein synthesis arrest in response to low concentrations of type 2 RIPs (Horrix *et al.*, 2011). These reports confirm the idea that the inhibition of protein synthesis cannot be the only and the main cause of programmed cell death.

By summarizing all of the studies performed over the last 20 years, three different hypotheses have been formulated concerning the rRNA N-glycosidase activity of RIPs, which seems to be (i) indispensable, (ii) necessary but not sufficient or (iii) unimportant for the induction of apoptosis (Das *et al.*, 2012).

In addition to the inhibition of translation, alternative mechanisms were proposed to explain how RIPs induce apoptosis, such as (a) the binding of the B chain to cell receptors, (b) the activation of UPR genes, (c) DNase activity, (d) interactions with anti-oxidant proteins and (e) the production of reactive oxygen species (Fig. 4.1).

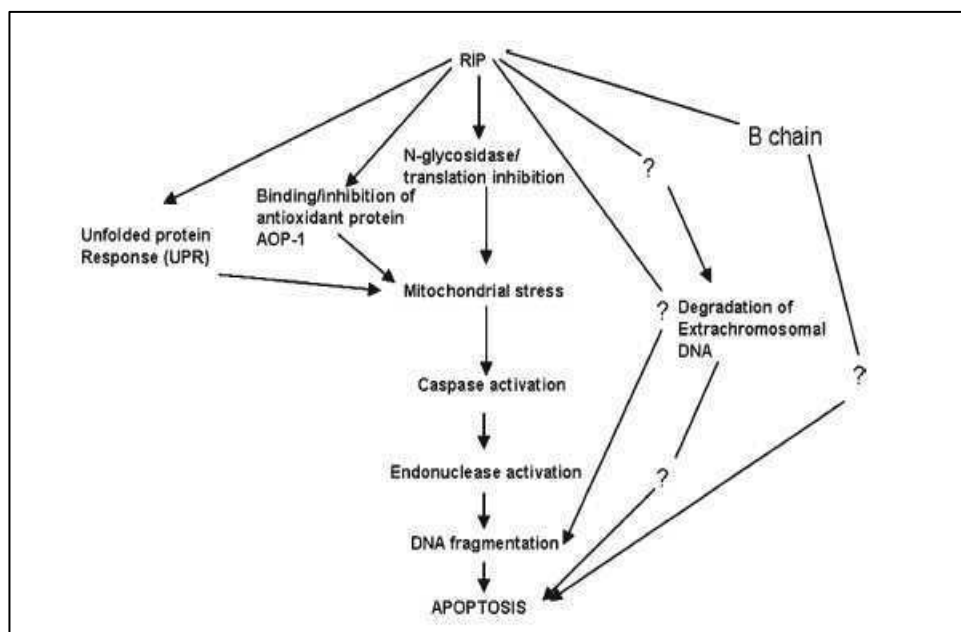


**Fig. 4.1.** Some possible mechanism of apoptosis induced by RIPs (Das *et al.*, 2012).

The B chain is a lectin that binds cell surface receptors that contain sugar. Low concentration (nM) of *Sambucus nigra* agglutinins II (SNAII), which consist only of the carbohydrate-binding B chains, induced caspase-dependent apoptosis in sensitive midgut CF-203 cells (Shahidi-Noghabi *et al.*, 2010). In U937 cells, the B chain of ricin also produced DNA fragmentation and the morphological changes that are typical of apoptosis at a concentration that did not inhibit protein synthesis (Hasewaga *et al.*, 2000).

qRT-PCR was used to identify genes connected with the UPR, such as activating transcription factor 3 (ATF3), growth arrest and DNA damage inducible gene 153 (GADD153) and IL24; these genes are upregulated in a dose dependent manner after RIP treatment. Their overexpression suggests that the cells experience endoplasmic reticulum stress, with subsequent apoptosis (Horrix *et al.*, 2011).

An alternative apoptotic pathway induced by RIPs could be caused to their DNase activity. Different RIPs (e.g., ricin, cinnamomin, gelonin, saporin-6 and dianthin 30) introduce specific cleavages into supercoiled DNA (Ling *et al.*, 1994; Roncuzzi and Gasperi-Campani, 1996; Brigotti *et al.*, 2002). Moreover, studies on saporin mutant, show that for the complete cytotoxic activity of saporin both the RNA glycosidase the genomic DNA fragmentation activity are required (Bagga *et al.*, 2003b). Using immunofluorescence assays and transmission electron microscopy, Bolognesi and co-workers found a nuclear localization of saporin-6. The presence of saporin in the nucleus suggests that one mechanism of cell death induced by the toxin could be DNA damage (Bolognesi *et al.*, 2012).

In a study by Nicolas and co-workers, the cytotoxic effect of gelonin on *Plasmodium falciparum* was reported to be caused by the loss of parasite mitochondrial DNA and not the inhibition of protein synthesis (Nicolas *et al.*, 1997).

Another mechanism proposed to induce apoptosis was found in abrin-treated cells. Using a yeast two-hybrid system and an abrin mutant that lacks the N-glycosidase activity, the authors discovered an interaction between the toxin and the antioxidant protein-1 (AOP-1). AOP-1 is located in the mitochondria and protects the mitochondria from the action of reactive oxygen species. The abrin mutant interacted directly with AOP-1 to inactivate its antioxidant activity, with a consequent release of cytochrome *c* and activation of caspases (Shih *et al.*, 2001).

RIPs can also induce apoptosis by increasing the reactive oxygen species (ROS) and intracellular calcium levels. Trichosanthin causes ROS production in human choriocarcinoma cells (JAR cells) after it interacts with a membrane-bound receptor. In addition, the ROS levels increased in parallel with calcium level, suggesting that ROS production in trichosanthin-treated cells might be a consequence of calcium signaling (Zhang *et al.*, 2001). In U937 cells, the toxin mistletoe lectin II (MLII) generated high levels of H<sub>2</sub>O<sub>2</sub>, which activated the intracellular stress signaling and JNK/SAPK pathways, concomitant with apoptosis. Treatment with an ROS scavenger was able to rescue the treated cells from apoptosis (Kim *et al.*, 2003). The same cell line treated with a low dose of abrin showed an increase in ROS levels, followed by DNA damage (Bhaskar *et al.*, 2008).

The mitochondria play a major role in different stress-induced cell death pathways, and damage to the mitochondria induces the loss of mitochondrial membrane potential, which is the point at which apoptosis is inevitable. Most of the mechanisms through which RIPs trigger the apoptotic pathway occur through the mitochondria. Bussing and co-workers found an increase in the expression of APO2.7 mitochondrial protein in ricin- and MLI-treated cells. APO2.7 is a 38 kDa mitochondrial membrane protein that is present in early apoptotic cells (Bussing *et al.*, 1999). The involvement of the mitochondria was confirmed by the increased levels of Bak protein in hepatoma (BEL7404) cells after intoxication with ricin. Bak constitutively resides in the mitochondria and, after oligomerization, forms the mitochondrial permeability transition pore, which releases apoptosis factors (Hu *et al.*, 2001). The mitochondrial pathway of apoptosis was also reported after intoxication with abrin. Treating Jurkat cells with abrin induced caspase 3 activation and subsequently DNA fragmentation, but its cytotoxic effect was independent by caspase 8 (Narayanan *et al.*, 2004). The involvement of the intrinsic pathway was also observed in saporin-6-treated cells. After intoxication with this toxin, a time-dependent increase in caspase 9 activity and the release of cytochrome *c* in

the cytosolic fraction was observed. Because caspase 8 was not activated, no change in the level of Bid (a proapoptotic Bcl-2 member) was observed, and the Fas receptor was not overexpressed; these results indicated that the extrinsic pathway was not involved (Sikriwal *et al.*, 2008).

Recently, Bolognesi and co-workers found that ricin and saporin were able to induce the intrinsic and extrinsic pathways (i.e., after 4 h treatment by both RIPs) in a human Hodgkin's lymphoma cell line (L540). However, ricin is more efficient than saporin at activating caspases 8 and 3/7, and its strong activation may be due to the lectin property of the B chain. Moreover, they proposed a mechanism of cell death that is at least partially independent of both caspase activation and necrosis because a pan caspase inhibitor (Z-Vad) and a non-apoptotic death inhibitor (necrostatin-1) could only partially rescue the cells from death (Polito *et al.*, 2009a).

The involvement of an alternative cell death pathway was also described by Bora and co-workers. They found that treating a human B cell line (U266B1) with abrin increased the ROS levels and lysosomal membrane permeabilization, resulting in the release of cathepsin; in contrast, they did not observe apoptosis and caspase activation. The authors speculated that caspase-independent programmed necrosis was involved (Bora *et al.*, 2010). Interestingly, the same toxin causes more than one death mechanism; Jurkat cells treated with abrin die via apoptosis in a caspase-dependent manner (Narayanan *et al.*, 2005).

Based on these data, RIPs clearly inhibit protein synthesis. Despite the different studies that have been conducted to elucidate the mechanism through which the RIPs trigger apoptosis, many unanswered questions remain. Figure 4.2 shows the different signaling cascades and pathways that are induced by RIPs.

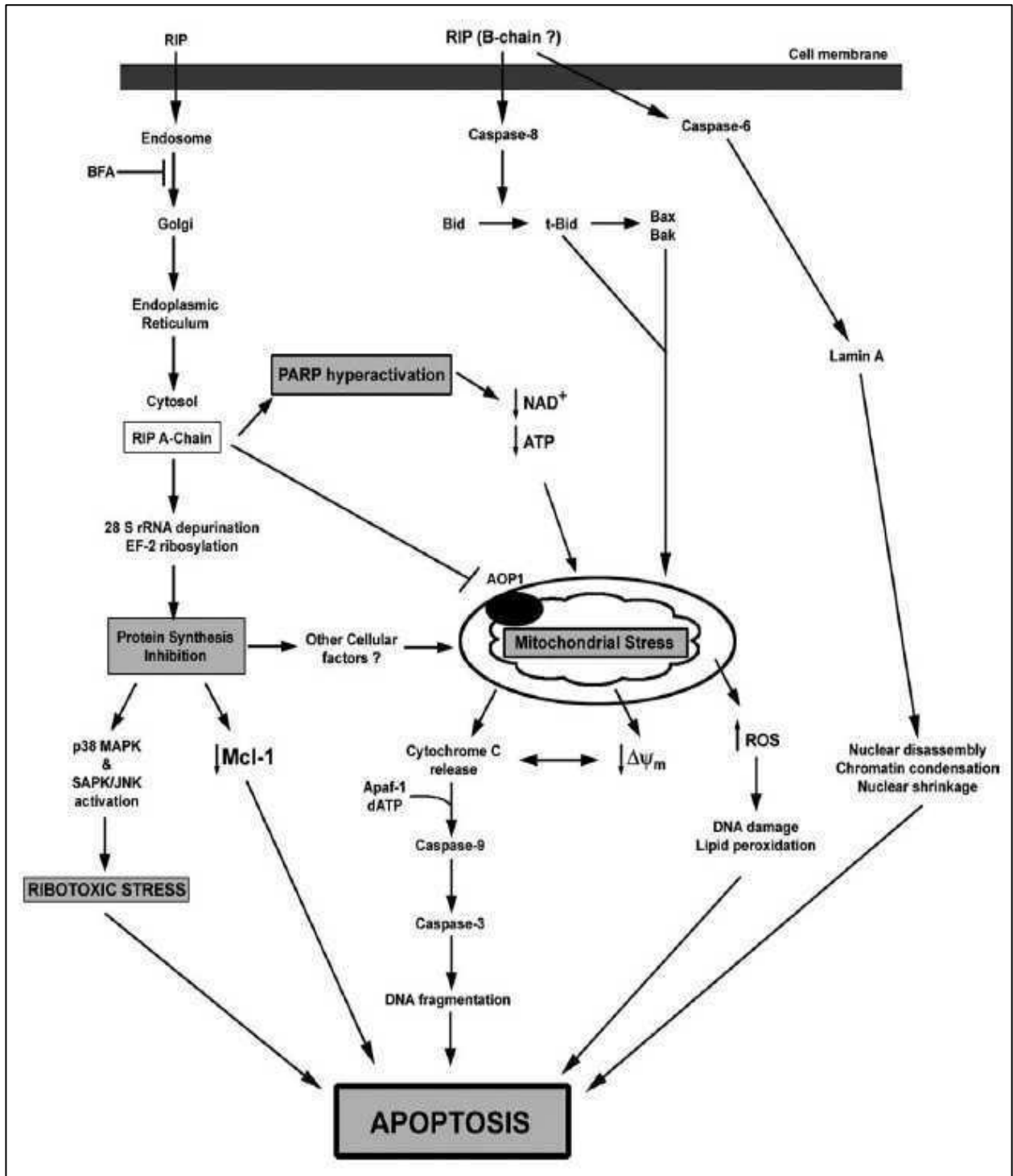


Fig. 4.2. Different types of mechanism of RIPs-induced apoptosis (Narayanan *et al.*, 2005).

## **AIM OF THE WORK**

RIPs have been used alone or as the toxic component of immunotoxins that are used to experimentally treat many diseases, such as cancer, hematological disorders, and graft-versus-host disease (GVHD), and as an antiviral agent in the therapy of AIDS; RIPs are used both for systemic and loco-regional treatments (Stirpe and Battelli, 2006). The best results have been reported in hematological neoplasias (Polito *et al.*, 2011). For the clinical application of RIPs and other cytotoxic substances, it is preferable that the drug kills the target cells by apoptosis rather than necrosis because the latter causes an inflammatory response in the surrounding tissues. Knowledge of the cell death pathway(s) induced by RIPs could be useful for designing specific immunotherapies and for clarifying the mechanism of damage.

Thus the purpose of the project was to understand the pathogenesis of cell intoxication caused by stenodactylin. Stenodactylin, which is extracted from the caudex of *A. stenodactyla*, was selected because little is known about its cytotoxic mechanisms even though it is the most toxic RIP.

The experiments were performed using the neuroblastoma cell line NB100, which our laboratory has previously shown to be very sensitive to RIPs. Its high sensitivity allows us to conduct experiments with very low doses of toxin that are comparable to the doses that could be reached *in vivo* in immunotherapy.

The cell death mechanisms induced by RIPs may depend on the cell type, the toxin, and the dose utilized.

To better understand the cell death pathway(s) induced by stenodactylin in NB100 cells, two different concentrations of the toxin were used. The first series of experiments was performed using stenodactylin at its IC<sub>100</sub> (value representing the protein concentration required to kill 100% of the cells). The cell death mechanisms were evaluated using inhibitors of apoptosis and necroptosis and ROS scavengers.

In the second series of experiments, stenodactylin cytotoxicity was evaluated by treating cells with a toxin concentration corresponding to the IC<sub>50</sub>. The role of rRNA N-glycosidase activity was evaluated by studying the temporal sequence of the key events that lead to cell damage induced by RIP. Caspase activation and protein and gene expression levels were quantified to understand the cell death mechanisms induced by stenodactylin.

## RESULTS AND DISCUSSION

### 4.1 Cell viability and protein synthesis inhibition assays

Cell viability and protein synthesis inhibition assays were performed on a neuroblastoma cell line (NB100). The experiments were performed using stenodactylin (extracted from the caudex of *A. stenodactyla*), the most toxic type 2 RIP yet discovered and purified. The results were compared with two other RIPs: ricin (type 2 RIP, purified from the seeds of *R. communis*), and saporin (type 1 RIP, extracted from the seeds of *S. officinalis*). These RIPs are among the best known and most studied RIPs, and part of the death pathways are already known.

The cytotoxicity of the RIPs was evaluated at 48 h using two indirect methods: the inhibition of protein synthesis and the viability. Protein synthesis was estimated from the inhibition of [<sup>3</sup>H] leucine incorporation, while the viability was assayed using a colorimetric method by MTS reduction. Both techniques were performed simultaneously to assess the correlation between translation impairment and cell viability (Fig. 4.3).

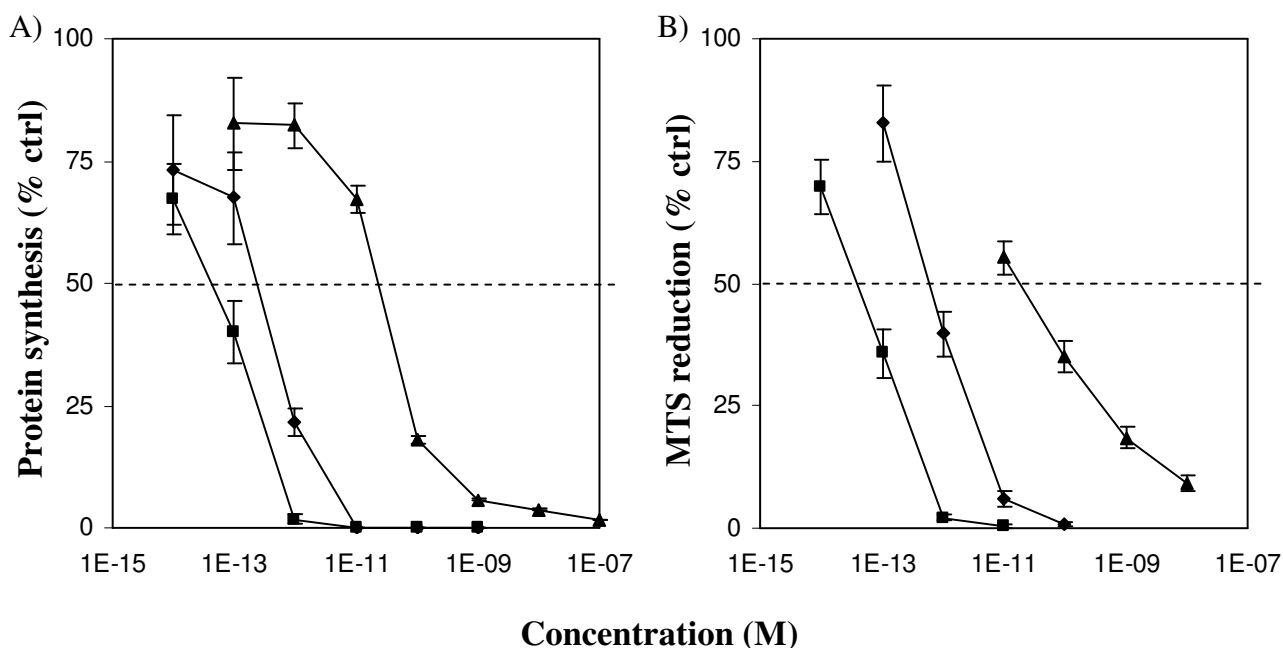


**Fig. 4.3.** Effect of stenodactylin (■), ricin (◆) and saporin (▲) on protein synthesis and viability in NB100 cells. Cells ( $2 \times 10^4$ ) were seeded in 24-wells plates in a total volume of 250  $\mu$ l of complete medium containing various concentrations of RIPs. After 48 h of incubation and an additional 4 h with [4,5 <sup>3</sup>H]-leucine, the incorporated radioactivity was determined (A). Viability of NB100 cells ( $3 \times 10^3$  in 100  $\mu$ l of complete medium) was evaluated after a 48 h exposure to the indicated concentrations of RIPs using a colorimetric assay based on MTS reduction (B). In both panels the results are the means of three independent experiments each performed in triplicate and are presented as the percentage of control values obtained from cultures grown in the absence of RIPs.

Dose-response curves, shown in Figure 4.3, demonstrated that protein synthesis and viability proceed in a parallel manner. As previously reported in other experimental models, the type 2 RIPs exhibited a higher cytotoxicity compared with the type 1 RIP saporin (Polito *et al.*, 2009a). Protein synthesis and viability were completely inhibited by stenodactylin and ricin at  $10^{-12}$  and  $10^{-11}$  M, respectively. The same cytotoxic effect was produced by saporin but at concentration of  $10^{-8}$  M.

The concentration of RIPs causing 50% and 100% inhibition of leucine incorporation ( $IC_{50}$ , half maximal inhibitory concentration, and  $IC_{100}$ , maximal inhibitory concentration) and of viability ( $EC_{50}$ , effective concentration 50% and  $EC_{100}$ , effective concentration 100%) was calculated by a linear regression analysis (Table 4.1).

**Table 4.1.**  $IC_{50}$ ,  $IC_{100}$ ,  $EC_{50}$ ,  $EC_{100}$  of stenodactylin, ricin, saporin on NB100 cell line.

	<b>STENODACTYLIN (M)</b>	<b>RICIN (M)</b>	<b>SAPORIN (M)</b>
<b>EC<sub>50</sub></b>	$2.5 \times 10^{-14}$	$6.5 \times 10^{-13}$	$1.8 \times 10^{-11}$
<b>IC<sub>50</sub></b>	$4.0 \times 10^{-14}$	$2.4 \times 10^{-13}$	$2.0 \times 10^{-11}$
<b>EC<sub>100</sub></b>	$1.24 \times 10^{-12}$	$1.1 \times 10^{-10}$	$>10^{-8}$
<b>IC<sub>100</sub></b>	$1.26 \times 10^{-12}$	$1.0 \times 10^{-11}$	$6.0 \times 10^{-7}$

Stenodactylin showed a stronger effect on both protein synthesis and viability, with  $IC_{50}$  and  $EC_{50}$  that were 1 and 3 log lower than ricin and saporin, respectively, and an  $IC_{100}$  that was 1 log lower than ricin and 5 log lower than saporin. The  $EC_{100}$  of stenodactylin was 2 log lower than ricin and more than 4 log lower than saporin.

The high toxicity of stenodactylin, at very low dose, could be advantageous for its use in loco-regional treatment. By injecting a low amount of the RIP, which would be immediately taken up by cells without spreading to the surrounding tissue, a strong toxic effect could be reached, with a reduction of unwanted side effects.

Moreover, these results demonstrated that the NB100 cell line was very sensitive to RIPs. In particular, saporin was more toxic in this cell line compared with the cell lines reported in the literature (Barbieri *et al.*, 1993).

## 4.2 Evaluation of the cytotoxic effect of stenodactylin at the IC<sub>100</sub> concentration

### 4.2.1 Assessment of apoptosis

Apoptosis was first evaluated in cells treated with stenodactylin at a concentration of  $10^{-12}$  M, and morphological changes were examined with phase contrast microscopy and fluorescence microscopy. A visual inspection of NB100 cells treated with stenodactylin ( $10^{-12}$  M) with phase contrast microscopy showed that the cells displayed the morphological features that are characteristic of apoptotic cells.

After overnight exposure to the RIP (24 h), cell shrinkage, cell membrane blebbing, and cytoplasmic condensation became clearly evident. Apoptosis was monitored by fluorescence microscopy using DAPI nuclear staining and Annexin V-EGFP/PI staining. DAPI staining showed that the intoxication with the RIP led to nuclear blebs and nuclear condensation (Fig. 4.4).

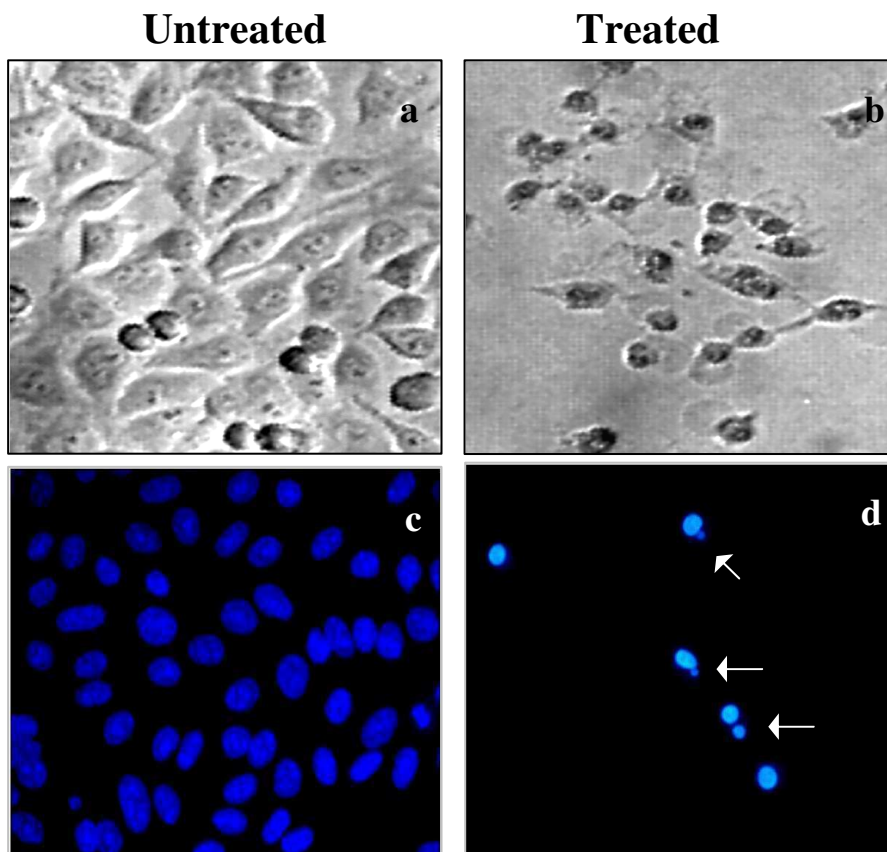


**Fig. 4.4.** NB100 cell morphology without (a,c) and with stenodactylin ( $10^{-12}$  M) for 24 h (b,d). NB100 cells morphology assessed by phase contrast microscopy (a,b, 60× magnification) and fluorescence microscopy (c,d, 60× magnification).

Annexin V is a sensitive probe for identifying apoptotic cells and binds with high affinity to phosphatidylserine (PS), which is flipped to the outer side of the plasma membrane during the early stage of apoptosis. Propidium iodide (PI) is a viability probe and is used to distinguish necrotic cells. Viable cells with intact membranes exclude PI, whereas the membranes of dead and damaged cells are permeable to PI. Cells that stain positive for Annexin V-EGFP and negative for PI are undergoing apoptosis (green). Cells that stain positive for both Annexin V-EGFP and PI are in the end stage of apoptosis (green and red). Cells that stain negative for Annexin V-EGFP and positive for PI are necrotic (red).

Double staining with Annexin V-EGFP/PI demonstrated that NB100 cells treated with stenodactylin ( $10^{-12}$  M) for 24 h showed the typical features of the late stage of apoptosis (Fig. 4.5).

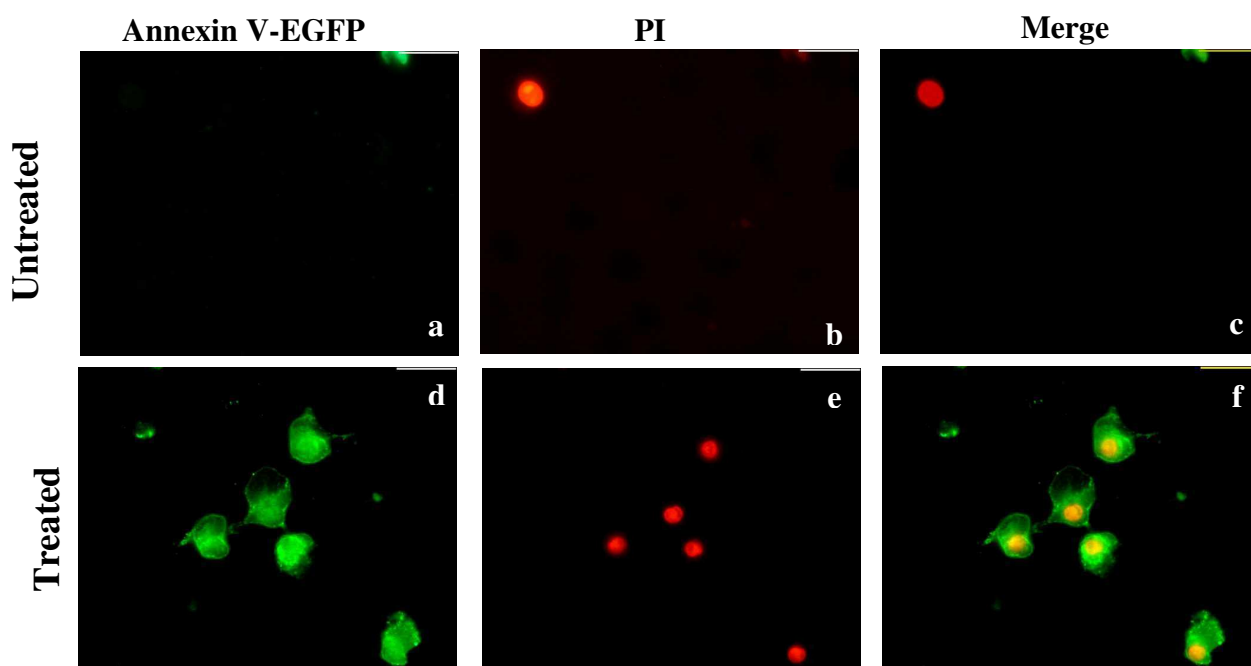


**Fig. 4.5.** Apoptosis as detected with Annexin V-EGFP/PI in control cells (a-c) and stenodactylin ( $10^{-12}$  M)-treated cells (d-f). After 24 h, NB100 cells were stained with Annexin V-EGFP/PI and observed under a fluorescent microscope. (a, d) The membranes of apoptotic cells stained green with Annexin V-EGFP; (b, e) the nuclei of late stage of apoptosis or necrotic cells stained red with PI; (c, f) a dual-channel fluorescence view was created by overlaying the images.

To quantify the percentage of apoptotic cells after stenodactylin treatment, NB100 cells were stained with Annexin V-EGFP/PI and then analyzed by flow cytometry (Fig. 4.6). PI-positive cells are in the upper left quadrant, while cells in late apoptosis and early apoptosis are in the upper and lower right quadrants, respectively. After 24 h intoxication, most of the cells were in the late apoptotic stage (86.2%). Interestingly, a small percentage of cells (9.4%) were

positive only for PI, thus suggesting that these cells undergo a mechanism of cell death that is different from apoptosis.

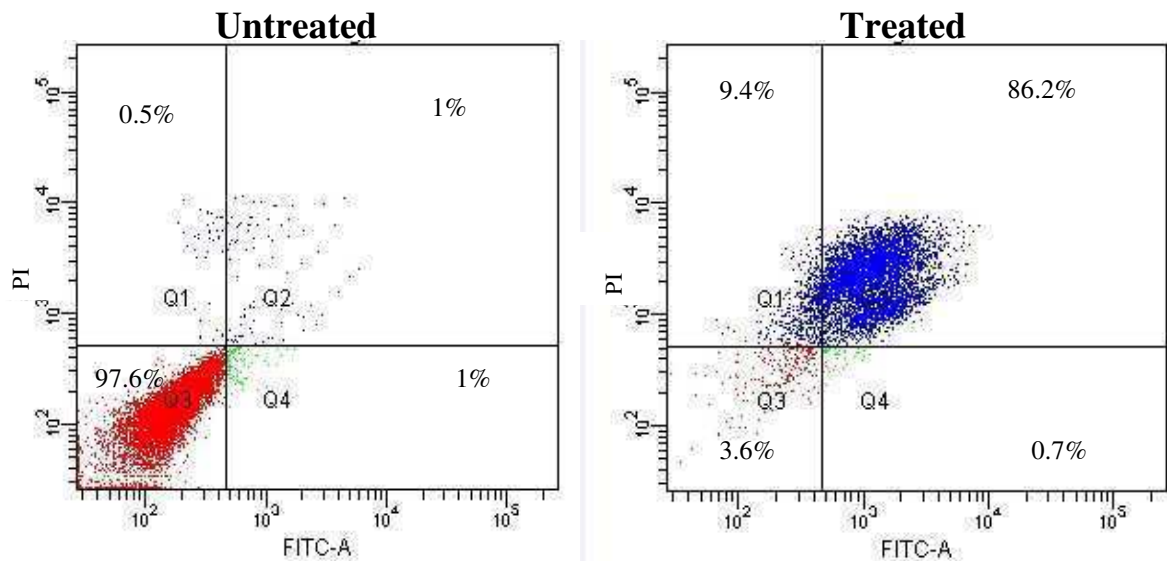


**Fig.4.6.** Evaluation of apoptosis by Annexin V-EGFP/PI staining, followed by flow cytometry analysis. Representative plots of annexin V-EGFP/PI staining of NB100 cells cultured in the absence of presence of stenodactylin ( $10^{-12}$  M).

A distinctive feature of programmed cell death is the disruption of active mitochondria. This mitochondrial disruption includes changes in the membrane potential and alterations to the mitochondria redox state.

Alterations of the mitochondrial membrane potential ( $\Delta\psi_m$ ) were detected by fluorescent microphotographs in cells that were exposed to stenodactylin ( $10^{-12}$  M) for 24 h and stained with JC-1 (Fig. 4.7).

JC-1 is a lipophilic, cationic dye that can selectively enter the mitochondria and reversibly change color from green to red as the membrane potential increases. In healthy cells with high mitochondrial  $\Delta\psi_m$ , JC-1 spontaneously forms J-aggregates with intense red fluorescence. In apoptotic or unhealthy cells with low  $\Delta\psi_m$ , JC-1 remains in the monomeric form, which fluoresces green.

In the mitochondria of control cells, JC-1 formed the characteristic J-aggregates, yielding red fluorescence, while in stenodactylin-treated cells, the JC-1 remained in the monomeric form producing a green fluorescence.

These results confirm that the cells undergo apoptotic programmed cell death after RIP intoxication and that the mitochondria are involved.

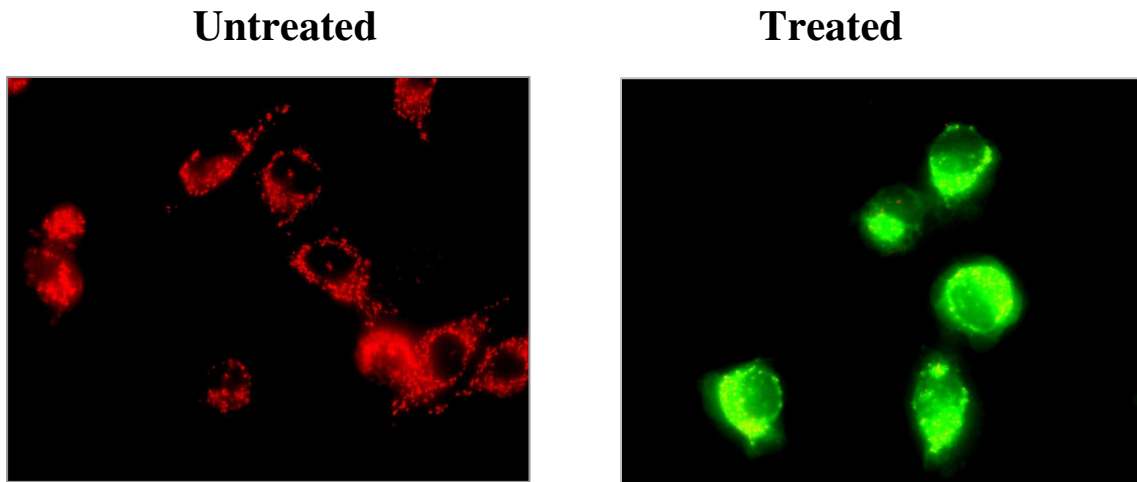


**Fig. 4.7.** Mitochondrial transmembrane potential in NB100 cells treated with stenodactylin ( $10^{-12}$  M) for 24 h, stained with JC-1 and then analyzed with fluorescence microscopy. The untreated cells showed a strong red fluorescence, indicating intact mitochondrial membrane potential. Treated cells presented a green fluorescence that represents the monomeric form of JC-1, indicating dissipation of the  $\Delta\psi_m$ .

To confirm that the cells undergo caspase-dependent apoptosis, caspase 3/7 activation was measured in cells exposed to  $10^{-12}$  M stenodactylin for 4, 6 and 8 h (Fig. 4.8). This experiment showed a time-dependent, strong activation of the effector caspases. After 8 h of intoxication, caspases 3/7 activation increased 770% compared with untreated cells. The high activation level of effector caspases confirmed that the cells underwent the caspase-dependent apoptosis, which was previously reported in cells treated with high doses of both type 1 and type 2 RIPs (Polito *et al.*, 2009a).

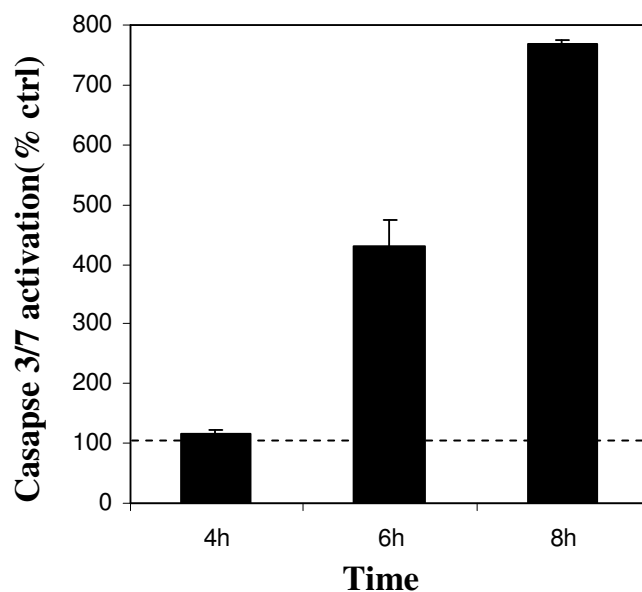


**Fig. 4.8.** Caspase 3/7 activation in NB100 cells ( $3 \times 10^3$  cells) treated with stenodactylin ( $10^{-12}$  M). Caspases activity was expressed as the percentage of control values obtained from cultures grown in the absence of RIPs.

To determine the role of caspase-dependent programmed cell death, the pan-caspase inhibitor Z-Vad-fmk was used. Z-Vad-fmk (Z-Vad) irreversibly binds to the catalytic site of caspase proteases and inhibits apoptosis.

NB100 cells were pretreated and maintained in 100  $\mu$ M Z-Vad, and cell viability was determined with the MTS assay at different time points (24, 48, 72, 96 h). As shown in Figure 4.9, Z-Vad significantly inhibited the cytotoxicity of stenodactylin after 24 h from intoxication, yielding a viability of  $98\% \pm 9\%$ . The protective effect of the pan caspase inhibitor decreased over time, leading to 10% of viability at 96 h.

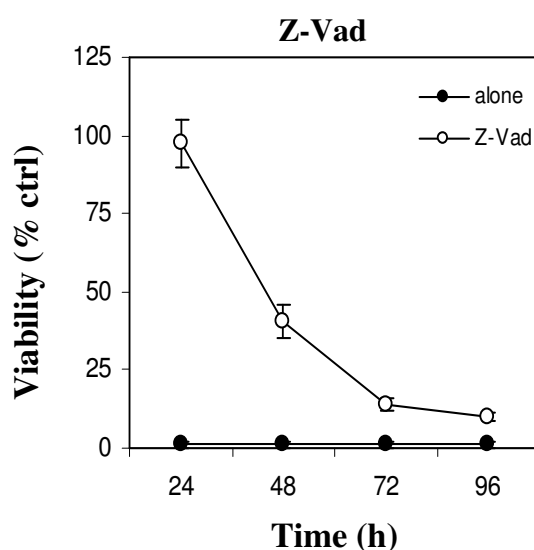


**Fig. 4.9.** Viability of NB100 cells ( $3 \times 10^3$  cells/well) treated with stenodactylin ( $10^{-12}$  M) alone (black circle) or in the presence (white circle) of 100  $\mu$ M Z-Vad. The pan-caspase inhibitor was added 3 h before the RIP was added, while stenodactylin was added for 2 h and the viability was observed after the indicating times. Viability was evaluated using a colorimetric assay based on MTS reduction. The results are the means of three independent experiments, with each performed in triplicate, and are presented as the percentage of control values obtained from cultures grown in the absence of RIPs.

A loss of protection from cell death by the pan-caspase inhibitor starting at 48 h was not caused by its inactivation. Z-Vad was added every 24 h, and as reported in Figure 4.10, the effector caspases were effectively maintained at the basal level.

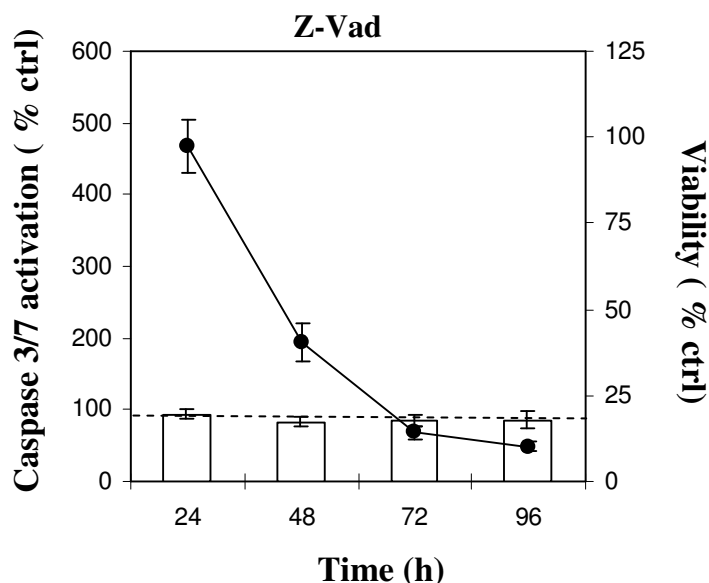


**Fig. 4.10.** Effect of stenodactylin ( $10^{-12}$  M) on the viability of (•) and caspase 3/7 activity in (columns) NB100 cells. Cells were pretreated for 3 h with Z-Vad (100  $\mu$ M) and then for 2 h with stenodactylin. The viability of NB100 cells ( $3 \times 10^3$  in 100  $\mu$ l of complete medium) was evaluated at the indicate times with a colorimetric assay based on MTS reduction. Caspase 3/7 activity is expressed as the percentage of control values obtained from cultures grown in the absence of RIPs. The results are the means of three independent experiments, each performed in triplicate.

Because Z-Vad rescued the cells from death 24 h from intoxication with stenodactylin, the apoptotic pathway appears to be the dominant and the fastest cell death mechanism induced by stenodactylin. However, the lack of total protection over time suggests that the toxin kills cells by activating more than one cell death mechanism, including probably necroptosis. Indeed, abrin can cause both caspase-dependent apoptosis and necroptosis (Bora *et al.*, 2010). When programmed cell death is inhibited by Z-Vad, cells can still die through necroptosis (Declercq *et al.*, 2009). Necroptosis is a programmed necrosis that occurs due to tumor necrosis factor receptor (TNF-R) activation. Like apoptosis, this programmed necrosis is highly regulated, and the cells show the same morphological features as cells undergoing necrosis (Gunther *et al.*, 2012).

Because necroptotic cells are similar to necrotic cells in terms of membrane changes, the Annexin V-EGFP/PI staining was used to confirm the necroptosis pathway in cells pretreated with Z-Vad (Fig. 4.11).

Double staining was evaluated at 48 h, when the cell viability was < 50%. At this time, only red fluorescence was observed, indicating that cell membranes were damaged, and the typical PI staining of non-apoptotic dead cells was observed.

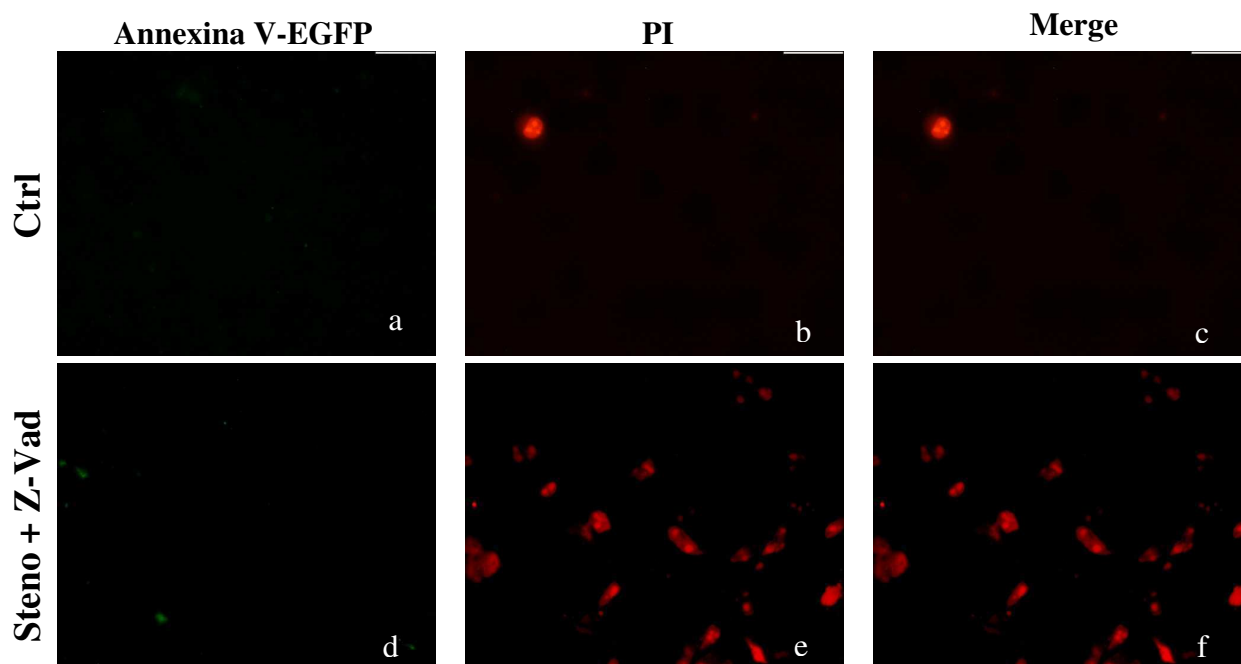


**Fig. 4.11.** Apoptosis as detected with Annexin V-EGFP/PI in control cells (a-c) and cells pretreated for 3 h with Z-Vad (100 $\mu$ M) and then intoxicated for 2 h with stenodactylin, steno, ( $10^{-12}$  M) (d-f). After 48 h, NB100 cells were stained with Annexin V-EGFP/PI and observed under a fluorescent microscope. (a, d) The membranes of apoptotic cells stained green with Annexin V-EGFP; (b, e) the nuclei of late stage of apoptosis or necrotic cells stained red with PI; (c, f) a dual-channel fluorescence view was creating by overlaying the images

#### 4.2.2 Necroptosis

To verify necroptosis in these cells, a set of experiments were performed using the inhibitor of necroptosis necrostatin-1.

Necroptosis depends on the serine-threonine kinase receptor-interacting proteins 1 (R.I.P1) and 3 (R.I.P3), and other proteins. R.I.P1 plays a critical role in necroptosis, and its kinase activity is inhibited by necrostatin-1 (Christofferson and Yuan, 2010).

In the presence of necrostatin, cell death was strongly but not completely inhibited at 24 h, with a viability of  $70\% \pm 7\%$ . Subsequently at 48, 72 and 96 h, cell viability decreased to approximately 25%. Therefore, necrostatin seems to be slightly more effective than Z-Vad in protecting cells from long-term intoxication (Fig. 4.12).

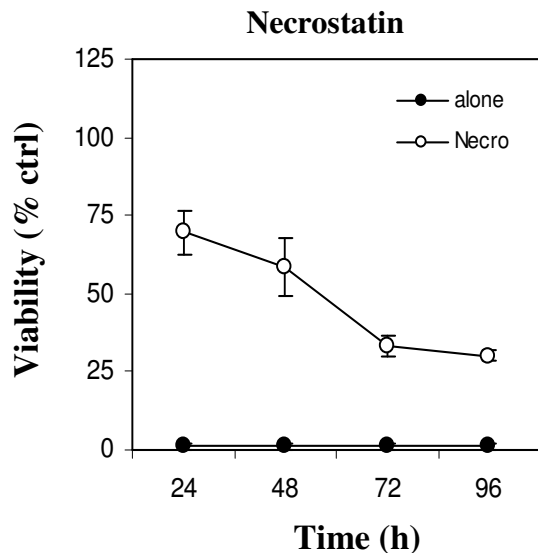


**Fig. 4.12.** Viability of NB100 cells ( $3 \times 10^3$  cells/well) treated with stenodactylin ( $10^{-12}$  M) alone (black circle) or in the presence (white circle) of necrostatin (Necro)  $100 \mu\text{M}$ . Necrostatin-1 was added 3 h before the RIP was added, while stenodactylin was added for 2 h and the viability was observed after the indicating times. Viability was evaluated using a colorimetric assay based on MTS reduction. The results are the means of three independent experiments, with each performed in triplicate, and are presented as the percentage of control values obtained from cultures grown in the absence of RIP.

The 30% of cells that died by 24 h most likely died via the apoptotic pathway, as demonstrated by the activation of caspases 3/7. Moreover, the further decrease in cell viability was accomplished by a corresponding strong increase in the effector caspases' activity (Fig. 4.13).

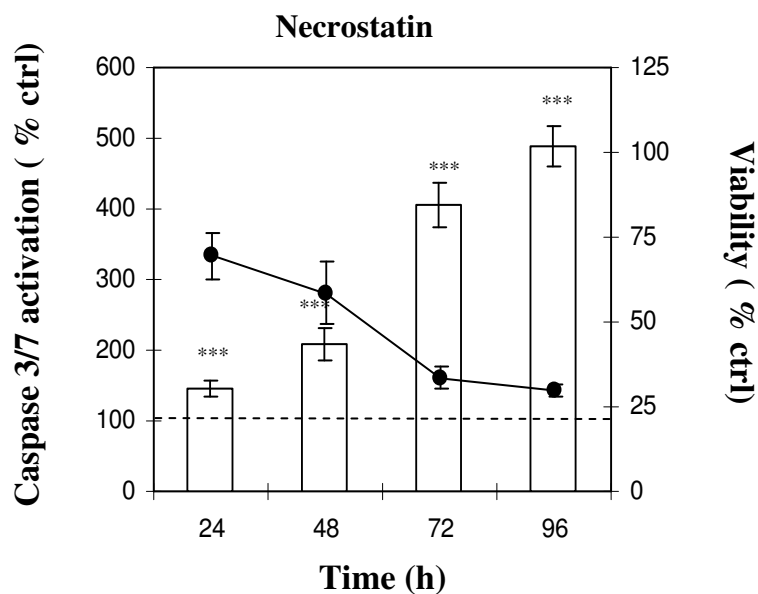


**Fig. 4.13.** Effect of stenodactylin ( $10^{-12}$  M) on the viability of (•) and caspase 3/7 activity in (columns) NB100 cells. Cells were pretreated for 3 h with necrostatin ( $100 \mu\text{M}$ ) and then for 2h with stenodactylin. The viability of NB100 cells ( $3 \times 10^3$  in  $100 \mu\text{l}$  of complete medium) was evaluated at the indicate times with a colorimetric assay based on MTS reduction. Caspase 3/7 activity is expressed as the percentage of control values obtained from cultures grown in the absence of RIP. The results are the means of three independent experiments, each performed in triplicate. Asterisks indicate level of significance in ANOVA, Dunnett's test \*\*\* $p=0.001$ .

The hypothesis that the cells underwent apoptosis in the presence of necrostatin and stenodactylin was confirmed by Annexin V-EGFP/PI staining. The apoptotic pathway was evaluated after 48 h from intoxication, when the viability was < 60%. In these conditions, cells showed characteristics of both early and late apoptosis (Fig. 4.14).

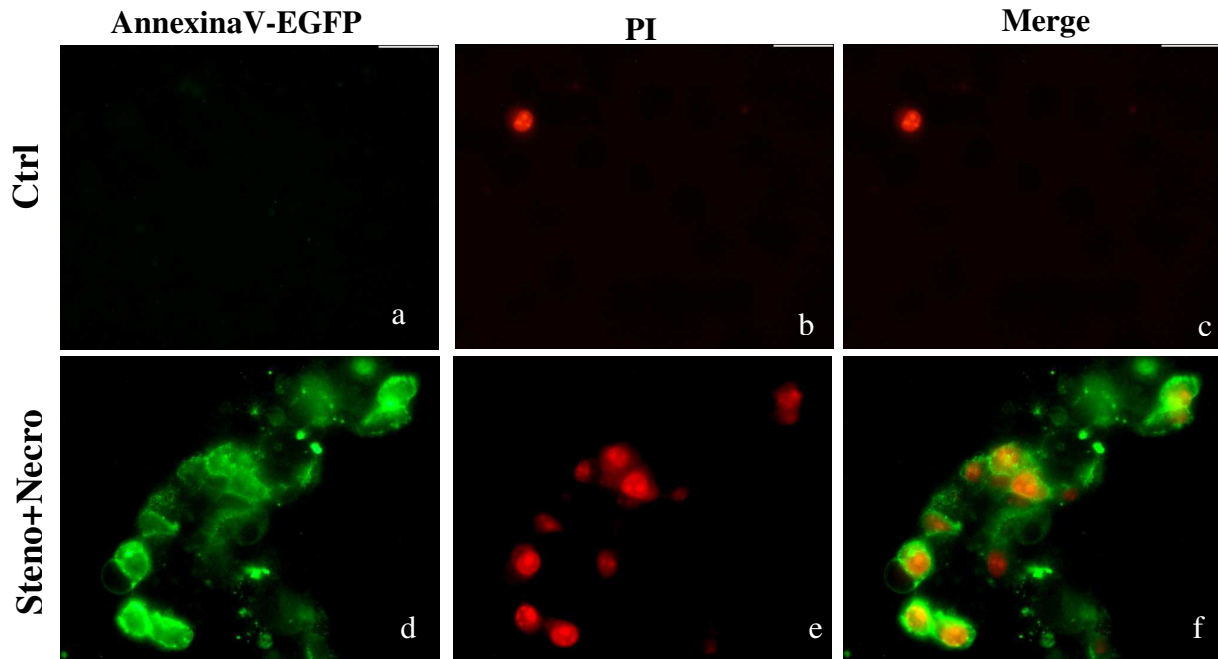


**Fig. 4.14.** Apoptosis as detected with Annexin V-EGFP/PI in control cells (a-c) and cells pretreated for 3 h with 100 $\mu$ M necrostatin (Necro) and then intoxicated for 2 h with stenodactylin, steno, ( $10^{-12}$  M) (d-f). After 48 h, NB100 cells were stained with Annexin V-EGFP/PI and observed under a fluorescent microscope. (a, d) The membranes of apoptotic cells stained green with Annexin V-EGFP; (b, e) the nuclei of late stage of apoptosis or necrotic cells stained red with PI; (c, f) a dual-channel fluorescence view was created by overlaying the images

Apoptotic morphological changes were examined by phase contrast microscopy. After 24 h, cells treated with one of the inhibitors and stenodactylin resemble the untreated cells, while morphological alterations were present after longer times of exposition. However, different morphological features were visible in cells treated with the RIP alone or in combination with Z-Vad or necrostatin-1, suggesting that more than one cell death mechanism was triggered (Fig. 4.15).

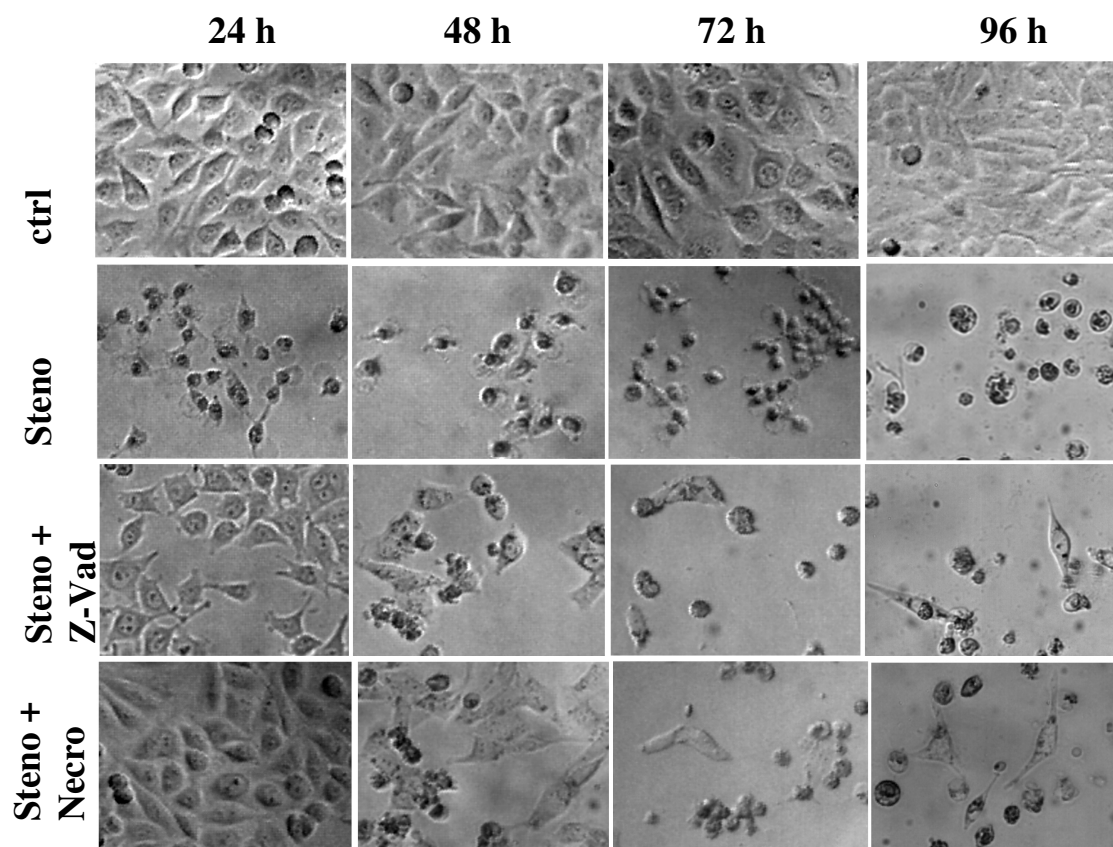


**Fig. 4.15.** NB100 cell morphology of cells treated with stenodactylin ( $10^{-12}$  M) in the absence (steno) or in the presence of the pan-caspase inhibitor Z-Vad, and in the presence of necrostatin 1 (necro). The cells ( $2 \times 10^4$  / 500  $\mu$ l of complete RPMI) were incubated with RIP for the indicated time and analyzed by phase contrast microscopy.

#### 4.2.3 Evaluation of oxidative stress

Previous studies showed a significant increase in reactive oxygen species (ROS) production in cells treated with RIP (e.g., HeLa cells intoxicated with ricin). The authors suggest that the apoptotic cells death induced by the RIP is correlated with the production of reactive oxygen species (Rao *et al.*, 2005).

The involvement of ROS after treatment with stenodactylin was measured both directly and indirectly through fluorescence microscopy and a viability evaluation after the addition of scavenger molecules, respectively.

The presence of total ROS and superoxide was evaluated in NB100 cells that were treated with stenodactylin ( $10^{-12}$  M) for 8 h.

The total ROS detection dye reacts directly with a wide range of reactive species, such as hydrogen peroxide, peroxynitrite and hydroxyl radicals, to yield a green fluorescent product. The superoxide detection dye is a cell-permeable probe that reacts specifically with superoxide, generating a red fluorescent product.

The results showed both red and green coloration, indicating an involvement of superoxide and others reactive species (Fig. 4.16).

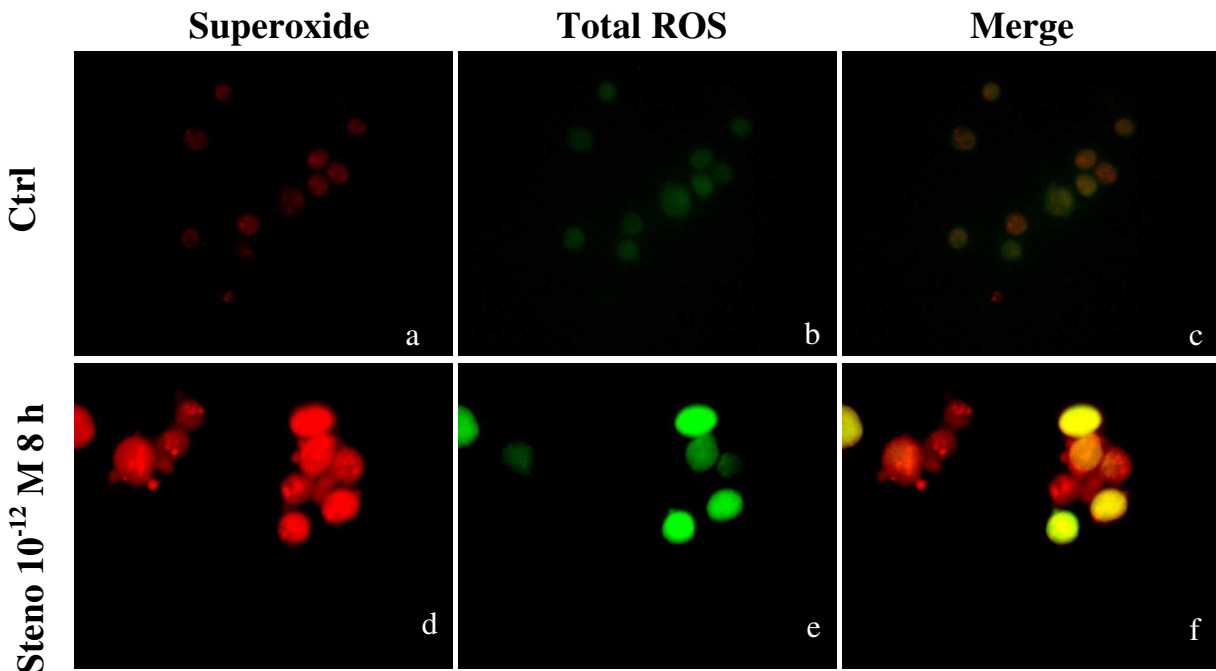


**Fig. 4.16.** Fluorescent microscopy profiling of reactive oxygen species formation in NB100 cells that were untreated (a-c) and treated with stenodactylin ( $10^{-12}$  M) for 8 h (d-f) and loaded with ROS/superoxide detection reagents. Superoxide production was detected in the orange channel (a, d), while general oxidative stress levels were monitored in the green channel (b, e), dual-channel fluorescence view was created by overlaying the images (c, f).

To quantify the superoxide production after 8 h of intoxication with stenodactylin, NB100 cells were stained with superoxide detection kit and analyzed by flow cytometry.

Figure 4.17 shows that in treated sample, 11.3% of cells were positive to superoxide, while in the untreated sample the superoxide positive cells were 1.2%.

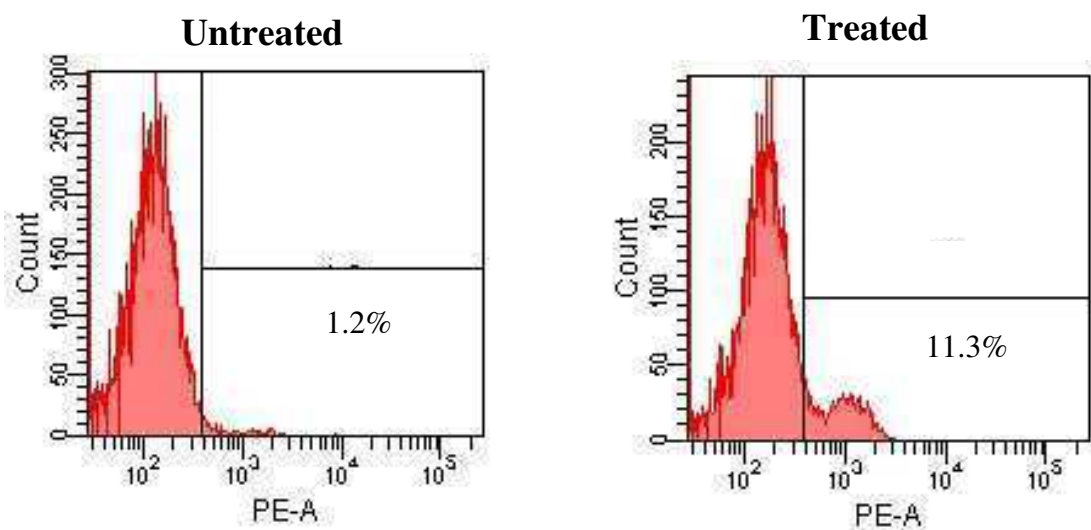


**Fig. 4.17.** NB100 cells that were untreated or treated with stenodactylin ( $10^{-12}$  M) for 8 h and then stained with a superoxide detection kit and analyzed with flow cytometry.

Together, the results obtained by fluorescence and flow cytometry suggest that after a short intoxication with stenodactylin, superoxide production is increased. This result supports the idea that the RIP lead to a very early formation of radical species and that ROS are important mediators of stenodactylin-induced cell death.

To demonstrate the possible formation of ROS induced by stenodactylin, two ROS scavengers, superoxide dismutase (SOD) and catalase (Cat), were used in time-course experiments. SODs catalyze the dismutation of superoxide into oxygen and hydrogen peroxide. There are three different types of SODs, depending on the metal cofactor: cytoplasmatic  $\text{Cu}^{2+}/\text{Zn}^{2+}$  SOD, mitochondrial  $\text{Mn}^{2+}$  SOD and extracellular  $\text{Cu}^{2+}/\text{Zn}^{2+}$  SOD. Catalase catalyzes the decomposition of hydrogen peroxide to water and oxygen, and it is localized in the peroxisomes.

The viability of NB100 cells pretreated with the scavenger and then with stenodactylin ( $10^{-12}$  M) was measured at different timepoints (24, 48, 72, 96 h). The  $\text{H}_2\text{O}_2$  scavenger catalase completely suppressed stenodactylin-induced cell death after 24 h from intoxication. This protective effect decreased over time, reaching a plateau of 50% 48 h from intoxication (Fig. 4.18A). No protective effect was detected when the cells were pretreated with SOD at any evaluated time point. The same results were obtained using either the extracellular  $\text{Cu}^{2+}/\text{Zn}^{2+}$  SOD or the mitochondrial  $\text{Mn}^{2+}$  SOD (Fig. 4.18B).

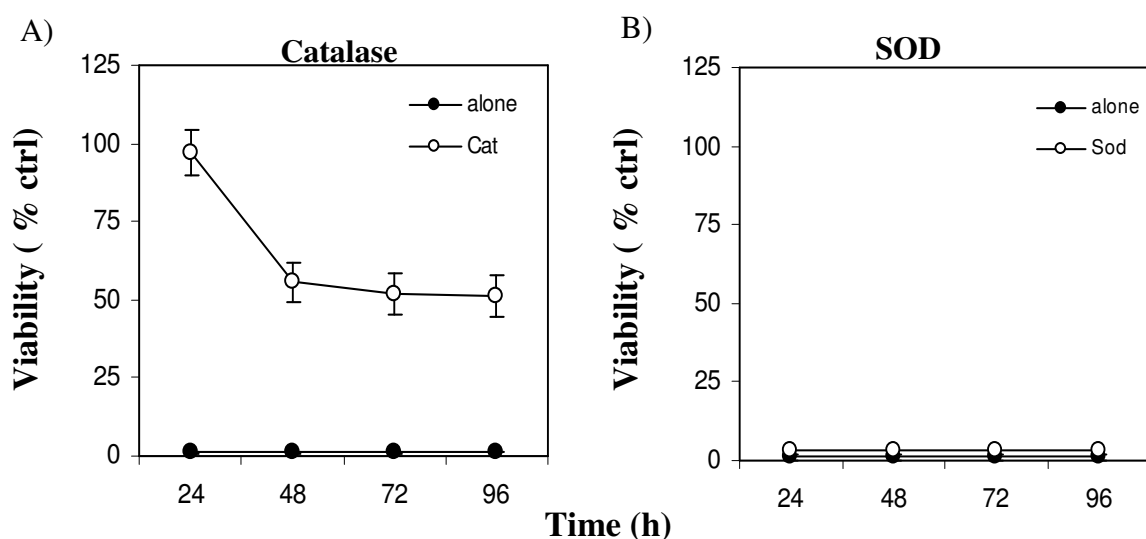


**Fig. 4.18.** Viability of NB100 cells ( $3 \times 10^3$  cells/well) treated with stenodactylin ( $10^{-12}$  M) alone (black circle) or in the presence (white circle) of Cat (10 U/ml) (A) or  $\text{Cu}^{2+}/\text{Zn}^{2+}$ SOD (100 U/ml) (B). The scavengers were added 3 h before RIP was added, while stenodactylin was added for 2 h and the viability was observed after the indicating times. Viability was evaluated using a colorimetric assay based on MTS reduction. The results are the means of three independent experiments, with each performed in triplicate, and are presented as the percentage of control values obtained from cultures grown in the absence of RIP.

These data suggest that stenodactylin induces the production of superoxide but that it is immediately converted to hydrogen peroxide, and this conversion appear to be very important because SOD was unable to protect cell from RIP-induced cell death. Moreover, hydrogen peroxide appears to have an important role in the pathogenic mechanism because catalase was able to rescue the cells from death.

There are controversial reports about the role of caspase 3 in the formation of ROS. In some cases, caspase 3 assumes an important function in the production of reactive species, while other reports indicate that the hydrogen peroxide activates caspase-dependent cell death (Zhang *et al.*, 2001).

Earlier, stenodactylin was shown to activate caspases 3/7 to >750% of control activity levels after 8 h from intoxication (Fig. 4.8). To determine whether the effector caspases are activated by ROS or by other mechanisms that activate the effector caspases, the activation of effector caspases was evaluated in the presence of catalase. Time-course experiments showed that caspases started to be significantly activated starting after 48 h of incubation with the RIP, reaching 300% of control activity after 96 h from treatment, at which point cell viability was 50% in the presence of catalase (Fig. 4.19). The maximal caspases 3/7 activation obtained in the presence of catalase was lower than stenodactylin-treated cells, indicating that a percentage of caspase 3/7 is activated through other RIP-induced mechanisms (e.g., DNA damage, intrinsic-extrinsic pathway).

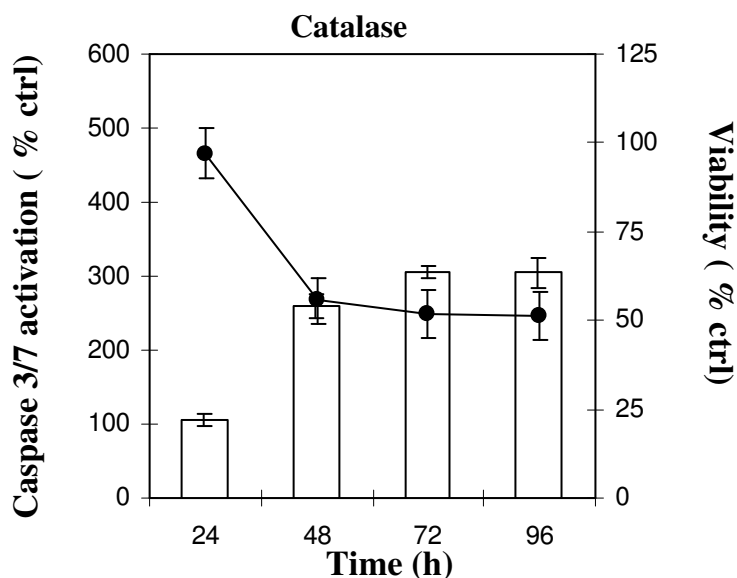


**Fig. 4.19.** Effect of stenodactylin ( $10^{-12}$  M) on the viability of (•) and caspase 3/7 activity in (columns) NB100 cells. Cells were pretreated for 3 h with Cat (10 U/ml) and then for 2 h with stenodactylin. The viability of NB100 cells ( $3 \times 10^3$  in 100  $\mu$ l of complete medium) was evaluated at the indicate times with a colorimetric assay based on MTS reduction. Caspase 3/7 activity is expressed as the percentage of control values obtained from cultures grown in the absence of RIPs. The results are means of three independent experiments each performed in triplicate.

To confirm that stenodactylin activates the caspases 3/7 via ROS and other mechanisms, cell viability was evaluated after co-treatment with Z-Vad and catalase. The time-course experiments showed that the combination of Z-Vad and the scavenger led to complete protection from cell death over time, even at 96 h (Fig. 4.20). Previous studies demonstrated 100% viability in the presence of Z-Vad (Fig. 4.9) or catalase (Fig. 4.18) but only for 24 h. These data suggest that the caspase-dependent pathway and the ROS production are the main cell death mechanisms involved.

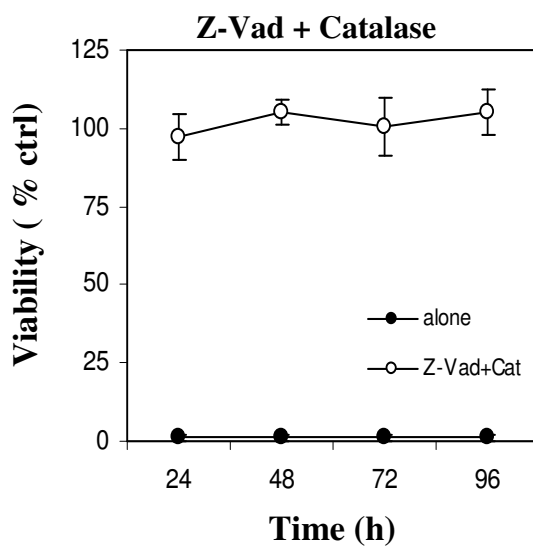


**Fig. 4.20.** Viability of NB100 cells ( $3 \times 10^3$  cells/well) treated with stenodactylin ( $10^{-12}$  M) alone (black circle) or in the presence (white circle) of Z-Vad ( $100 \mu\text{M}$ ) + Cat ( $10 \text{ U/ml}$ ). The scavengers were added 3 h before the RIP was added, while stenodactylin was added for 2 h and the viability was observed after the indicating times. Viability was evaluated using a colorimetric assay based on MTS reduction. The results are the means of three independent experiments, which each performed in triplicate, and are presented as the percentage of control values obtained from cultures grown in the absence of RIP.

To confirm that the apoptotic pathway is activated in cells pretreated with catalase, the cells were stained with Annexin V EGFP/PI. The cells showed the typical pattern of early and late apoptotic cells (Fig. 4.21).

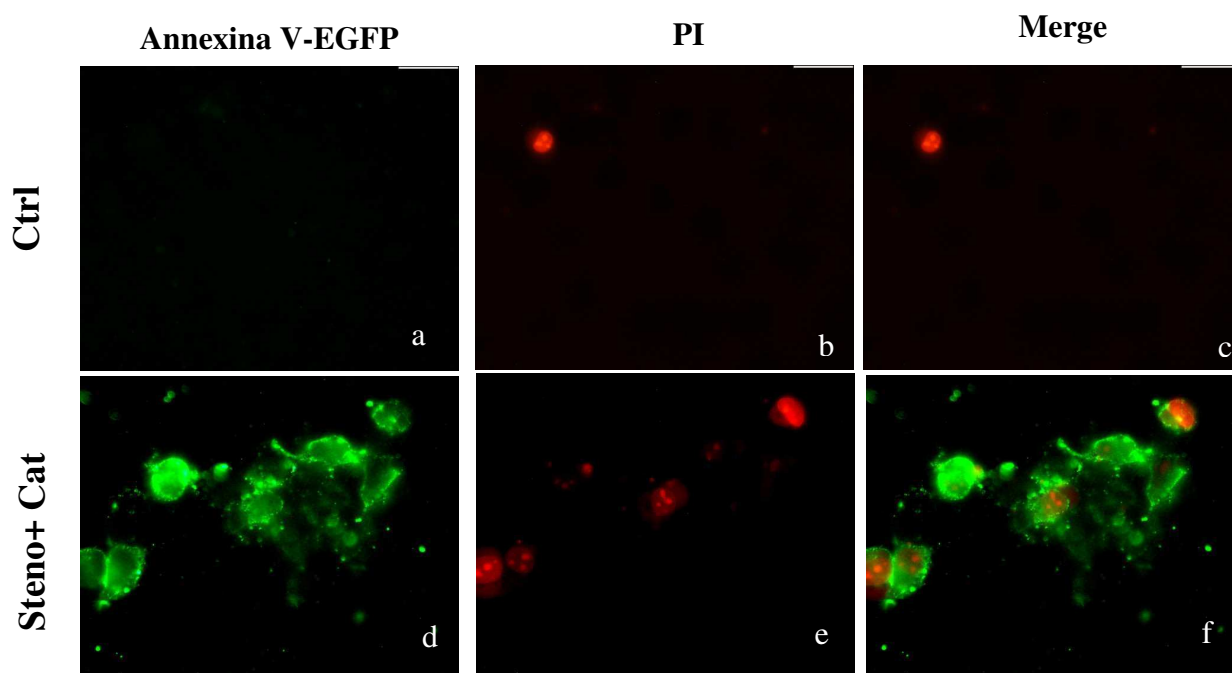


**Fig. 4.21.** Apoptosis as detected with AnnexinV-EGFP/PI in control cells (a-c) and cells pretreated for 3 h with Cat (10U/ml) and then intoxicated for 2 h with stenodactylin, steno, ( $10^{-12}$  M) (d-f). After 48 h, NB100 cells were stained with AnnexinV-EGFP/PI and observed under a fluorescent microscope. (a, d) The membranes of apoptotic cells stained green with AnnexinV-EGFP; (b, e) the nuclei of late stage of apoptosis or necrotic cells stained red with PI; (c, f) a dual-channel fluorescence view was creating by overlaying the images

To confirm that the enzymatic activity of catalase was important for its protective effect, cells were pretreated using heat-inactivated catalase (Cat HI). In addition, the cells were pretreated with another scavenger, sodium pyruvate (NaPyruvate or NaPyr). NaPyruvate is a strong hydrogen peroxide scavenger that reacts stoichiometrically with  $H_2O_2$  to protect cells from peroxide toxicity.

Viability was measured after 24 h from the intoxication. Cells that were pretreated with Cat HI were completely dead, similar to cells treated with stenodactylin, while pretreatment with NaPyruvate decreased cell death, but less efficiently than catalase (80% vs. 100% viability with NaPyr and Cat, respectively). These results confirmed that stenodactylin induces the production of hydrogen peroxide and that the total protective effect of Cat occurs through its enzymatic activity (Fig. 4.22).

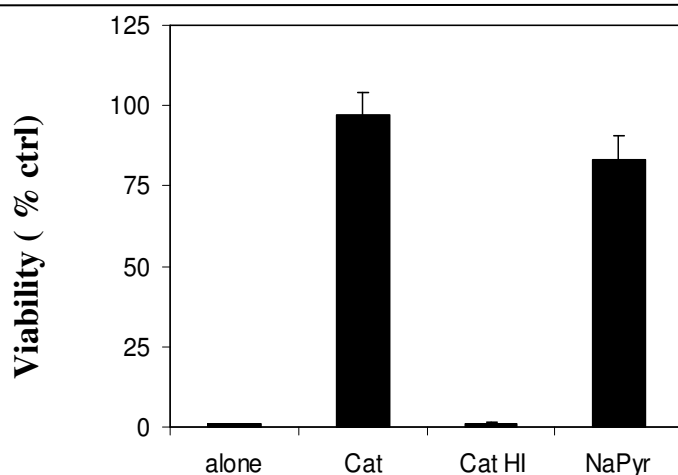


**Fig. 4.22.** Viability of NB100 cells treated with stenodactylin alone or in the presence of Cat (10 U/ml), heat inactivated catalase, Cat HI (10 U/ml) or NaPyruvate, NaPyr (1mM). The scavengers were added 3 h before RIP was added, while stenodactylin was added for 2 h and the viability was observed after 24 h from the intoxication with the RIP. The results are the means of three independent experiments, each performed in triplicate, and are presented as the percentage of control values obtained from cultures grown in the absence of the RIP.

To ensure that the result obtained with catalase was not due to an experimental artifact, inhibition of protein synthesis in a cell-free system, native PAGE and fluorescence analysis of stenodactylin cell binding were performed in the presence of catalase, stenodactylin or both. Catalase and stenodactylin together inhibited protein synthesis *in vitro* by 35%, comparable to the inhibition measured with the RIP alone (45%). This result indicates that the scavenger does not modify the enzymatic activity of stenodactylin (data not shown).

The native PAGE analysis showed only two bands when the RIP and the scavenger were incubated together. These bands correspond to catalase and stenodactylin. The results indicate that the scavenger did not block the RIP; indeed, no band was higher than the one corresponding to catalase, indicating that the scavenger did not produce steric hindrance. Moreover, no band was lower than the one corresponding to the RIP, indicating that the disulfide bridge was not reduced (Fig. 4.23).

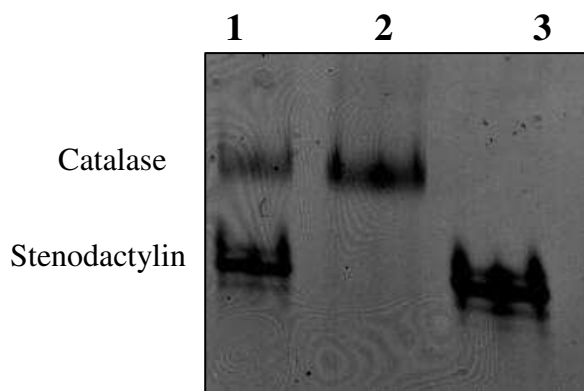


**Fig. 4.23.** Native PAGE under non-reducing conditions of the combination of catalase and stenodactylin (lane 1), catalase alone (lane 2), and stenodactylin alone (lane 3).

Catalase did not compete for the same binding site receptor of stenodactylin. Indeed, in cells treated with stenodactylin and subsequently with an anti-stenodactylin antibody, the RIP (red dots) was observed inside the cells, both in the presence and in the absence of the scavenger (Fig. 4.24).

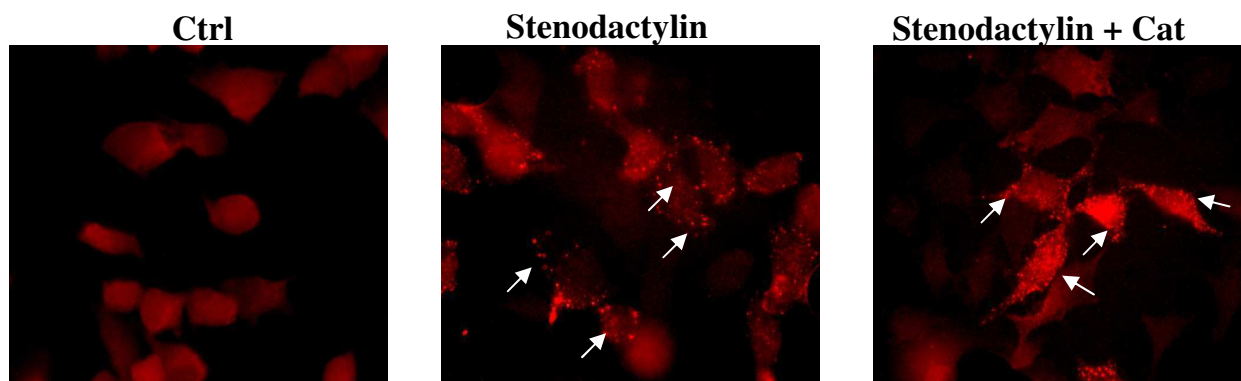


**Fig. 4.24.** Fluorescence microscopy of NB100 cells loaded with an anti-stenodactylin antibody after incubation with stenodactylin in the presence or absence of catalase. White arrows indicate stenodactylin red dots.

#### 4.2.4 Assessment of autophagy

Autophagy is a cellular degradation process that involves the lysosomal breakdown of cytoplasmic components. It is maintained at basal level in most cells and contributes to the routine turnover of cytoplasmic components. After stress or pathological stimuli, its activation is increased. Reactive oxygen species are implicated in the activation of this cellular mechanism. There are two controversial hypotheses concerning the induction of autophagy by ROS. Autophagy could be a cell-survival mechanism and cause a decrease in ROS levels by disrupting ROS-producing compartments. Alternatively, autophagy could act as a cell death mechanism when high levels of ROS are present. In these conditions, autophagy self-digests components of the cell and leads to cell death (Huang *et al.*, 2011).

The microtubule-associated protein light chain 3 (LC3) is a marker of autophagy and is a major constituent of autophagosome, a double membrane structure that sequesters the target organelle/protein and then fuses with endo/lysosomes. During autophagy, LC3 is cleaved to generate the cytosolic form LC3I, which is subsequently conjugated to phosphatidylethanolamine to form LC3II, which is in turn recruited to autophagosomal membranes (Kabeya *et al.*, 2000; Tanida *et al.*, 2008).

To verify the activation of autophagy, a preliminary experiment was performed in cells treated with stenodactylin ( $10^{-12}$  M) for 8 h. The experiment was conducted at 8 h because, as reported previously, the formation of ROS was already detected at this time. Western blot

analysis showed the presence of the two bands of LC3: LC3I (18 kDa) and LC3II (16 kDa), thus confirming that autophagy is triggered (Fig. 4.25A). Densitometric analysis of band intensity showed that stenodactylin induced an increase of LC3II levels compared with untreated cells, while the cytosolic form of LC3 decreased (Fig. 4.25B). The data are significantly different with a confidence range of 90%.

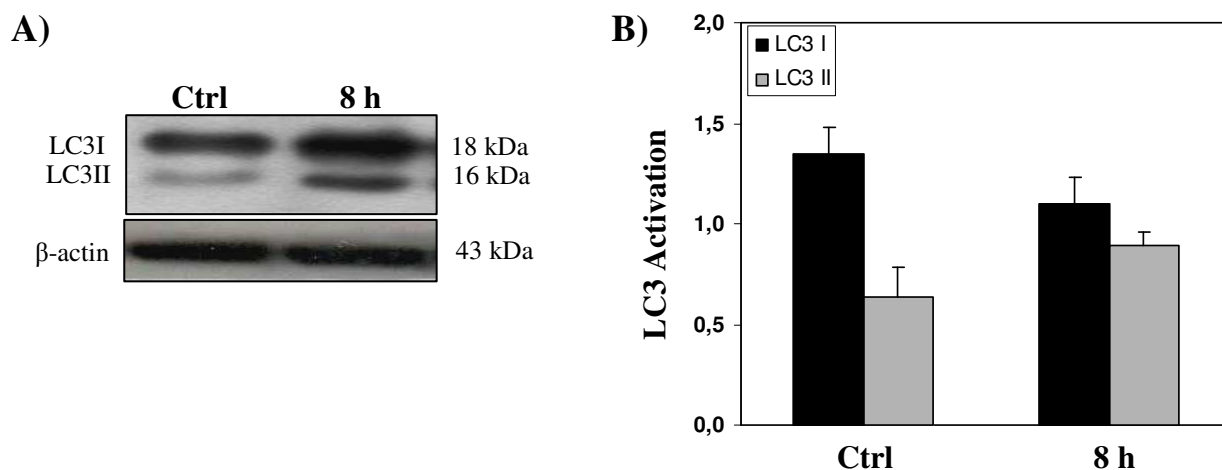


**Fig. 4.25.** Expression of LC3 by western blot analysis in NB100 cells treated with stenodactylin ( $10^{-12}$  M) for 8 h. The band at 18 kDa corresponds to LC3I, while the band at 16 kDa correspond to LC3 II. The same blot was hybridized with anti- $\beta$ -actin as loading control (A). Densitometric analysis of LC3 expression by western blot analysis in cells treated with stenodactylin ( $10^{-12}$  M). The data were normalized to the respective loading control ( $\beta$ -actin). The columns represent the bands density calculated by Image J software. The values are the means  $\pm$  SD of two independent experiments. Data were analyzed by ANOVA, followed by a comparison with Dunnett's test, using a 90% confidence interval.

Summarizing all the results obtained in NB100 cells intoxicated with the  $IC_{100}$  of stenodactylin ( $10^{-12}$  M), we speculate that the RIP can activate the effector caspases (perhaps through the DNA damage and/or by intrinsic and extrinsic pathways) and causes the formation of the superoxide radical. The latter is immediately converted to hydrogen peroxide, which causes or contributes to caspase-dependent apoptosis.  $H_2O_2$  can also activate other cell death mechanisms, such as necroptosis and/or autophagy (Fig. 4.26A).

Pretreatment with Z-Vad protects the cells from apoptosis for a limited time spare, after which the cells start to die, most likely of catalase consumption and accumulation of  $H_2O_2$ , which could cause necroptosis and/or autophagy. Several reports have indicated that autophagy can be caused by necroptosis and Z-Vad (Degterev *et al.*, 2005; Bell *et al.*, 2008; Bonapace *et al.*, 2010). Indeed, Z-Vad can cause autophagic degradation of catalase, thus inducing an increase in ROS accumulation. (Yu *et al.*, 2006) (Fig. 4.26B).

With catalase, hydrogen peroxide is converted to water and oxygen. Over time, the cells start to die, perhaps through other mechanisms that activate the effector caspases (Fig. 4.26C).

Co-treatment with catalase and Z-Vad rescues the cells from death even after 96 h from the treatment. The hydrogen peroxide formed after treatment with *stenodactylin* is converted to water and  $O_2$  by catalase, while Z-Vad protects the cells from caspase-dependent cell death (Fig. 4.26D).

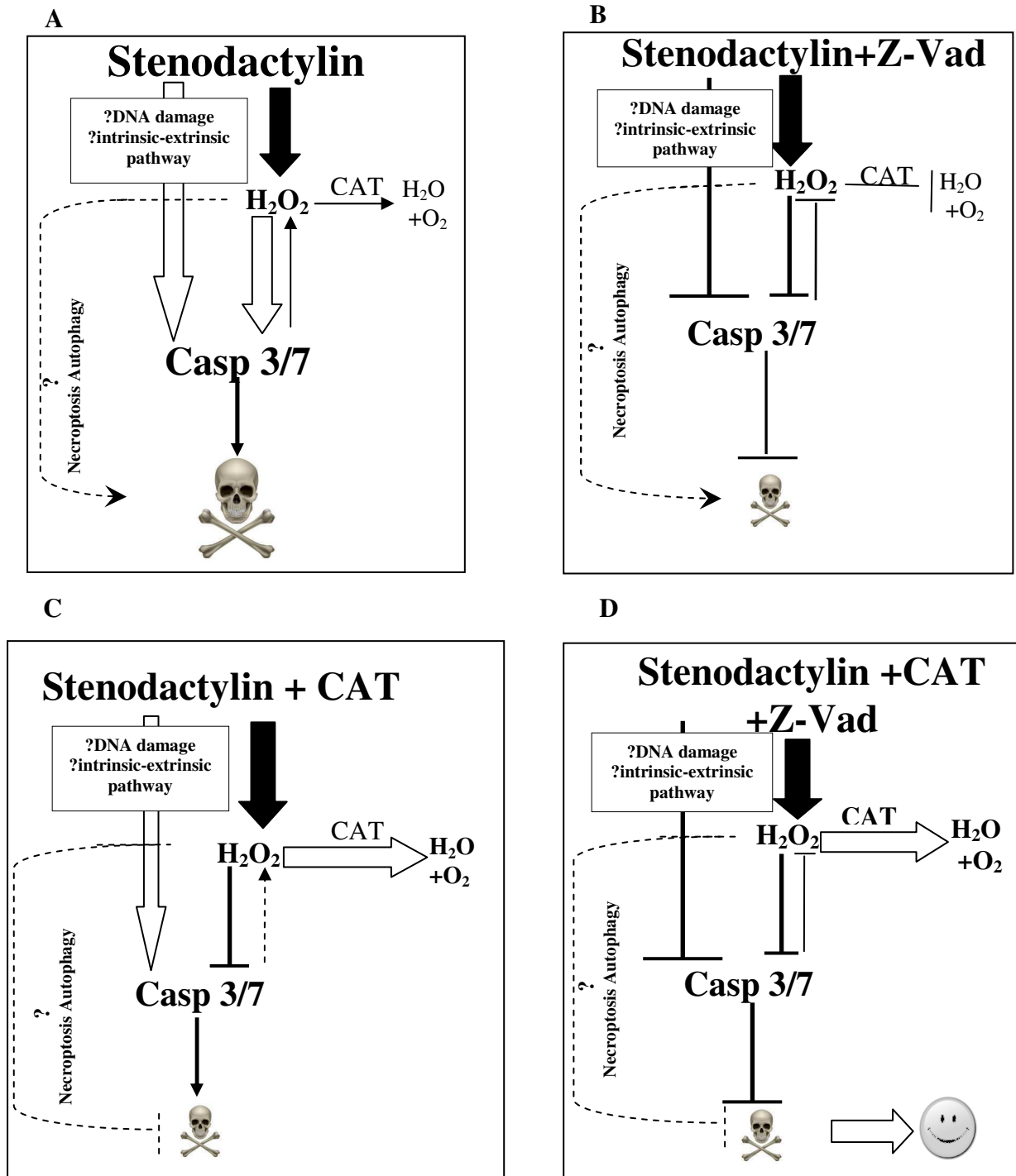


**Fig. 4.26.** A probably scheme for cell death mechanisms of induced by *stenodactylin*: alone(A), with Z-Vad (B), with the scavenger catalase (CAT) (C), and in the presence of catalase and Z-Vad (D).

### 4.3 The cytotoxic effect of RIPs at IC<sub>50</sub> concentration

#### 4.3.1 Inhibition of protein synthesis and activation of caspases 3/7

Many open questions remain about the importance of inhibiting protein synthesis during the induction of apoptosis. To understand the mechanism underlying RIP-induced cell death, in particular the role of rRNA N-glycosidase activity, the activation of effector caspases 3/7 and the inhibition of protein synthesis were evaluated in parallel experiments. In this set of experiments, stenodactylin was compared with another type 2 RIP (ricin) and a type 1 RIP (saporin) to evaluate possible differences in the dynamics of intoxication between mono- and bichain RIPs. All time-course experiments were performed using the IC<sub>50</sub> calculated above: 10<sup>-14</sup> M, 10<sup>-13</sup> M and 10<sup>-11</sup> M for stenodactylin, ricin, and saporin, respectively. The IC<sub>50</sub> were chosen for the following reasons: (i) high doses could be too strong and cause fast cell death, which would prevent studying the temporal events induced by RIPs and (ii) high RIP concentrations could be more favorable to one cell death mechanism than another. In these experiments with IC<sub>50</sub>, type 2 RIPs induced a strong activation of caspases 3/7, which was significant after only 4 h of incubation, followed by an exponential increase over time (Fig. 4.27). Activity was increased approximately 1500 and 1200% of control activity levels with stenodactylin and ricin, respectively. In contrast, protein synthesis became significant inhibited only after 24 h of incubation with both RIPs.

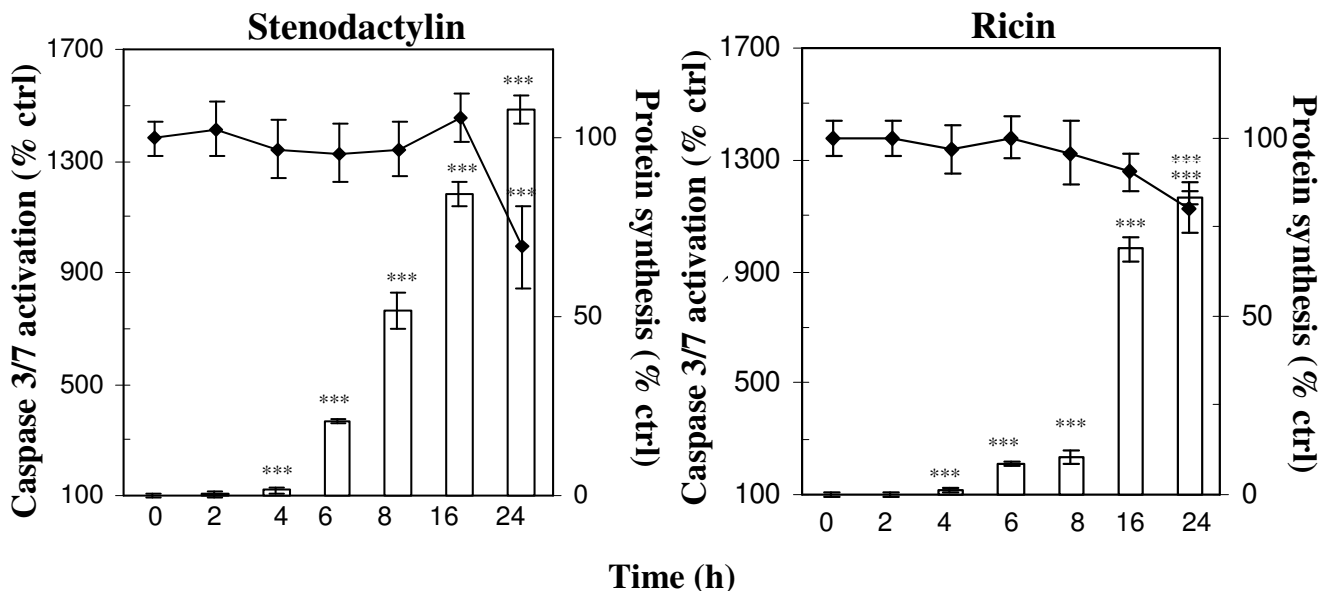


**Fig. 4.27.** Effect of the type 2 RIPs, stenodactylin (10<sup>-14</sup> M) and ricin (10<sup>-13</sup> M), on protein synthesis (◆) and caspase 3/7 activity (columns) in NB100 cells. Caspases 3/7 activity is expressed as the percentage of control values obtained from cultures grown in the absence of RIPs. The results are the means of three independent experiments, each performed in triplicate. Asterisks indicate the level of significance as determined by ANOVA, Dunnett's test \*\*\* p=0.001.

In cells treated with saporin, the effector caspases started being significantly activated only after 16 h of incubation, reaching 600% at 24 h. As observed with type 2 RIPs, the inhibition of protein synthesis became significant after 24 h of intoxication (Fig. 4.28).

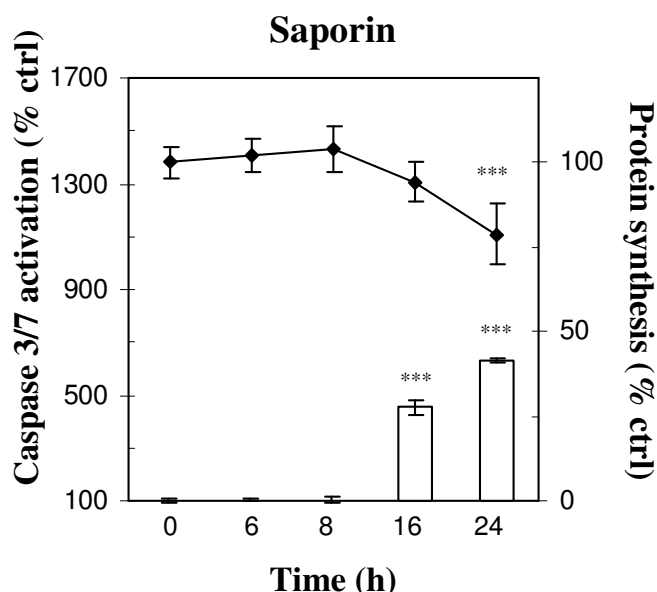


**Fig. 4.28.** Effect of the type 1 RIP saporin ( $10^{-11}$  M) on protein synthesis ( $\blacklozenge$ ) and caspase 3/7 activation (columns) in NB100 cells. Caspases 3/7 activity is expressed as the percentage of control values obtained from cultures grown in the absence of RIP. The results are the means of three independent experiments each performed in triplicate. Asterisks indicate level of significance as determined by ANOVA, Dunnett's test \*\*\*  $p=0.001$ .

These data demonstrate that in cells treated with a relatively low dose of RIP, the first effect produced is the activation of caspases 3/7, even before the inhibition of protein synthesis is detectable. Indeed, the effector caspases activation increased starting at 4 h for stenodactylin and ricin and from 16 h for saporin, while the protein synthesis was not inhibited until 24 h for all the three RIPs. The delayed activation of caspases 3/7 in saporin-treated cells was caused by its less efficient entry into cells due to the lack of the B chain.

These results show that caspase activation occurs independently from the inhibition of protein synthesis. This finding suggests that the different mechanisms of cell death induced by RIPs are distinct from rRNA deadenylation. Moreover, the toxicity of the RIPs was primarily due to caspases activation and not to inhibition of protein synthesis.

Activation of caspases 3/7 is the most common hallmark of apoptosis. To confirm this cell death pathway, Annexin V-EGFP/PI staining was performed on NB100 cells treated with stenodactylin  $10^{-14}$  M, ricin  $10^{-13}$  M and saporin  $10^{-11}$  M, 48 h of intoxication (Fig. 4.29).

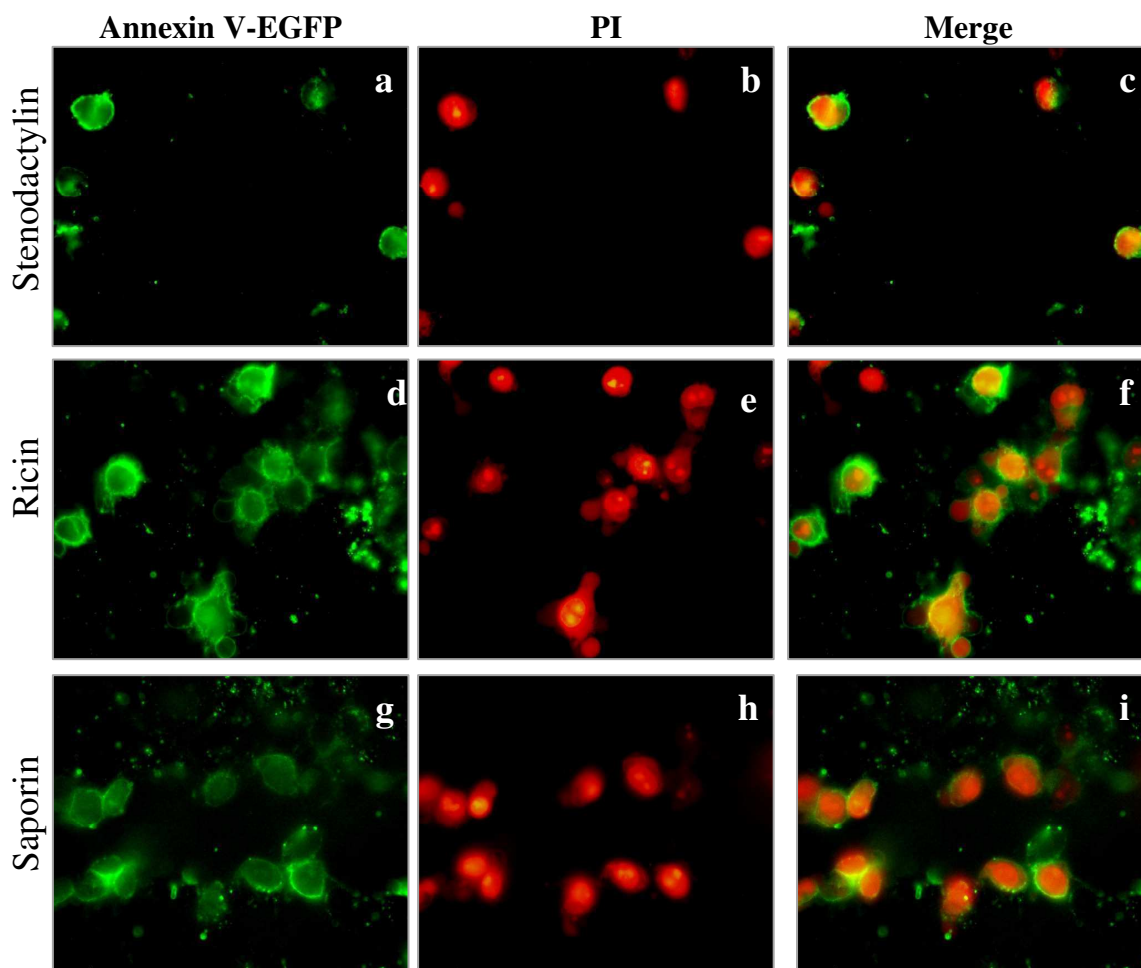


**Fig. 4.29.** Apoptosis as detected with Annexin V-EGFP/PI in (a-c) stenodactylin-, (d-f) ricin-, (g-i) saporin-treated cells. After 48 h NB100 cells ( $2 \times 10^4/500\mu\text{l}$  complete RPMI) intoxicated with RIPs were stained with Annexin V-EGFP/PI and observed under fluorescence microscope. (a, d, g) The membranes of apoptotic cells stained green with Annexin V-EGFP; (b, e, h) the nuclei of apoptotic or dead cells stained red stained with PI; (c, f, i) a dual-channel fluorescence view was creating by overlaying the images.

All three RIPs caused apoptosis; indeed, after 48 h of intoxication with RIPs, the majority of cells were positive for Annexin V-EGFP and PI, thus indicating that the cells were in the end stage of apoptosis.

#### 4.3.2 Evaluation of apoptotic cell death

As earlier observed, intoxication with stenodactylin  $10^{-14}$  M led to activation of caspases 3/7 in a time- dependent manner.

The early activation of effector caspases in cells treated with stenodactylin ( $10^{-14}$  M) was confirmed by the change of poly(ADP ribose) polymerase (PARP).

PARP is one of the first identified cellular substrates that is cleaved during apoptosis by caspase 3, and it is important for DNA repair. Whole cell extracts were analyzed for PARP by immunoblotting. In stenodactylin-treated cells, intact 116-kDa PARP was degraded to the 85-

kDa form at 8 h when caspase-3 activation was highly detectable (800%) (Fig. 4.30A). Moreover, densitometric analysis of band intensity showed increases expression of PARP in treated cells compared with untreated cells, which may have been caused by a stress response to the RIP intoxication (Fig. 4.30B).

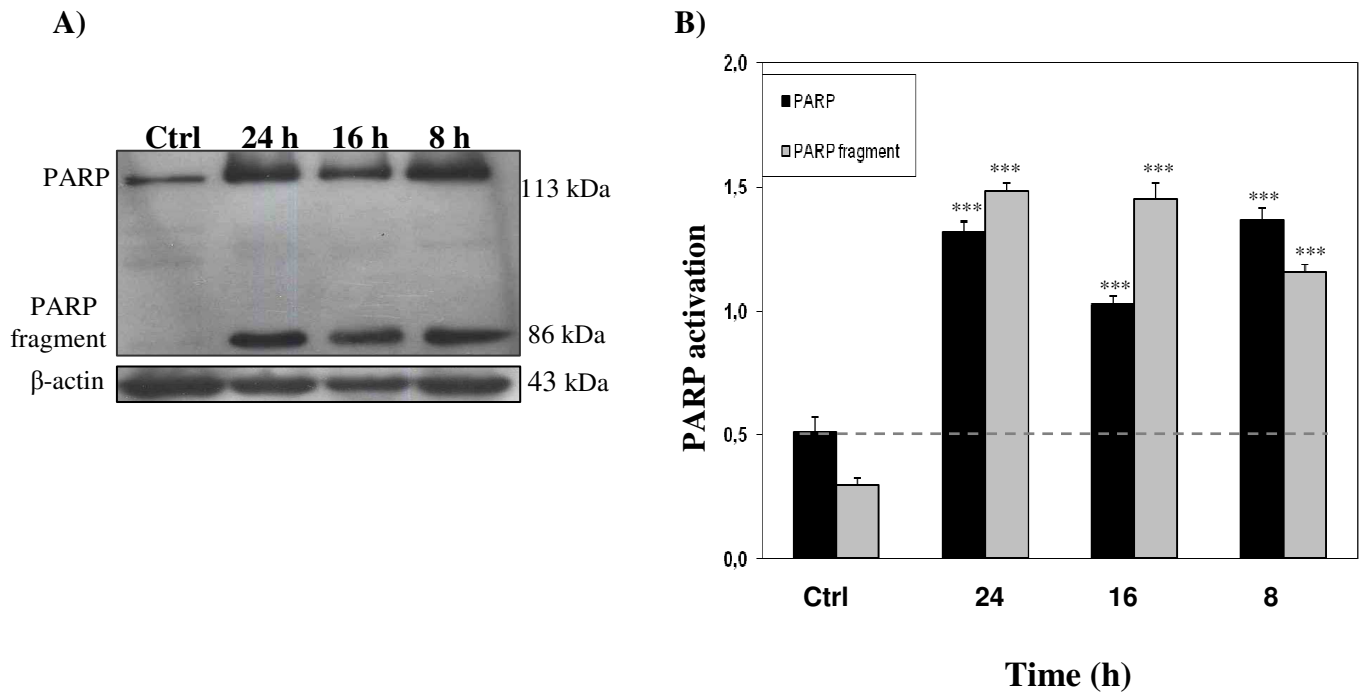


**Fig. 4.30.** Expression of PARP analyzed, by western analysis in NB100 cells treated with stenodactylin ( $10^{-14}$  M) for 8, 16, 24 h. The band of 113 kDa corresponds to PARP, while the band of 86 kDa correspond to PARP fragment. The same blot was hybridized with anti- $\beta$ -actin as loading control (A). Densitometric analysis of PARP expression by western blot analysis in cells treated with stenodactylin ( $10^{-14}$  M). The data were normalized to the respective loading control ( $\beta$ -actin). The columns represent the bands density calculated by Image J software. The values are the means  $\pm$  SD of two independent experiments. Asterisks indicate level of significance as determined ANOVA, Dunnett's test \*\*\*  $p=0.001$  (B).

#### 4.3.2.1 Involvement of the intrinsic and extrinsic apoptotic cell death pathways

Cell death through apoptosis occurs through two primary pathways, an extrinsic pathway involving death receptors, and an intrinsic pathway through the mitochondria. The receptor-mediated pathway is triggered by an external stimulus and activates initiator caspases such as caspases 8 and 2. The mitochondrial pathway is normally triggered by internal stresses that activate caspase 9. The caspases activate effector caspases 3/7.

To study the involvement of the intrinsic and extrinsic pathways in stenodactylin-induced apoptosis, the activation of caspases 8, 2 and 9 was evaluated in time-course experiments (Fig. 4.31).

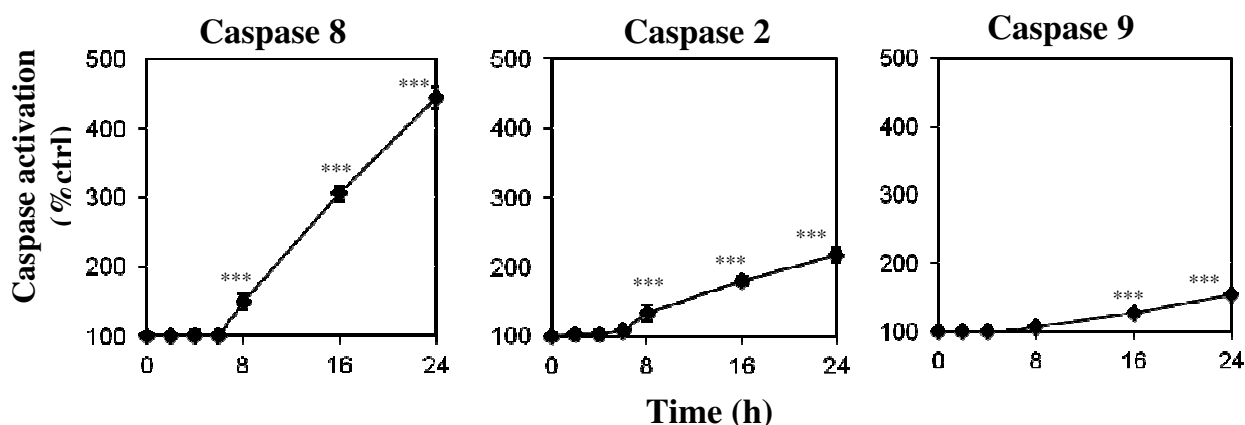


**Fig. 4.31.** Caspases activation in NB100 cells ( $4 \times 10^3$  cells) exposed to stenodactylin ( $10^{-14}$  M). The enzymatic activity of caspases were measured by luminometric assay. Caspases activity is expressed as the percentage of control values obtained from cultures grown in the absence of RIP. Asterisks indicate level of significance as determined by ANOVA, Dunnett's test \*\*\*  $p=0.001$ .

The results showed that all the caspases had a similar trend but a variable activation time. Caspase 8 and 2 were significantly activated after 8 h of intoxication, while the intrinsic caspase 9 was significantly activated after 16 h. Caspase 8 can also induce the intrinsic pathway. Indeed, caspase 8 causes the cleavage of Bid protein to a truncated form (tBid), which translocates to the mitochondria and subsequently activates caspase 9 (Li *et al.*, 1998). From the results obtained, we assume that (i) the caspase 9 is not activated directly by RIP but most likely by caspase 8 because caspase 9 activation was detectable 8 h after caspase 8 and/or (ii) the activation of caspase 9 requires more time.

Moreover, the highest levels of caspase activation were observed for caspase 8 (400 % at 24 h). The earliest activation of the extrinsic pathway was reported for lymphoma cells treated with ricin and saporin (Polito *et al.*, 2009a).

The role of the intrinsic apoptosis pathway was evaluated using the caspase 8 inhibitor Z-IETD-fmk. The activation of caspases 3/7 in the presence of the caspase 8 inhibitor was tested 16 h after the beginning of the treatment with RIP, when the effector caspases were highly activated. In the presence of the Z-IETD, the caspase 8 activity was completely inhibited, while the activation of caspases 3/7 were only 28% lower than in the absence of the inhibitor (Fig. 4.32).

These results suggest that although the caspase 8 was the most active caspase, other caspases activated the effector caspases. Thus, at this time, the activated caspase 2 and caspase 9 may play an important role in the activation of effector caspases.

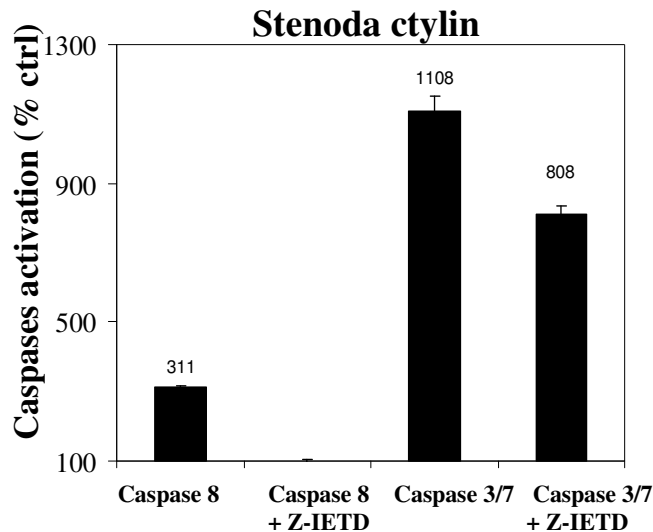


**Fig. 4.32.** Effect of caspase-8-inhibitor Z-IETD (25 $\mu$ M) on caspase 8 and 3/7. Inhibitor was added to NB100 cell 3 h before the RIPs. The caspases activation were valuated after 16 h of exposure to stenodactylin ( $10^{-14}$  M), ricin ( $10^{-13}$  M).

As mentioned above, in cells treated with stenodactylin ( $10^{-14}$  M) caspase 9 began to be significantly activated after 16 h of incubation, although with a very low value when compared with caspase 8 activity. To confirm that the intrinsic pathway was partially involved in the apoptotic cell death pathway, the dissipation of mitochondrial membrane ( $\Delta\psi_m$ ) was evaluated. The cells were treated with stenodactylin ( $10^{-14}$  M) for 16 h and the  $\Delta\psi_m$  was examined by evaluating the changes in fluorescence intensity of cells stained with JC-1. In healthy cells with high  $\Delta\psi_m$ , JC-1 forms J-aggregates with intense red fluorescence. In apoptotic cells with low  $\Delta\psi_m$ , JC-1 remains in the monomeric form (green fluorescence). As shown in Figure 4.33 the treatment did not affect JC-1 fluorescence; indeed, there were not differences between untreated and treated cells, indicating a lack of mitochondrial involvement.

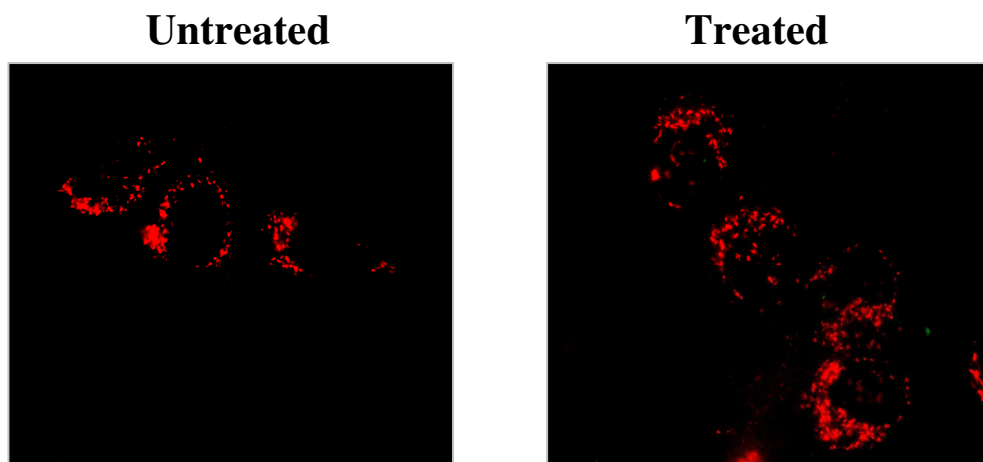


**Fig. 4.33.** Mitochondrial transmembrane potential in NB100 cells ( $2 \times 10^4/500\mu$ l complete RPMI) treated with stenodactylin ( $10^{-14}$  M) for 16 h, stained with JC-1 and then analyzed with fluorescence microscopy. The untreated and treated cells showed a strong red fluorescence, indicating intact mitochondrial membrane potential.

To further evaluate the intrinsic apoptotic signaling pathway in cell treated with stenodactylin, the expression of two proapoptotic member of Bcl-2 protein family, Bax and Bad, was evaluated.

Bad is involved in initiating apoptosis. It can form a heterodimers with anti-apoptotic proteins and prevent them from inhibiting apoptosis. Bax increases the opening of the mitochondrial voltage-dependent anion channel (VDAC), which leads to the loss of the mitochondrial membrane potential and the release of cytochrome *c*.

Total cellular proteins from NB100 cells treated with  $10^{-14}$  M stenodactylin were analyzed by western blot using anti-Bax and anti-Bad primary antibodies, at different time points.

Western blot and quantitative densitometric analysis showed only a slight decrease of Bad expression at 4 h, while the expression of Bax protein was slightly lower when compared with untreated cells at all time points. However, the two markers involved in intrinsic apoptosis did not show any significant differences when compared with the controls (Fig. 4.34).

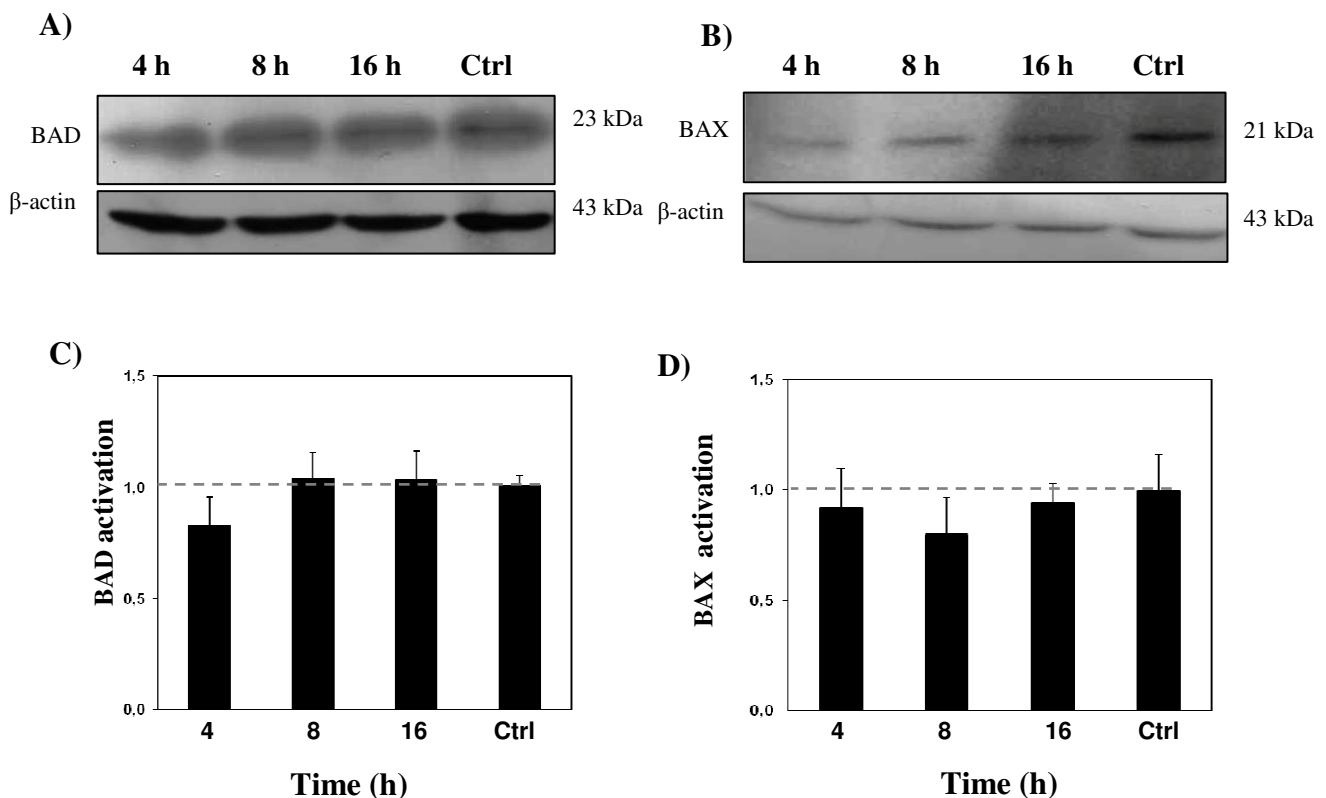


**Fig. 4.34** Total cellular proteins from NB100 cells that were treated with stenodactylin ( $10^{-14}$  M) were analyzed by western blot using anti-Bad and anti-Bax antibodies, followed by reprobing with a  $\beta$ -actin antibody. The Bad (A) and Bax (B) protein levels remained unchanged. The quantitative densitometric analyses for the Bad (C) and Bax (D) proteins normalized to  $\beta$ -actin. Values are presented as the mean  $\pm$  SD of two independent experiments.

Subsequently using the quantitative real-time PCR, the mRNA expression levels of the Bad and Bax genes were analyzed. All values were adjusted for the expression of glyceraldehyde-3-phosphate dehydrogenase GAPDH, which was determined to be the most stable

housekeeping gene in this cell line. After stenodactylin treatment, a small increase of Bad was observed, but in both genes, no significant differences were observed compared with control cells (Fig. 4.35).

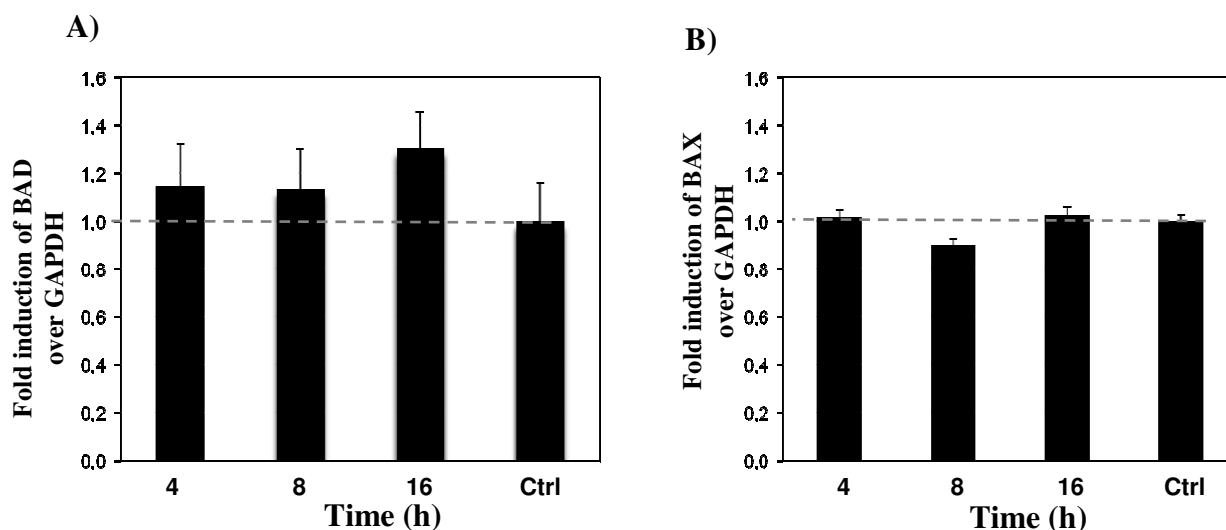


**Fig. 4.35.** Mean fold expression of mRNA of pro-apoptotic genes after treatment of stenodactylin ( $10^{-14}$  M) in NB100 cells. A EvaGreen (SBYR) real-time PCR was used to detect mRNA of Bad (A) and Bax (B). Analysis of mRNA levels was evaluated by the  $2^{-\Delta\Delta Ct}$  method. Values were normalized to GAPDH mRNA expression and the data presented are the mean of three experiments.

The involvement of the extrinsic cell death pathway was investigated by evaluating the expression of Receptor Interacting Protein-1 (R.I.P.1) by western blot analysis.

R.I.P.1 contains a death domain that may be recruited to the TNFR1 and Fas (CD95) receptor signal complexes following ligand binding. It is important for NF- $\kappa$ B activation and the triggering of apoptosis or necroptosis. Upon stimulation, two different complexes can be formed within the cell: complex I and complex II (A and B). In complex I, R.I.P.1 is polyubiquitinated, which activates NF- $\kappa$ B pathway and leads to the expression of prosurvival genes. When R.I.P.1 is deubiquitinated by A20 and Cyld, it translocates to complex II. There are two complexes II: TRADD- dependent complex IIA and R.I.P.1 kinase-dependent complex IIB. Complex IIA is formed by TRADD, FADD and activated caspase 8, which causes the cleavage of R.I.P.1 and R.I.P.3, thereby blocking necroptosis and inducing apoptosis. Complex IIB acts independently of TRADD through a R.I.P.1-FADD scaffold to activate caspase 8 in a R.I.P.1 kinase-dependent manner, which induces the apoptosis pathway.

When caspase 8 is inactivated (e.g., by Z-Vad), R.I.P.1 and R.I.P.3 assemble a complex that contains FADD and caspase 8 (and eventually TRADD), and the interdependent phosphorylation of R.I.P.1 and R.I.P.3 activates necroptotic signaling (Declercq *et al.*, 2009; Gunther *et al.*, 2012).

Figure 4.36 demonstrates an increase in R.I.P.1 expression after intoxication with  $10^{-14}$  M stenodactylin for only 8 h, and this increase became significant at 24 h.

Because caspase 8 is activated and R.I.P.1 is expressed after 24 h of intoxication with stenodactylin, the complex IIA may have formed within the cells.

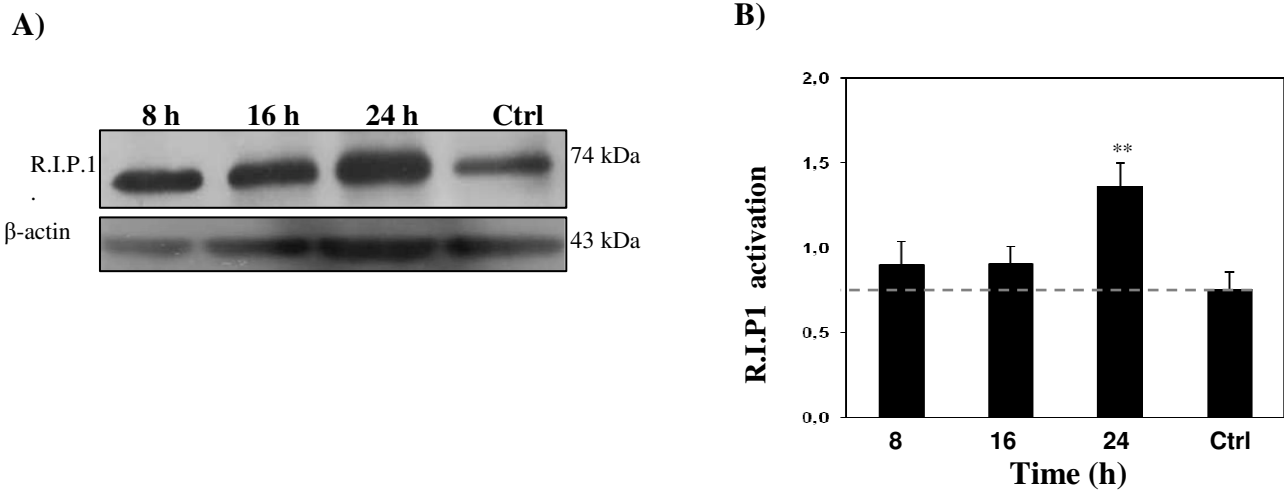


**Fig. 4.36.** Total cellular proteins from NB100 cells treated with stenodactylin ( $10^{-14}$  M) were analyzed by western blot using anti-R.I.P.1 antibody, the same blot was hybridized with anti- $\beta$ -actin as loading control. A long-time exposure an increase of R.I.P.1 protein level was observed (A). Densitometric analyses of R.I.P.1 expression by western blot analysis in cells treated with stenodactylin ( $10^{-14}$  M). The data were normalized to the respective loading control ( $\beta$ -actin). The columns represent the bands density calculated by Image J software. The values are the mean  $\pm$  SD of two independent experiments (B). Asterisks indicate level of significance by ANOVA, Dunnett's test \*\*  $p=0.01$ .

Altogether, apoptosis appears to be the main mechanism of cell death induced by RIPs because protein synthesis is inhibited after programmed cell death begins. Moreover, our data suggest that the extrinsic apoptotic pathway is the most relevant death mechanism induced by stenodactylin intoxication.

*Chapter 5*

**Effects of ebulin l and nigrin b  
on NB100 cells**

## **BACKGROUND: Ribosome inactivating proteins from Sambucus**

The *Sambucus* genus is composed of approximately 20 species. Numerous type 1 and type 2 RIPs and homolectins have been found in *Sambucus*, and all types can coexist in diverse tissues of the same plant. For example, type 1 RIPs ebulitins ( $\alpha$ ,  $\beta$ ,  $\gamma$ ), the heterodimeric type 2 RIP ebulin 1 and monomeric and homodimeric lectins (SELIm and SELId) are observed in the leaves of *S. ebulus*. The fruits of *S. nigra* express the type 1 RIPs nigrins (f1 and f2), both heterodimeric and tetrameric type 2 RIPs (nigrin f and SNAIf), and monomeric and homodimeric lectins (SNAIV and SELfd). The RIP level can change with plant development and during the seasons. Indeed, in young leaves of *S. ebulus*, the ebulin 1 level was higher than the level of the lectin SELId, but with the development of the plant, the ebulin 1 level decreased and disappeared during senescence, whereas the level of lectin increased (Rojo *et al.*, 2003). Nigrin b, which is extracted from the bark of *S. nigra* provides another example of seasonal variation. High levels of this toxin are present in spring and summer, but not in winter (Ferrerias *et al.*, 2010).

A sequence analysis of the RIPs of *Sambucus* demonstrated that they share an homology with ricin and other type 2 RIPs. The identity between the A chain and the B chain of ricin and ebulin 1 are 34 % and 48%, respectively (Pascal *et al.*, 2001).

Based on X-ray diffraction analysis, ebulin 1 was shown to possess A and B chains similar to ricin, but with different galactose-binding properties. Ricin binds galactose and lactose in both subdomains 1 and 2 (at the  $1\alpha$  and  $2\gamma$  sites, respectively). Ebulin 1 binds galactose and lactose similar to ricin, at the  $1\alpha$  sites, but it is unable to bind lactose at the  $2\gamma$  site. Galactose binds differently within the  $2\gamma$  site of ebulin as compared with ricin; galactose bound is further into the binding cleft, and the different orientation and position may cause steric interference with the sugar attached to the C1 hydroxyl. The altered mode of galactose binding could alter the binding of this RIP to the cell surface and explain the low toxicity of this protein (Ferrerias *et al.*, 2010).

Both type 1 and type 2 RIPs from *Sambucus* depurinate the rRNA and inhibit the protein synthesis, similar to ricin, in a cell-free system (rabbit reticulocytes) ( $IC_{50}$  of 0.15 nM, 0.003 nM, and 0.10 nM for ebulin 1, nigrin b and ricin, respectively) (Girbes *et al.*, 1993a,b). Despite the high inhibition of protein synthesis in rabbit reticulocytes, the type 2 RIPs from *Sambucus* showed low cytotoxicity compared with ricin and other type 2 RIPs. For example, in HeLa cells, the  $IC_{50}$  was 64.3 nM and 27.6 nM for ebulin 1 and nigrin b, respectively, whereas it was 0.00067 nM for ricin-treated cells (Citores *et al.*, 1996). Their low toxic effect

was also observed in mice. The LD<sub>50</sub> of ebulin 1 and nigrin b are 2 and 12 mg/kg body weight, respectively, whereas it is 0.003 mg/kg for ricin-treated mice (Girbes *et al.*, 1993b; Battelli *et al.*, 1997). Treating mice with an intravenous injection of a lethal dose of nigrin b (16 mg/kg) causes lesions in the intestine, with the disappearance of the villi and crypt structures. With sublethal doses (e.g., 5 mg/kg), the mice was completely recovered 9 days after the injection. In both cases, nigrin b caused apoptotic changes in the highly proliferating stem cells of the intestinal crypts (Gayoso *et al.*, 2005). Recently, apoptotic changes were also observed in ebulin-treated mice (Jiménez *et al.*, 2013).

The different cytotoxicity among non-toxic and toxic type 2 RIPs, seems to be related to these proteins' diverse interactions with cells and to the different routes used to enter the cells. The first hypothesis is supported by the finding that (i) ebulin 1 had a lower affinity for galactosides and, thus, for the galactose-containing glycoproteins and glycolipids present on the cell surface (Pascal *et al.*, 2001) and (ii) nigrin b has lower affinity than ricin for HeLa cells (Battelli *et al.*, 2004). The second hypothesis is based in part on the finding that volkensin, another highly toxic type 2 RIP, has low affinity for HeLa cells, suggesting that the low cytotoxicity of ebulin 1 and nigrin b is not only caused by a weaker interaction with cells but could also depend on intracellular trafficking and processing pathways that are different from those of toxic type 2 RIPs. Nigrin b is distributed between cytoplasmic dots and Golgi compartment and is rapidly degraded; thus, exocytosed nigrin b is completely inactive (Battelli *et al.*, 2004). Nigrin b may bind different glycoproteins on the plasma membrane and utilize a different intracellular routing than ricin. After internalization into the endosome, both toxic and non-toxic RIPs can be partially degraded in the lysosomes and then excreted, while another percentage of these RIPs can be recycled. After internalization into the endosomes, some ricin molecules can reach the Golgi apparatus and then be retrogradely transported to the ER, where the disulfide bridge is reduced, and the A chain can translocate into the cytosol, where it inactivates the ribosomes. In contrast, nigrin b is translocated from the endosome to the cytosol when its extracellular concentration is very high, and then it can reach the ribosomes (Ferrerias *et al.*, 2010).

Structure analysis showed that ricin possesses a lipase catalytic site, whereas ebulin 1 lacks this site. That absence of this lipolytic site, which has been implicated in the translocation and cytotoxicity of ricin, may also explain the lower cytotoxicity of ebulin 1 compared with ricin (Morloy-Guyot *et al.*, 2003).

## **AIM OF THE PROJECT**

Nigrin b and ebulin l have been used to construct immunotoxins directed toward the transferring receptor (TfR), which is over-expressed in some cancer cells (Citores *et al.*, 2002), and to endothelial receptor CD105 (endoglin), which is strongly expressed in the blood vessels of tumor tissues (Benítez *et al.*, 2005; Muñoz *et al.*, 2007). These immunotoxins showed high cytotoxicity, with IC<sub>50</sub> in the picomolar range. The previously obtained results suggest that non-toxic type 2 RIPs could be used for cancer therapy. Nigrin b and ebulin l show some advantages compared with toxic type 2 RIPs: (i) vascular leak syndrome should be less likely to develop; (ii) the free toxins released after hydrolysis of the conjugate do not cause significant toxic effects; and (iii) they are less dangerous to prepare than ricin (Ferrerias *et al.*, 2011).

The aim of this work was to study the cell death mechanisms induced by the non-toxic type 2 RIPs ebulin l and nigrin b because little is known about their pathogenic effects. The identification of the death pathway may be helpful for the selection of toxins that cause less necrosis, and thus fewer side effects, when used to construct immunotoxins.

The pathogenesis of cell toxicity induced by these two RIPs was compared with the toxicity induced by toxic type 2 RIPs ricin and stenodactylin and the type 1 RIP saporin because of their different interactions with cells and their different internalization strategies.

The ebulin l and nigrin b cytotoxicities were evaluated by studying caspase activation and viability in the presence of inhibitors of apoptosis and necroptosis.

## RESULTS AND DISCUSSION

### 5.1 The cytotoxic effects of Ebulin 1 and Nigrin b

#### 5.1.1 Inhibition of protein synthesis *in vitro*

The enzymatic activity of two non-toxic type 2 RIP proteins purified from the leaves of *S. ebulus* (ebulin 1) and the bark of *S. nigrin* (nigrin b) was evaluated *in vitro* in a cell-free system (rabbit reticulocyte lysate) using a non-radioactive method based on luciferase mRNA translation.

The proteins were tested in reduced conditions to eliminate the steric hindrance of the B chain.

The  $IC_{50}$ , which were calculated by linear regression analysis, for the inhibition of protein translation were 8.7 ng/ml and 5.4 ng/ml for ebulin 1 and nigrin b, respectively (Fig. 5.1).

These results are comparable to the  $IC_{50}$  already reported in literature (Ferrerias *et al.* 2011).

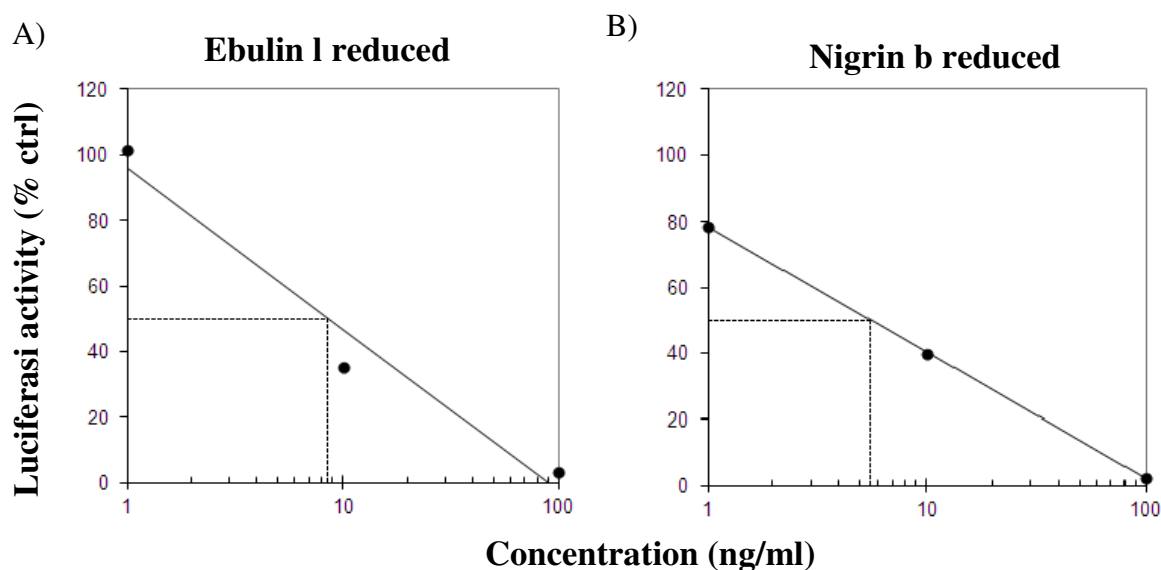


**Fig. 5.1.** Effect of ebulin 1 (A) and nigrin b (B) on protein synthesis of a rabbit reticulocyte lysate cell-free system

These results indicate that both RIPs efficiently inactivate ribosomes through their rRNA N-glycosylase activity.

Table 5.1 shows that the  $IC_{50}$  of ebulin 1 and nigrin b are very similar to the values reported for the toxic type 2 RIP ricin and the type 1 RIP saporin, indicating that they have comparable enzymatic activity.

**Table 5.1.** Effect of type 2 and type 1 RIPs on protein synthesis using the rabbit reticulocyte lysate system

Rabbit Lysate IC <sub>50</sub> (ng/ml)				
Ebulin l	Nigrin b	Ricin	Stenodactylin	Saporin
8.7	5.4	6	498*	1.8

(\* the high IC<sub>50</sub> value of stenodactylin has been caused by an incomplete reduction of the molecule)

### 5.1.2 Cell viability

A previous study showed that nigrin b has a very low toxicity in different cell lines (Munoz *et al.*, 2001). It is noteworthy that cell lines have different sensitivity to the lectins.

A cell viability assay was performed using two cell lines: the human neuroblastoma NB100 (Fig. 5.2) and the human colon carcinoma COLO320 (Fig. 5.3). NB100 was chosen for its high sensitivity to other RIPs that were previously tested in our laboratory.

The cells were treated with RIP concentrations ranging from 10<sup>-13</sup> M to 10<sup>-7</sup> M, and the cytotoxicity was evaluated after 48 h using the MTS assay.

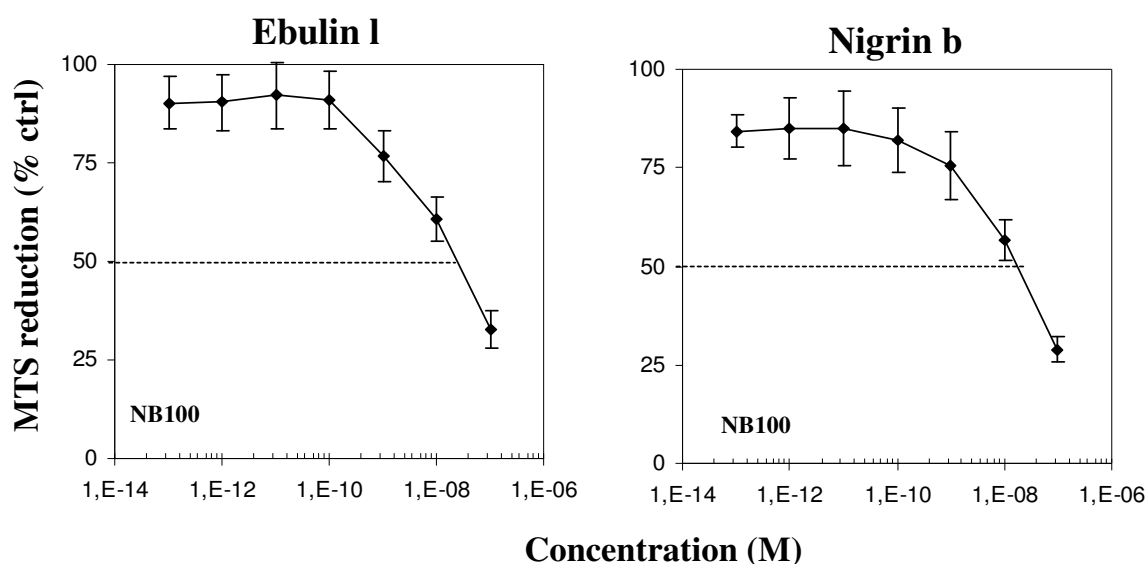


**Fig. 5.2.** Effects of ebulin l and nigrin b on NB100 cell viability after 48 h at the indicated concentrations of the RIPs. Viability was evaluated using a colorimetric assay based on MTS reduction. The results are the means of three independent experiments, each performed in triplicate, and are presented as the percentage of control values obtained from cultures grown in the absence of RIPs

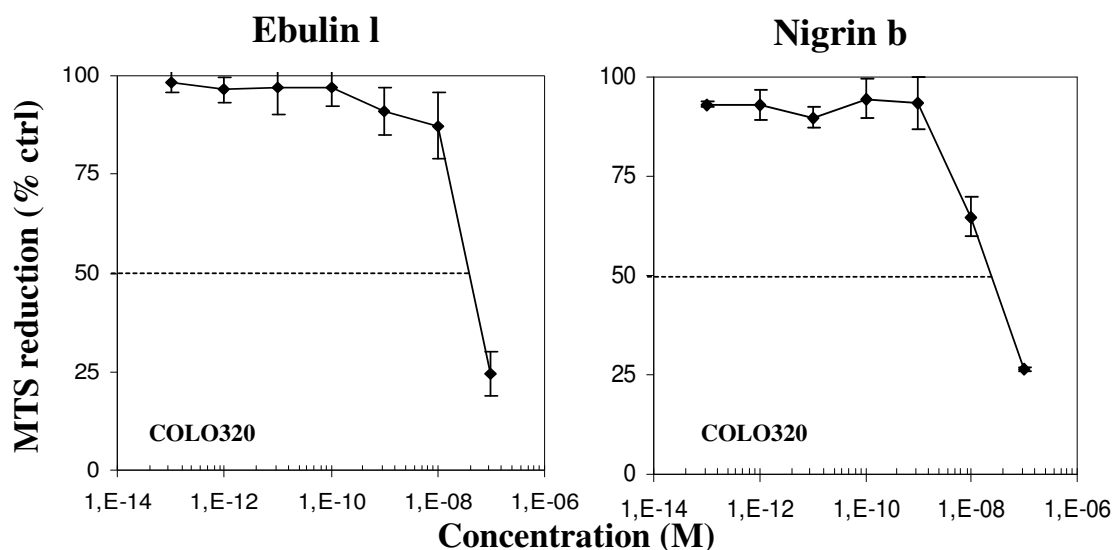


**Fig. 5.3.** Effects of ebulin I and nigrin b on COLO320 cell viability after 48 h at the indicated concentrations of the RIPs. Viability was evaluated using a colorimetric assay based on MTS reduction. The results are the means of three independent experiments, each performed in triplicate, and are presented as the percentage of the control values obtained from cultures grown in the absence of RIPs.

The  $EC_{50}$  values were very similar both between the two toxins and between the two cell lines (Table 5.2). The NB100 cell line was not very sensitive to these two toxins, as compared with the other RIPs.

**Table 5.2.** Comparison of  $EC_{50}$  values calculated for the RIP ebulin I and nigrin b on NB100 and COLO320 cells

$EC_{50}$ (M)		
Cell line	Ebulin I	Nigrin b
NB100	$2.0 \times 10^{-8}$	$1.4 \times 10^{-8}$
COLO320	$2.6 \times 10^{-8}$	$2.2 \times 10^{-8}$

When comparing the  $EC_{50}$  of the toxic type 2 RIPs stenodactylin and ricin and the type 1 RIP saporin, which were calculated previously (Chapter 4), with those of ebulin I and nigrin b in NB100 cells (Table 5.3), it is notable that the RIPs from Sambucus showed lower cytotoxicity than the other RIPs, even than saporin. The  $EC_{50}$  were almost the same for both ebulin I and

*nigrin b*; and the EC<sub>50</sub> of both non-toxic type 2 RIPs were 3, 5 and 6 orders of magnitude higher than the EC<sub>50</sub> of saporin, ricin and stenodactylin, respectively. The enzymatic activity was almost identical between the RIPs, whereas the cytotoxic activity was very different between the non-toxic and the toxic RIPs. These differences could be caused by a diverse number of cell receptors, and/or by different sugar binding sites between the *Sambucus* RIPs and the toxic type 2 RIPs. However, the non-toxic type 2 RIPs were less toxic than even saporin, which present low (if any) binding affinity to the receptors. These results confirm the hypothesis that a different routing and possibly intracellular modifications may explain the low cytotoxicity of *ebulin 1* and *nigrin b*.

**Table 5.3.** Comparison of type 2 (toxic and non-toxic) and type 1 RIPs toxicities to NB100 cells

EC <sub>50</sub> (M)				
<b>Ebulin 1</b>	<b>Nigrin b</b>	<b>Ricin</b>	<b>Stenodactylin</b>	<b>Saporin</b>
2.0×10 <sup>-8</sup>	1.4×10 <sup>-8</sup>	6.5×10 <sup>-13</sup>	2.5×10 <sup>-14</sup>	1.8×10 <sup>-11</sup>

### 5.1.3 Evaluation of cell death

Because the non-toxic type 2 RIPs exhibited low cytotoxicity, the experiments were conducted with a concentration that was 10 times higher than the IC<sub>50</sub>, corresponding to 10<sup>-7</sup> M.

To understand the cell death mechanism induced by *ebulin 1* and *nigrin b*, NB100 cells were stained with Annexin V-EGFP/PI and analyzed by flow cytometry. PI-positive cells are in the upper left quadrant, while cells in late and early apoptosis are in the upper and lower right quadrants, respectively. After a 48 h of intoxication, more than 10% of the treated cells were in the late apoptosis stage; this percentage increased with time, reaching 35.8% and 31.2% for *ebulin 1* and *nigrin b*, respectively. Interestingly, a small percentage of cells (higher in *nigrin b*-treated cells) were only positive for PI, suggesting death through a mechanism other than apoptosis (Fig. 5.4).

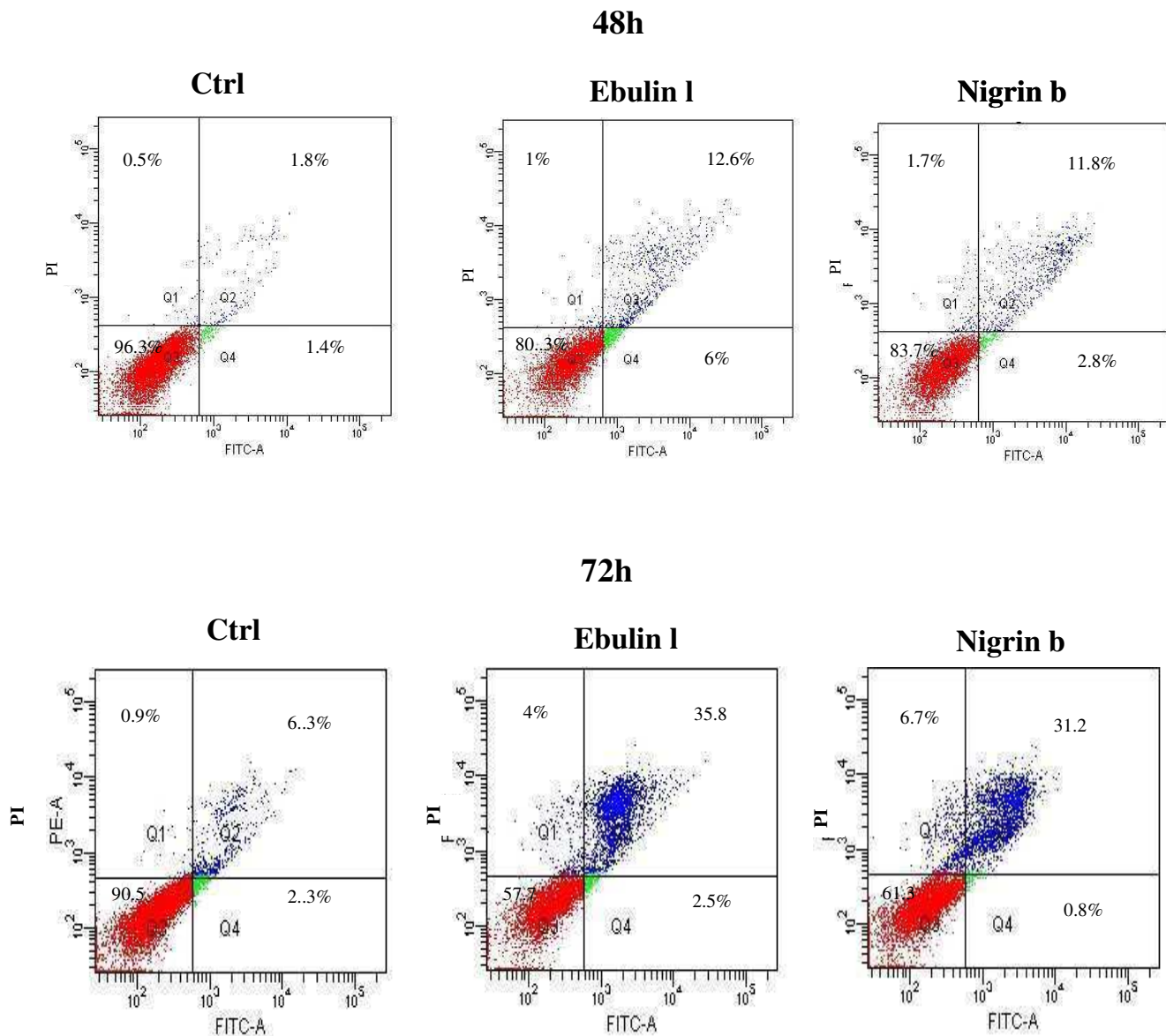


**Fig. 5.4.** Apoptosis as detected with Annexin V-EGFP/PI staining followed by flow cytometry analysis. Representative plots of Annexin V-EGFP/PI staining of NB100 cells cultured in the absence or presence of ebulin I ( $10^{-7}$  M) and nigrin b ( $10^{-7}$  M) at 48 h and 72 h.

To evaluate whether ebulin I and nigrin b could induce caspase-dependent apoptosis, caspase 3/7 activation was assessed at different time points. The results showed that the two RIPs activated caspases 3/7 in a time-dependent manner. The effector caspases became significantly activated after 8 h of intoxication and increased exponentially over time, reaching 700% and 450% with ebulin I and nigrin b, respectively, after 24 h of intoxication (Fig. 5.5).

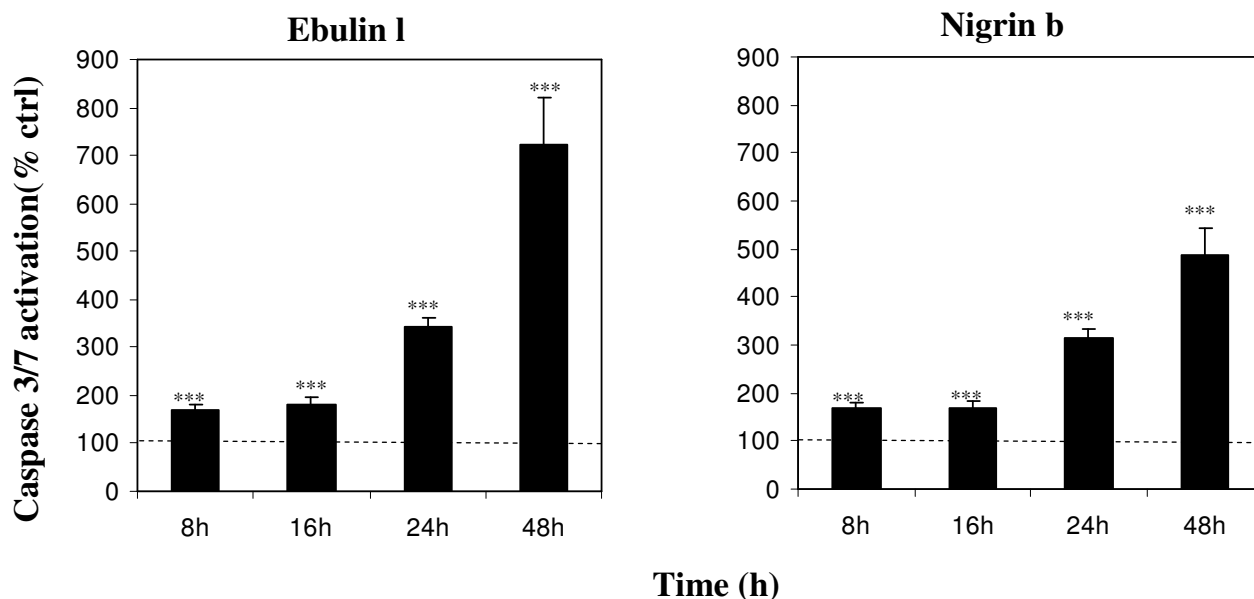


**Fig. 5.5.** Caspases 3/7 activation in NB100 cells treated with ebulin I ( $10^{-7}$  M) and nigrin b ( $10^{-7}$  M). Caspase activity was expressed as the percentage of control values obtained from cultures grown in the absence of RIPs. Means results  $\pm$  S.D are reported. The asterisk indicate level of significance in ANOVA Dunnett's test (\*\*\*)  $p=0.001$ ).

Previous studies, reported in chapter 4, have shown that stenodactylin and ricin, at their  $IC_{50}$  concentration, could induce caspases 3/7 activation in NB100 cells after 4 h of exposition to the toxin, whereas with saporin, the effector caspases began being significantly activated after 16 h of exposure to the toxin.

Comparing the caspase 3/7 activity after 24 h with stenodactylin, ricin, and saporin and the non-toxic type 2 RIPs, the activation of effector caspases was much lower with ebulin I and nigrin b than with the other RIPs, including saporin (Table 5.4). These results suggest that ebulin I and nigrin b induce a caspase-dependent apoptosis but require longer time than the type 2 RIPs, not to initiate activation but to significantly induce caspases activation.

**Table 5.4.** Caspase 3/7 activation of type 2 RIP (toxic and non-toxic) and type 1 RIP after 24 h of treatment

Caspase 3/7 activation (24h)				
Ebulin I	Nigrin b	Ricin	Stenodactylin	Saporin
342%	316 %	1164%	1484%	631%

To evaluate the role of different cytotoxic mechanisms induced by the Sambucus toxins, NB100 cells were pretreated with two inhibitors, the pan-caspase inhibitor Z-Vad and the inhibitor of necroptosis, necrostatin-1 (Fig 5.6).

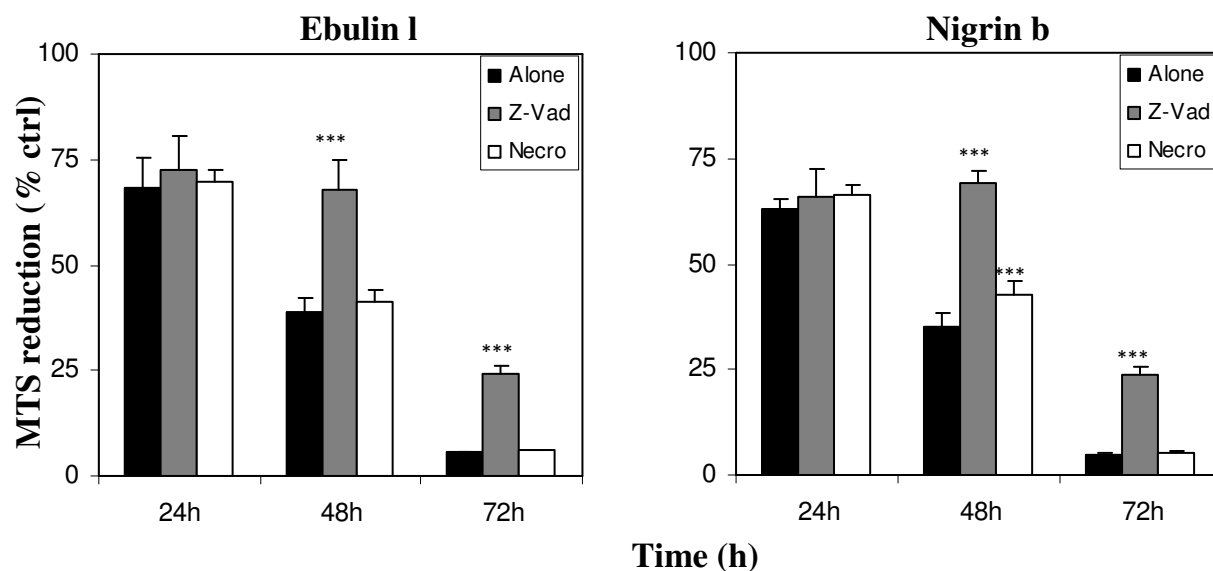


**Fig 5.6.** Time-course experiments with NB100 cells exposed to ebulin l ( $10^{-7}$  M) and nigrin b ( $10^{-7}$  M) after a pretreatment with  $100\mu\text{M}$  necrostatin (Necro) or  $100\mu\text{M}$  Z-Vad or exposed to RIP alone. The inhibitors were added every 24 h Viability was evaluated at the indicate times with a colorimetric assay based on MTS reduction. The results are the means of three independent experiments, with each performed in triplicate, and are presented as the percentage of control values obtained from cultures grown in the absence of RIPs. Asterisks indicate level of significance in ANOVA, Dunnett's test (\*\*\*) $p=0.001$ .

Surprisingly, these preliminary results showed that at 24 h, there was no difference in viability in the presence or absence of the inhibitors. At 48 h and 72 h, the presence of Z-Vad improved cell survival. In particularly, at 48 h, viability increased from 39% to 68% in ebulin l-treated cells and from 35% to 69% in nigrin b-treated cells, whereas at 72 h viability increased from 5% to 24% in ebulin l- and nigrin b-treated cells. In contrast, necrostatin did not rescue ebulin l-induced cell death, whereas a slight, but significant, protective effect was observed after 48 h of treatment with nigrin b. However, the rescue observed was much lower than the rescue observed with Z-Vad. These data suggest that the cell death mechanism induced by non-toxic type 2 RIPs is partially due to a caspase-dependent apoptotic pathway. However, because Z-Vad does not provide total protection and because necrostatin-1 offers little or no protection, a different type of cell death, in addition to apoptosis, should be present in NB100 cells treated with ebulin l, and nigrin b. Necrosis or necroptosis may be partially involved in cell death mechanism.

When L540 cells are incubated with saporin and ricin, Z-Vad caused a strong improvement in cell survival (Polito *et al.*, 2009a). A strong protective effect of Z-Vad has been observed also in NB100 cells treated with stenodactylin (Chapter 4). In treated L540 and NB100, the effect of necrostatin-1 was smaller than the effect observed with Z-Vad. Taking together, these observations and the data for caspases 3/7 suggest that in stenodactylin-, ricin- and saporin-treated cells, the apoptotic pathway is the faster, dominant cell death mechanism, whereas the same is not observed for ebulin l- and nigrin b- treated cells.

*Chapter 6*

**Conclusions**

RIPs are a family of plant proteins that damage ribosomes, with consequent arrest of protein synthesis. Although various pathways have been proposed by which type 1 and type 2 RIPs can trigger cell death, the detailed molecular mechanisms are still unclear.

The purpose of this research project was to increase the knowledge about the most toxic type 2 RIPs stenodactylin (by studying the amino acid sequence and its cytotoxic effect), and the pathogenic effect of non-toxic type 2 RIPs ebulin I and nigrin B.

**The amino acid sequence of stenodactylin** showed a high degree of identity with volkensin and with amino acid residues that are involved in the active site of both type 1 RIPs and the A chain of type 2 RIPs. The carbohydrate-binding sites of the B chain were highly homologous between stenodactylin and the other RIPs. The B chain of stenodactylin contains a positive charge in the 2 $\gamma$  binding site; substitution for this charge seems to be correlated with the lower cytotoxicity of other RIPs. Moreover, a phylogenetic tree showed that the B chain of stenodactylin is more related to non toxic type 2 RIPs than to ricin. Both results are surprising because stenodactylin is actually the most toxic type 2 RIP.

The knowledge of the amino acid sequence of stenodactylin will allow studies of site-directed mutagenesis to construct less immunogenic recombinant immunotoxins and to identify the residues that underlie its high cytotoxicity. Moreover, the amino acid sequence, together with the previously published crystallographic analysis, will be used to determinate the three-dimensional structure, which could further clarify the molecular basis of the high toxicity of this protein.

**The studies on the cell death mechanisms induced by stenodactylin** on NB100 cells showed that high doses of this toxin can activate the effector caspases (perhaps through the DNA damage and/or intrinsic/extrinsic pathways) and also causes ROS generation, which appear to be important mediators of stenodactylin-induced cell death. The results suggest that the production of ROS in stenodactylin-treated cells mainly causes caspase-dependent apoptosis, but other cell death mechanisms, such as necroptosis, are also induced. These results indicate that stenodactylin induces damage as a consequence of a multi-directional pathway, and apoptosis appears to be the fastest and most strongly induced cell death mechanism.

Testing low doses of stenodactylin, ricin and saporin has allowed us to observe that the caspases activation is independent from the inhibition of protein synthesis. Moreover, the

extrinsic apoptotic pathway seems to be the main mechanism that is activated in stenodactylin- treated cells.

Future studies will clarify the alternative cell death mechanisms induced by low doses of stenodactylin, for example, by studying the expression of genes that are involved in necroptosis or other cell death pathways (e.g., autophagy). The same studies will be conducted in various cell lines because different cell lines show different sensitivity to RIPs, most likely due to the induction of alternative cell death mechanisms. Because several factors that affect cell machinery could be responsible for cell death, a better knowledge of the cell death mechanisms induced by stenodactylin may have important consequences for its medicinal use.

**The assessment of toxicity induced by ebulin I and nigrin b** showed a strong enzymatic activity in a cell-free system compared with ricin, stenodactylin and saporin but a low cytotoxic effect on NB100 cells even when compared with saporin. The two non-toxic type 2 RIPs induced the activation of caspases 3/7 but to a lower extent than the other RIPs. These preliminary studies showed that caspase-dependent apoptosis is only partially involved in the cell death mechanism induced by ebulin I and nigrin b. Moreover, nigrin b caused a slight but significant activation of the necroptotic pathway.

Future studies are required to understand the other cell death mechanisms induced by ebulin I and nigrin b, and the involvement of reactive oxygen species and autophagy.

*Chapter 7*

**Bibliography**

- Bagga S, Hosur MV, Batra JK. Cytotoxicity of ribosome-inactivating protein saporin is not mediated through alpha2-macroglobulin receptor. *FEBS Lett.* 2003a Apr 24;541(1-3):16-20.
- Bagga S, Seth D, Batra JK. The cytotoxic activity of ribosome-inactivating protein saporin-6 is attributed to its rRNA N-glycosidase and internucleosomal DNA fragmentation activities. *J Biol Chem.* 2003b Feb 14;278(7):4813-20.
- Balint GA. Ricin: the toxic protein of castor oil seeds. *Toxicology.* 1974 Mar;2(1):77-102.
- Barbieri L, Battelli MG, Stirpe F. Ribosome-inactivating proteins from plants. *Biochim Biophys Acta.* 1993 Dec 21;1154(3-4):237-82. Review.
- Barbieri L, Gasperi-Campani A, Derenzini M, Betts CM, Stirpe F. Selective lesions of acinar pancreatic cells in rats poisoned with abrin. A morphological and biochemical study. *Virchows Arch B Cell Pathol Incl Mol Pathol.* 1979 May 4;30(1):15-24.
- Barbieri L, Gorini P, Valbonesi P, Castiglioni P, Stirpe F. Unexpected activity of saporins. *Nature.* 1994 Dec 15;372(6507):624.
- Barbieri L, Stoppa C, Bolognesi A. Large scale chromatographic purification of ribosome-inactivating proteins. *J. Chromat. A.* 1987; 408: 235-243.
- Barbieri L, Valbonesi P, Bondioli M, Alvarez ML, Dal Monte P, Landini MP, Stirpe F. Adenine glycosylase activity in mammalian tissues: an equivalent of ribosome-inactivating proteins. *FEBS Lett.* 2001 Sep 7;505(1):196-7.
- Barbieri L, Valbonesi P, Bonora E, Gorini P, Bolognesi A, Stirpe F. Polynucleotide:adenosine glycosidase activity of ribosome-inactivating proteins: effect on DNA, RNA and poly(A). *Nucleic Acids Res.* 1997 Feb 1;25(3):518-22.
- Barbieri L, Valbonesi P, Righi F, Zuccheri G, Monti F, Gorini P, Samorí B, Stirpe F. Polynucleotide:Adenosine glycosidase is the sole activity of ribosome-inactivating proteins on DNA. *J Biochem.* 2000 Nov;128(5):883-9.
- Battelli MG, Barbieri L, Stirpe F. Toxicity of, and histological lesions caused by, ribosome-inactivating proteins, their IgG-conjugates, and their homopolymers. *APMIS.* 1990 Jul;98(7):585-93.
- Battelli MG, Citores L, Buonamici L, Ferreras JM, de Benito FM, Stirpe F, Girbés T. Toxicity and cytotoxicity of nigrin b, a two-chain ribosome-inactivating protein from *Sambucus nigra*: comparison with ricin. *Arch Toxicol.* 1997;71(6):360-4.
- Battelli MG, Musiani S, Buonamici L, Santi S, Riccio M, Maraldi NM, Girbés T, Stirpe F. Interaction of volkensin with HeLa cells: binding, uptake, intracellular localization, degradation and exocytosis. *Cell Mol Life Sci.* 2004 Aug;61(15):1975-84.
- Battelli MG, Scicchitano V, Polito L, Farini V, Barbieri L, Bolognesi A. Binding and intracellular routing of the plant-toxic lectins, lanceolin and stenodactylin. *Biochim Biophys Acta.* 2010 Dec;1800(12):1276-82.
- Bell BD, Leverrier S, Weist BM, Newton RH, Arechiga AF, Luhrs KA, Morrissette NS, Walsh CM. FADD and caspase-8 control the outcome of autophagic signaling in proliferating T cells. *Proc Natl Acad Sci U S A.* 2008 Oct 28;105(43):16677-82.
- Benítez J, Ferreras JM, Muñoz R, Arias Y, Iglesias R, Córdoba-Díaz M, del Villar R, Girbés T. Cytotoxicity of an ebulin I-anti-human CD105 immunotoxin on mouse fibroblasts (L929) and rat myoblasts (L6E9) cells expressing human CD105. *Med Chem.* 2005 Jan;1(1):65-70.
- Bergamaschi G, Perfetti V, Tonon L, Novella A, Lucotti C, Danova M, Glennie MJ, Merlini G, Cazzola M. Saporin, a ribosome-inactivating protein used to prepare immunotoxins, induces cell death via apoptosis. *Br J Haematol.* 1996 Jun;93(4):789-94.

- Bhaskar AS, Deb U, Kumar O, Lakshmana Rao PV. Abrin induced oxidative stress mediated DNA damage in human leukemic cells and its reversal by N-acetylcysteine. *Toxicol In Vitro*. 2008 Dec;22(8):1902-8.
- Bolognesi A, Polito L, Scicchitano V, Orrico C, Pasquinelli G, Musiani S, Santi S, Riccio M, Bortolotti M, Battelli MG. Endocytosis and intracellular localisation of type 1 ribosome-inactivating protein saporin-s6. *J Biol Regul Homeost Agents*. 2012 Jan-Mar;26(1):97-109.
- Bolognesi A, Polito L. Immunotoxins and other conjugates: pre-clinical studies. *Mini Rev Med Chem*. 2004 Jun;4(5):563-83. Review.
- Bolognesi A, Tazzari PL, Olivieri F, Polito L, Falini B, Stirpe F. Induction of apoptosis by ribosome-inactivating proteins and related immunotoxins. *Int J Cancer*. 1996 Nov 4;68(3):349-55.
- Bonapace L, Bornhauser BC, Schmitz M, Cario G, Ziegler U, Niggli FK, Schäfer BW, Schrappe M, Stanulla M, Bourquin JP. Induction of autophagy-dependent necroptosis is required for childhood acute lymphoblastic leukemia cells to overcome glucocorticoid resistance. *J Clin Invest*. 2010 Apr;120(4):1310-23.
- Bora N, Gadadhar S, Karande AA. Signaling different pathways of cell death: Abrin induced programmed necrosis in U266B1 cells. *Int J Biochem Cell Biol*. 2010 Dec;42(12):1993-2003.
- Brigotti M, Alfieri R, Sestili P, Bonelli M, Petronini PG, Guidarelli A, Barbieri L, Stirpe F, Sperti S. Damage to nuclear DNA induced by Shiga toxin 1 and ricin in human endothelial cells. *FASEB J*. 2002 Mar;16(3):365-72.
- Büssing A, Suzart K, Bergmann J, Pfüller U, Schietzel M, Schweizer K. Induction of apoptosis in human lymphocytes treated with *Viscum album L.* is mediated by the mistletoe lectins. *Cancer Lett*. 1996 Jan 19;99(1):59-72.
- Büssing A, Wagner M, Wagner B, Stein GM, Schietzel M, Schaller G, Pfüller U. Induction of mitochondrial Apo2.7 molecules and generation of reactive oxygen-intermediates in cultured lymphocytes by the toxic proteins from *Viscum album L.* *Cancer Lett*. 1999 May 3;139(1):79-88.
- Byers VS, Levin AS, Waites LA, Starrett BA, Mayer RA, Clegg JA, Price MR, Robins RA, Delaney M, Baldwin RW. A phase I/II study of trichosanthin treatment of HIV disease. *AIDS*. 1990 Dec;4(12):1189-96.
- Carzaniga R, Sinclair L, Fordham-Skelton AP, Harris N, Croy RRD. Cellular and subcellular distribution of saporins, type-1 ribosome-inactivating proteins in soapwort (*Saponaria officinalis L.*). *Planta*. 1994 ;194:461-470.
- Cavallaro U, Soria MR. Targeting plant toxins to the urokinase and alpha 2-macroglobulin receptors. *Semin Cancer Biol*. 1995 Oct;6(5):269-78. Review.
- Chambery A, Di Maro A, Monti MM, Stirpe F, Parente A. Volkensin from *Adenia volkensii* Harms (kilyambiti plant), a type 2 ribosome-inactivating protein. *Eur J Biochem*. 2004 Jan;271(1):108-17.
- Chow TP, Feldman RA, Lovett M, Piatak M. Isolation and DNA sequence of a gene encoding alpha-trichosanthin, a type I ribosome-inactivating protein. *J Biol Chem*. 1990 May 25;265(15):8670-4.
- Christiansen SP, Peterson D, To T, Youle R, McLoon L. Long-term effects of ricin-mAb 35 on extraocular muscles of rabbits: potential treatment for strabismus. *Invest Ophthalmol Vis Sci*. 2002 Mar;43(3):679-85.
- Christofferson DE, Yuan J. Necroptosis as an alternative form of programmed cell death. *Curr Opin Cell Biol*. 2010 Apr;22(2):263-8.
- Citores L, Ferreras JM, Muñoz R, Benítez J, Jiménez P, Girbés T. Targeting cancer cells with transferrin conjugates containing the non-toxic type 2 ribosome-inactivating proteins nigrin b or ebulin l. *Cancer Lett*. 2002 Oct 8;184(1):29-35.
- Citores L, Muñoz R, De Benito FM, Iglesias R, Ferreras JM, Girbes T. Differential sensitivity of HELA cells to the type 2 ribosome-inactivating proteins ebulin l, nigrin b and nigrin f as compared with ricin. *Cell Mol Biol (Noisy-le-grand)*. 1996 Jun;42(4):473-6.

- Colombatti M, Colombatti A, Blythman HE, Bron C. Thy 1.2+ leukemia cells eradicated from in vitro leukemia-bone marrow cell mixtures by antibody-toxin conjugates. *J Natl Cancer Inst.* 1984 May;72(5):1095-9.
- Das MK, Sharma RS, Mishra V. Induction of apoptosis by ribosome inactivating proteins: importance of N-glycosidase activity. *Appl Biochem Biotechnol.* 2012 Mar;166(6):1552-61.
- de la Cruz RR, Baker R, Delgado-García JM. Behavior of cat abducens motoneurons following the injection of toxic ricin into the lateral rectus muscle. *Brain Res.* 1991 Mar 29;544(2):260-8.
- Declercq W, Vanden Berghe T, Vandenabeele P. RIP kinases at the crossroads of cell death and survival. *Cell.* 2009 Jul 23;138(2):229-32. doi: 10.1016/j.cell.2009.07.006. Review.
- Deeks ED, Cook JP, Day PJ, Smith DC, Roberts LM, Lord JM. The low lysine content of ricin A chain reduces the risk of proteolytic degradation after translocation from the endoplasmic reticulum to the cytosol. *Biochemistry.* 2002 Mar 12;41(10):3405-13.
- Degterev A, Huang Z, Boyce M, Li Y, Jagtap P, Mizushima N, Cuny GD, Mitchison TJ, Moskowitz MA, Yuan J. Chemical inhibitor of nonapoptotic cell death with therapeutic potential for ischemic brain injury. *Nat Chem Biol.* 2005 Jul;1(2):112-9. Epub 2005 May 29.
- Derenzini M, Bonetti E, Marionozzi V, Stirpe F. Toxic effects of ricin: studies on the pathogenesis of liver lesions. *Virchows Arch B Cell Pathol.* 1976 Feb 11;20(1):15-28.
- Di R, Kyu E, Shete V, Saidasan H, Kahn PC, Tumer NE. Identification of aminoacids critical for the cytotoxicity of Shiga toxin 1 and 2 in *Saccharomyces cerevisiae*. *Toxicon.* 2011 Mar 15;57(4):525-39.
- Duggar B.M. and Armstrong J.K. (1925). The effect of treating the virus of tobacco mosaic with the juices of various plants. *Ann. Missouri Bot. Gard.* 12: 359-366.
- Dumas M, Schwab ME, Thoenen H. Retrograde axonal transport of specific macromolecules as a tool for characterizing nerve terminal membranes. *J Neurobiol.* 1979 Mar;10(2):179-97.
- Eiklid K, Olsnes S, Pihl A. Entry of lethal doses of abrin, ricin and modeccin into the cytosol of HeLa cells. *Exp Cell Res.* 1980 Apr;126(2):321-6.
- Endo Y, Mitsui K, Motizuki M, Tsurugi K. The mechanism of action of ricin and related toxic lectins on eukaryotic ribosomes. The site and the characteristics of the modification in 28 S ribosomal RNA caused by the toxins. *J Biol Chem.* 1987 Apr 25;262(12):5908-12.
- Fernández-Puentes C, Carrasco L. Viral infection permeabilizes mammalian cells to protein toxins. *Cell.* 1980 Jul;20(3):769-75.
- Ferreras JM, Barbieri L, Girbés T, Battelli MG, Rojo MA, Arias FJ, Rocher MA, Soriano F, Mendéz E, Stirpe F. Distribution and properties of major ribosome-inactivating proteins (28 S rRNA N-glycosidases) of the plant *Saponaria officinalis* L. (Caryophyllaceae). *Biochim Biophys Acta.* 1993 Oct 19;1216(1):31-42.
- Ferreras JM, Citores L, Iglesias R, Jiménez P, Girbés T. Sambucus Ribosome-Inactivating Proteins and Lectins. Toxic Plant Proteins. *Plant Cell Monographs.* 2010, 18:107-131.
- Ferreras JM, Citores L, Iglesias R, Jiménez P, Girbés T. Use of ribosome-inactivating proteins from sambucus for the construction of immunotoxins and conjugates for cancer therapy. *Toxins (Basel).* 2011 May;3(5):420-41.
- Filipovich AH, Vallera DA, Youle RJ, Quinones RR, Neville DM Jr, Kersey JH. Ex-vivo treatment of donor bone marrow with anti-T-cell immunotoxins for prevention of graft-versus-host disease. *Lancet.* 1984 Mar 3;1(8375):469-72.
- Foà-Tomasi L, Campadelli-Fiume G, Barbieri L, Stirpe F. Effect of ribosome-inactivating proteins on virus-infected cells. Inhibition of virus multiplication and of protein synthesis. *Arch Virol.* 1982;71(4):323-32.

- Frankel A, Welsh P, Richardson J, Robertus JD. Role of arginine 180 and glutamic acid 177 of ricin toxin A chain in enzymatic inactivation of ribosomes. *Mol Cell Biol*. 1990 Dec;10(12):6257-63.
- Frankel AE, Neville DM, Bugge TA, Kreitman RJ, Leppla SH. Immunotoxin therapy of hematologic malignancies. *Semin Oncol*. 2003 Aug;30(4):545-57. Review.
- Gayoso MJ, Muñoz R, Arias Y, Villar R, Rojo MA, Jiménez P, Ferreras JM, Aranguez I, Gírbés T. Specific dose-dependent damage of Lieberkühn crypts promoted by large doses of type 2 ribosome-inactivating protein nigrin b intravenous injection to mice. *Toxicol Appl Pharmacol*. 2005 Sep 1;207(2):138-46.
- Gírbés T, Citores L, Ferreras JM, Rojo MA, Iglesias R, Muñoz R, Arias FJ, Calonge M, García JR, Méndez E. Isolation and partial characterization of nigrin b, a non-toxic novel type 2 ribosome-inactivating protein from the bark of *Sambucus nigra* L. *Plant Mol Biol*. 1993(a) Sep;22(6):1181-6.
- Gírbés T, Citores L, Iglesias R, Ferreras JM, Muñoz R, Rojo MA, Arias FJ, García JR, Méndez E, Calonge M. Ebulin 1, a nontoxic novel type 2 ribosome-inactivating protein from *Sambucus ebulus* L. leaves. *J Biol Chem*. 1993(b) Aug 25;268(24):18195-9.
- Girbes T, Ferreras JM, Arias FJ, Muñoz R, Iglesias R, Jimenez P, Rojo MA, Arias Y, Perez Y, Benitez J, Sanchez D, Gayoso MJ. Non-toxic type 2 ribosome-inactivating proteins (RIPs) from *Sambucus*: occurrence, cellular and molecular activities and potential uses. *Cell Mol Biol (Noisy-le-grand)*. 2003 Jun;49(4):537-45. Review.
- Gírbés T, Ferreras JM, Arias FJ, Stirpe F. Description, distribution, activity and phylogenetic relationship of ribosome-inactivating proteins in plants, fungi and bacteria. *Mini Rev Med Chem*. 2004 Jun;4(5):461-76. Review.
- Glennie MJ, McBride HM, Stirpe F, Thorpe PE, Worth AT, Stevenson GT. Emergence of immunoglobulin variants following treatment of a B cell leukemia with an immunotoxin composed of antiidiotypic antibody and saporin. *J Exp Med*. 1987 Jul 1;166(1):43-62.
- Görschen E, Dunaeva M, Hause B, Reeh I, Wasternack C, Parthier B. Expression of the ribosome-inactivating protein JIP60 from barely in transgenic tobacco leads to an abnormal phenotype and alterations on the level of translation. *Planta*. 1997;202(4):470-8.
- Grasso S, Shepherd RJ. Isolation and partial characterization of virus inhibitors from plants species taxonomically related to *Phytolacca*. *Phytopathol*. 1978; 68: 199-205.
- Griffiths GD, Leek MD, Gee DJ. The toxic plant proteins ricin and abrin induce apoptotic changes in mammalian lymphoid tissues and intestine. *J Pathol*. 1987 Mar;151(3):221-9.
- Gu YJ, Xia ZX. Crystal structures of the complexes of trichosanthin with four substrate analogs and catalytic mechanism of RNA N-glycosidase. *Proteins*. 2000 Apr 1;39(1):37-46.
- Günther C, Neumann H, Neurath MF, Becker C. Apoptosis, necrosis and necroptosis: cell death regulation in the intestinal epithelium. *Gut*. 2012 Jun 27.
- Hajto T, Hostanska K, Frei K, Rordorf C, Gabius HJ. Increased secretion of tumor necrosis factors alpha, interleukin 1, and interleukin 6 by human mononuclear cells exposed to beta-galactoside-specific lectin from clinically applied mistletoe extract. *Cancer Res*. 1990 Jun 1;50(11):3322-6.
- Hao Q, Van Damme EJ, Hause B, Barre A, Chen Y, Rougé P, Peumans WJ. Iris bulbs express type 1 and type 2 ribosome-inactivating proteins with unusual properties. *Plant Physiol*. 2001 Feb;125(2):866-76.
- Harper CG, Gonatas JO, Mizutani T, Gonatas NK. Retrograde transport and effects of toxic ricin in the autonomic nervous system. *Lab Invest*. 1980 Apr;42(4):396-404.
- Hasegawa N, Kimura Y, Oda T, Komatsu N, Muramatsu T. Isolated ricin B-chain-mediated apoptosis in U937 cells. *Biosci Biotechnol Biochem*. 2000 Jul;64(7):1422-9.

- Hatakeyama T, Yamasaki N, Funatsu G. Identification of the tryptophan residue located at the low-affinity saccharide binding site of ricin D. *J Biochem.* 1986 Sep;100(3):781-8.
- Henry MA, Westrum LE, Johnson LR, Canfield RC. Ultrastructure of degenerative changes following ricin application to feline dental pulps. *J Neurocytol.* 1987 Oct;16(5):601-11.
- Hino M, Sekizawa T, Openshaw H. Ricin injection eliminates latent herpes simplex virus in the mouse. *J Infect Dis.* 1988 Jun;157(6):1270-1.
- Horrix C, Raviv Z, Flescher E, Voss C, Berger MR. Plant ribosome-inactivating proteins type II induce the unfolded protein response in human cancer cells. *Cell Mol Life Sci.* 2011 Apr;68(7):1269-81.
- Hossann M, Li Z, Shi Y, Kreilinger U, Büttner J, Vogel PD, Yuan J, Wise JG, Trommer WE. Novel immunotoxin: a fusion protein consisting of gelonin and an acetylcholine receptor fragment as a potential immunotherapeutic agent for the treatment of Myasthenia gravis. *Protein Expr Purif.* 2006 Mar;46(1):73-84.
- Hott JS, Dalakas MC, Sung C, Hallett M, Youle RJ. Skeletal muscle-specific immunotoxin for the treatment of focal muscle spasm. *Neurology.* 1998 Feb;50(2):485-91.
- Hu R, Zhai Q, Liu W, Liu X. An insight into the mechanism of cytotoxicity of ricin to hepatoma cell: roles of Bcl-2 family proteins, caspases, Ca(2+)-dependent proteases and protein kinase C. *J Cell Biochem.* 2001;81(4):583-93.
- Huang J, Lam GY, Brumell JH. Autophagy signalling through reactive oxygen species. *Antioxidants & Redox Signaling.* 2011, 14 (11): 2215-31.
- Hudak KA, Bauman JD, Tumer NE. Pokeweed antiviral protein binds to the cap structure of eukaryotic mRNA and depurinates the mRNA downstream of the cap. *RNA.* 2002 Sep;8(9):1148-59.
- Hughes JN, Lindsay CD, Griffiths GD. Morphology of ricin and abrin exposed endothelial cells is consistent with apoptotic cell death. *Hum Exp Toxicol.* 1996 May;15(5):443-51.
- Hur Y, Hwang DJ, Zoubenko O, Coetzer C, Uckun FM, Tumer NE. Isolation and characterization of pokeweed antiviral protein mutations in *Saccharomyces cerevisiae*: identification of residues important for toxicity. *Proc Natl Acad Sci U S A.* 1995 Aug 29;92(18):8448-52.
- Jiménez P, Gayoso M, Tejero J, Cabrero P, Córdoba-Díaz D, Basterrechea JE, Gírbés T. Toxicity in mice of lectin ebulin f present in dwarf Elderberry (*Sambucus ebulus* L.). *Toxicon.* 2013 Jan;61:26-9.
- Kabeya Y, Mizushima N, Ueno T, Yamamoto A, Kirisako T, Noda T, Kominami E, Ohsumi Y, Yoshimori T. LC3, a mammalian homologue of yeast Apg8p, is localized in autophagosome membranes after processing. *EMBO J.* 2000 Nov 1;19(21):5720-8.
- Kalb VF Jr, Bernlohr RW. A new spectrophotometric assay for protein in cell extracts. *Anal Biochem.* 1977 Oct;82(2):362-71.
- Katzin BJ, Collins EJ, Robertus JD. Structure of ricin A-chain at 2.5 Å. *Proteins.* 1991;10(3):251-9.
- Kim MS, Lee J, Lee KM, Yang SH, Choi S, Chung SY, Kim TY, Jeong WH, Park R. Involvement of hydrogen peroxide in mistletoe lectin-II-induced apoptosis of myeloleukemic U937 cells. *Life Sci.* 2003 Jul 25;73(10):1231-43.
- Kochi SK, Collier RJ. DNA fragmentation and cytolysis in U937 cells treated with diphtheria toxin or other inhibitors of protein synthesis. *Exp Cell Res.* 1993 Sep;208(1):296-302.
- Kurinov IV, Rajamohan F, Venkatachalam TK, Uckun FM. X-ray crystallographic analysis of the structural basis for the interaction of pokeweed antiviral protein with guanine residues of ribosomal RNA. *Protein Sci.* 1999 Nov;8(11):2399-405.

- Lam SK, Ng TB. First simultaneous isolation of a ribosome inactivating protein and an antifungal protein from a mushroom (*Lyophyllum shimeji*) together with evidence for synergism of their antifungal effects. *Arch Biochem Biophys*. 2001 Sep 15;393(2):271-80.
- Langer M, Möckel B, Eck J, Zinke H, Lentzen H. Site-specific mutagenesis of mistletoe lectin: the role of RIP activity in apoptosis. *Biochem Biophys Res Commun*. 1999 Nov 2;264(3):944-8.
- Lehar SM, Pedersen JT, Kamath RS, Swimmer C, Goldmacher VS, Lambert JM, Blättler WA, Guild BC. Mutational and structural analysis of the lectin activity in binding domain 2 of ricin B chain. *Protein Eng*. 1994 Oct;7(10):1261-6.
- Li H, Zhu H, Xu CJ, Yuan J. Cleavage of BID by caspase 8 mediates the mitochondrial damage in the Fas pathway of apoptosis. *Cell*. 1998 Aug 21;94(4):491-501.
- Li J, Xia X, Ke Y, Nie H, Smith MA, Zhu X. Trichosanthin induced apoptosis in HL-60 cells via mitochondrial and endoplasmic reticulum stress signalling pathways. *Biochim Biophys Acta*. 2007 Aug;1770(8):1169-80.
- Li XP, Baricevic M, Saidasan H, Tumer NE. Ribosome depurination is not sufficient for ricin-mediated cell death in *Saccharomyces cerevisiae*. *Infect Immun*. 2007 Jan;75(1):417-28. Epub 2006 Nov 13.
- Licastro F, Morini MC, Bolognesi A, Stirpe F. Ricin induces the production of tumour necrosis factor-alpha and interleukin-1 beta by human peripheral-blood mononuclear cells. *Biochem J*. 1993 Sep 1;294 ( Pt 2):517-20.
- Lin JY, Tserng KY, Chen CC, Lin LT, Tung TC. Abrin and ricin: new anti-tumour substances. *Nature*. 1970 Jul 18;227(5255):292-3.
- Ling J, Liu WY, Wang TP. Cleavage of supercoiled double-stranded DNA by several ribosome-inactivating proteins in vitro. *FEBS Lett*. 1994 May30;345(2-3):143-6.
- Liu RS, Yang JH, Liu WY. Isolation and enzymatic characterization of lamjapin, the first ribosome-inactivating protein from cryptogamic algal plant (*Laminaria japonica* A). *Eur J Biochem*. 2002 Oct;269(19):4746-52.
- Lord JM, Roberts LM, Robertus JD. Ricin: structure, mode of action, and some current applications. *FASEB J*. 1994 Feb;8(2):201-8. Review.
- Lu PX, Jin YC. Ectopic pregnancy treated with trichosanthin. Clinical analysis of 71 patients. *Chin Med J (Engl)*. 1989 May;102(5):365-7.
- Madan S, Ghosh PC. Interaction of gelonin with macrophages: effect of lysosomotropic amines. *Exp Cell Res*. 1992 Jan;198(1):52-8.
- Masuda S, Sakuta C, Satoh S. cDNA cloning of a novel lectin-like xylem sap protein and its root-specific expression in cucumber. *Plant Cell Physiol*. 1999 Nov;40(11):1177-81.
- McGrath MS, Santulli S, Gaston I. Effects of GLQ223 on HIV replication in human monocyte/macrophages chronically infected in vitro with HIV. *AIDS Res Hum Retroviruses*. 1990 Aug;6(8):1039-43.
- Mehta AD, Boston RS. Ribosome-inactivating protein. In *A Look beyond Transcription: Mechanisms Determining mRNA Stability and Translation in Plants*. Eds Bailey-Serres J, Gallie DR (American Society of Plant Physiologists, Rockville, MD) 1998:145-152.
- Mlsna D, Monzingo AF, Katzin BJ, Ernst S, Robertus JD. Structure of recombinant ricin A chain at 2.3 Å. *Protein Sci*. 1993 Mar;2(3):429-35.
- Montanaro L, Sperti S, Mattioli A, Testoni G, Stirpe F. Inhibition by ricin of protein synthesis in vitro. Inhibition of the binding of elongation factor 2 and of adenosine diphosphate-ribosylated elongation factor 2 to ribosomes. *Biochem J*. 1975 Jan;146(1):127-31.
- Montanaro L, Sperti S, Stirpe F. Inhibition by ricin of protein synthesis in vitro. Ribosomes as the target of the toxin. *Biochem J*. 1973 Nov;136(3):677-83.

- Montfort W, Villafranca JE, Monzingo AF, Ernst SR, Katzin B, Rutenber E, Xuong NH, Hamlin R, Robertus JD. The three-dimensional structure of ricin at 2.8 Å. *J Biol Chem*. 1987 Apr 15;262(11):5398-403.
- Monti B, D'Alessandro C, Farini V, Bolognesi A, Polazzi E, Contestabile A, Stirpe F, Battelli MG. In vitro and in vivo toxicity of type 2 ribosome-inactivating proteins lanceolin and stenodactylin on glial and neuronal cells. *Neurotoxicology*. 2007 May;28(3):637-44.
- Morlon-Guyot J, Helmy M, Lombard-Frasca S, Pignol D, Piéroni G, Beaumelle B. Identification of the ricin lipase site and implication in cytotoxicity. *J Biol Chem*. 2003 May 9;278(19):17006-11.
- Muñoz R, Arias Y, Ferreras JM, Jiménez P, Rojo MA, Girbés T. Sensitivity of cancer cell lines to the novel non-toxic type 2 ribosome-inactivating protein nigrin b. *Cancer Lett*. 2001 Jun 26;167(2):163-9.
- Muñoz R, Arias Y, Ferreras JM, Rojo MA, Gayoso MJ, Nocito M, Benitez J, Jiménez P, Bernabéu C, Girbés T. Targeting a marker of the tumour neovasculature using a novel anti-human CD105-immunotoxin containing the non-toxic type 2 ribosome-inactivating protein nigrin b. *Cancer Lett*. 2007 Oct 18;256(1):73-80.
- Narayanan S, Surendranath K, Bora N, Surolia A, Karande AA. Ribosome inactivating proteins and apoptosis. *FEBS Lett*. 2005 Feb 28;579(6):1324-31. Review.
- Narayanan S, Surolia A, Karande AA. Ribosome-inactivating protein and apoptosis: abrin causes cell death via mitochondrial pathway in Jurkat cells. *Biochem J*. 2004 Jan 1;377(Pt 1):233-40.
- Nicolas E, Goodyer ID, Taraschi TF. An additional mechanism of ribosome-inactivating protein cytotoxicity: degradation of extrachromosomal DNA. *Biochem J*. 1997 Oct 15;327 ( Pt 2):413-7.
- Nicolson GL, Blaustein J, Etzler ME. Characterization of two plant lectins from *Ricinus communis* and their quantitative interaction with a murine lymphoma. *Biochemistry*. 1974 Jan 1;13(1):196-204.
- Nielsen K, Boston RS. Ribosome-inactivating proteins: a plant perspective. *Annu. Rev. Physiol. Plant Mol. Biol.* (2001) 52:785-816.
- Obrig TG. Shiga toxin mode of action in *E. coli* O157:H7 disease. *Front Biosci*. 1997 Dec 15;2:d635-42. Review.
- Olmo N, Turnay J, González de Buitrago G, López de Silanes I, Gavilanes JG, Lizarbe MA. Cytotoxic mechanism of the ribotoxin alpha-sarcin. Induction of cell death via apoptosis. *Eur J Biochem*. 2001 Apr;268(7):2113-23.
- Olsnes S. Ricin and ricinus agglutinin, toxic lectins from castor bean. *Methods Enzymol*. 1978;50:330-5.
- Parikh BA, Baykal U, Di R, Tumer NE. Evidence for retro-translocation of pokeweed antiviral protein from endoplasmic reticulum into cytosol and separation of its activity on ribosomes from its activity on capped RNA. *Biochemistry*. 2005 Feb 22;44(7):2478-90.
- Pascal JM, Day PJ, Monzingo AF, Ernst SR, Robertus JD, Iglesias R, Pérez Y, Ferreras JM, Citores L, Girbés T. 2.8-Å crystal structure of a nontoxic type-II ribosome-inactivating protein, ebulin I. *Proteins*. 2001 May 15;43(3):319-26.
- Pasqualucci L, Wasik M, Teicher BA, Flenghi L, Bolognesi A, Stirpe F, Polito L, Falini B, Kadin ME. Antitumor activity of anti-CD30 immunotoxin (Ber-H2/saporin) in vitro and in severe combined immunodeficiency disease mice xenografted with human CD30+ anaplastic large-cell lymphoma. *Blood*. 1995 Apr 15;85(8):2139-46.
- Peumans WJ, Van Damme E. Evolution of plant ribosome-inactivating proteins. *Toxic plant proteins*. 2010;18: 1-26.
- Polito L, Bortolotti M, Farini V, Battelli MG, Barbieri L, Bolognesi A. Saporin induces multiple death pathways in lymphoma cells with different intensity and timing as compared to ricin. *Int J Biochem Cell Biol*. 2009a, May;41(5):1055-61.

- Polito L, Bortolotti M, Farini V, Pedrazzi M, Tazzari PL, Bolognesi A. ATG-saporin-S6 immunotoxin: a new potent and selective drug to eliminate activated lymphocytes and lymphoma cells. *Br J Haematol.* 2009b, Dec;147(5):710-8.
- Polito L, Bortolotti M, Pedrazzi M, Bolognesi A. Immunotoxins and other conjugates containing saporin-s6 for cancer therapy. *Toxins (Basel).* 2011 Jun;3(6):697-720.
- Rajamohan F, Kurinov IV, Venkatachalam TK, Uckun FM. Deguanlylation of human immunodeficiency virus (HIV-1) RNA by recombinant pokeweed antiviral protein. *Biochem Biophys Res Commun.* 1999 Sep 24;263(2):419-24.
- Rao PV, Jayaraj R, Bhaskar AS, Kumar O, Bhattacharya R, Saxena P, Dash PK, Vijayaraghavan R. Mechanism of ricin-induced apoptosis in human cervical cancer cells. *Biochem Pharmacol.* 2005 Mar 1;69(5):855-65. Epub 2005 Jan 22.
- Ready M, Wilson K, Piatak M, Robertus JD. Ricin-like plant toxins are evolutionarily related to single-chain ribosome-inhibiting proteins from *Phytolacca*. *J Biol Chem.* 1984 Dec 25;259(24):15252-6.
- Ready MP, Brown DT, Robertus JD. Extracellular localization of pokeweed antiviral protein. *Proc Natl Acad Sci U S A.* 1986 Jul;83(14):5053-6.
- Ready MP, Kim Y, Robertus JD. Site-directed mutagenesis of ricin A-chain and implications for the mechanism of action. *Proteins.* 1991;10(3):270-8.
- Reinbothe S, Reinbothe C, Lehmann J, Becker W, Apel K, Parthier B. JIP60, a methyl jasmonate-induced ribosome-inactivating protein involved in plant stress reactions. *Proc.Natl.Acad.Sci.USA.* 1994. 91:7.12-16.
- Reisbig R, Olsnes S, Eiklid K. The cytotoxic activity of Shigella toxin. Evidence for catalytic inactivation of the 60 S ribosomal subunit. *J Biol Chem.* 1981 Aug 25;256(16):8739-44.
- Rennie DP, McGregor AM, Wright J, Weetman AP, Hall R, Thorpe P. An immunotoxin of ricin A chain conjugated to thyroglobulin selectively suppresses the antithyroglobulin autoantibody response. *Lancet.* 1983 Dec 10;2(8363):1338-40.
- Roberts LM, Lamb FI, Pappin DJ, Lord JM. The primary sequence of *Ricinus communis* agglutinin. Comparison with ricin. *J Biol Chem.* 1985 Dec 15;260(29):15682-6.
- Rojo MA, Citores L, Arias FJ, Ferreras JM, Jimenez P, Girbés T. cDNA molecular cloning and seasonal accumulation of an ebulin I-related dimeric lectin of dwarf elder (*Sambucus ebulus* L) leaves. *Int J Biochem Cell Biol.* 2003 Jul;35(7):1061-5.
- Roncuzzi L, Gasperi-Campani A. DNA-nuclease activity of the single-chain ribosome-inactivating proteins dianthin 30, saporin 6 and gelonin. *FEBS Lett.* 1996 Aug 19;392(1):16-20.
- Rutenber E, Robertus JD. Structure of ricin B-chain at 2.5 Å resolution. *Proteins.* 1991;10(3):260-9.
- Sandvig K, Olsnes S, Pihl A. Kinetics of binding of the toxic lectins abrin and ricin to surface receptors of human cells. *J Biol Chem.* 1976 Jul 10;251(13):3977-84.
- Sandvig K, van Deurs B. Delivery into cells: lessons learned from plant and bacterial toxins. *Gene Ther.* 2005 Jun;12(11):865-72. Review.
- Sandvig K, van Deurs B. Endocytosis, intracellular transport, and cytotoxic action of Shiga toxin and ricin. *Physiol Rev.* 1996 Oct;76(4):949-66. Review.
- Savino C, Federici L, Ippoliti R, Lendaro E, Tsernoglou D. The crystal structure of saporin SO6 from *Saponaria officinalis* and its interaction with the ribosome. *FEBS Lett.* 2000 Mar 31;470(3):239-43.
- Shahidi-Noghabi S, Van Damme EJ, Iga M, Smagghe G. Exposure of insect midgut cells to *Sambucus nigra* L. agglutinins I and II causes cell death via caspase-dependent apoptosis. *J Insect Physiol.* 2010 Sep;56(9):1101-7.

- Shih SF, Wu YH, Hung CH, Yang HY, Lin JY. Abrin triggers cell death by inactivating a thiol-specific antioxidant protein. *J Biol Chem*. 2001 Jun 15;276(24):21870-7. Epub 2001 Apr 2.
- Siena S, Lappi DA, Bregni M, Formosa A, Villa S, Soria M, Bonadonna G, Gianni AM. Synthesis and characterization of an antihuman T-lymphocyte saporin immunotoxin (OKT1-SAP) with in vivo stability into nonhuman primates. *Blood*. 1988 Aug;72(2):756-65.
- Sikriwal D, Ghosh P, Batra JK. Ribosome inactivating protein saporin induces apoptosis through mitochondrial cascade, independent of translation inhibition. *Int J Biochem Cell Biol*. 2008;40(12):2880-8.
- Soler-Rodríguez AM, Ghetie MA, Oppenheimer-Marks N, Uhr JW, Vitetta ES. Ricin A-chain and ricin A-chain immunotoxins rapidly damage human endothelial cells: implications for vascular leak syndrome. *Exp Cell Res*. 1993 Jun;206(2):227-34.
- Sperti S, Montanaro L, Derenzini M, Gasperi-Campani A, Stirpe F. Effect of modeccin on rat liver ribosomes in vivo. *Biochim Biophys Acta*. 1979 May 24;562(3):495-503.
- Spreafico F, Malfiore C, Moras ML, Marmonti L, Filippeschi S, Barbieri L, Perocco P, Stirpe F. The immunomodulatory activity of the plant proteins Momordica charantia inhibitor and pokeweed antiviral protein. *Int J Immunopharmacol*. 1983;5(4):335-43.
- Stirpe F, Bailey S, Miller SP, Bodley JW. Modification of ribosomal RNA by ribosome-inactivating proteins from plants. *Nucleic Acids Res*. 1988 Feb 25;16(4):1349-57.
- Stirpe F, Barbieri L, Gorini P, Valbonesi P, Bolognesi A, Polito L. Activities associated with the presence of ribosome-inactivating proteins increase in senescent and stressed leaves. *FEBS Lett*. 1996 Mar 18;382(3):309-12.
- Stirpe F, Battelli MG. Ribosome-inactivating proteins: progress and problems. *Cell Mol Life Sci*. 2006 Aug;63(16):1850-66. Review.
- Stirpe F, Bolognesi A, Bortolotti M, Farini V, Lubelli C, Pelosi E, Polito L, Dozza B, Strocchi P, Chambery A, Parente A, Barbieri L. Characterization of highly toxic type 2 ribosome-inactivating proteins from *Adenia lanceolata* and *Adenia stenodactyla* (Passifloraceae). *Toxicon*. 2007 Jul;50(1):94-105.
- Stirpe F. On the action of ribosome-inactivating proteins: are plant ribosomes species-specific? *Biochem J*. 1982 Jan 15;202(1):279-80.
- Stirpe F. Ribosome-inactivating proteins. *Toxicon*. 2004 Sep 15;44(4):371-83. Review.
- Strocchi P, Barbieri L, Stirpe F. Immunological properties of ribosome-inactivating proteins and a saporin immunotoxin. *J Immunol Methods*. 1992 Oct 19;155(1):57-63.
- Tanida I, Ueno T, Kominami E. LC3 and Autophagy. *Methods Mol Biol*. 2008;445:77-88.
- Tazzari PL, Polito L, Bolognesi A, Pistillo MP, Capanni P, Palmisano GL, Lemoli RM, Curti A, Biancone L, Camussi G, Conte R, Ferrara GB, Stirpe F. Immunotoxins containing recombinant anti-CTLA-4 single-chain fragment variable antibodies and saporin: in vitro results and in vivo effects in an acute rejection model. *J Immunol*. 2001 Oct 15;167(8):4222-9.
- Tomlinson JA, Walker VM, Flewett TH, Barclay GR. The inhibition of infection by cucumber mosaic virus and influenza virus by extracts from *Phytolacca americana*. *J Gen Virol*. 1974 Feb;22(2):225-32.
- Tosi G, Fermani S, Falini G, Polito L, Bortolotti M, Bolognesi A. Crystallization and preliminary X-ray diffraction data analysis of stenodactylin, a highly toxic type 2 ribosome-inactivating protein from *Adenia stenodactyla*. *Acta Crystallogr Sect F Struct Biol Cryst Commun*. 2010 Jan 1;66(Pt 1):51-3. Epub 2009 Dec 25.
- Tumer NE, Hwang DJ, Bonness M. C-terminal deletion mutant of pokeweed antiviral protein inhibits viral infection but does not dephosphorylate host ribosomes. *Proc Natl Acad Sci U S A*. 1997 Apr 15;94(8):3866-71.

- Vago R, Marsden CJ, Lord JM, Ippoliti R, Flavell DJ, Flavell SU, Ceriotti A, Fabbrini MS. Saporin and ricin A chain follow different intracellular routes to enter the cytosol of intoxicated cells. *FEBS J.* 2005 Oct;272(19):4983-95.
- Van Damme EJ, Hao Q, Charels D, Barre A, Rougé P, Van Leuven F, Peumans WJ. Characterization and molecular cloning of two different type 2 ribosome-inactivating proteins from the monocotyledonous plant *Polygonatum multiflorum*. *Eur J Biochem.* 2000 May;267(9):2746-59.
- Van Damme EJ, Roy S, Barre A, Rougé P, Van Leuven F, Peumans WJ. The major elderberry (*Sambucus nigra*) fruit protein is a lectin derived from a truncated type 2 ribosome-inactivating protein. *Plant J.* 1997 Dec;12(6):1251-60
- Van Damme EJM, Hao Q, Chen Y, Barre A, Vandenbussche F, Desmyter S, Rougé P, Peumans WJ. Ribosome-inactivating proteins: a family of plant proteins that do more than inactivate ribosomes. *Crit Rev Palnt Sci.*2001; 20:395-465.
- Vater CA, Bartle LM, Leszyk JD, Lambert JM, Goldmacher VS. Ricin A chain can be chemically cross-linked to the mammalian ribosomal proteins L9 and L10e. *J Biol Chem.* 1995 May 26;270(21):12933-40.
- Villafranca JE, Robertus JD. Ricin B chain is a product of gene duplication. *J Biol Chem.* 1981 Jan 25;256(2):554-6.
- Volkman DJ, Ahmad A, Fauci AS, Neville DM Jr. Selective abrogation of antigen-specific human B cell responses by antigen-ricin conjugates. *J Exp Med.* 1982 Aug 1;156(2):634-9.
- Wang BZ, Zou WG, Liu WY, Liu XY. The lower cytotoxicity of cinnamomin (a type II RIP) is due to its B-chain. *Arch Biochem Biophys.* 2006 Jul 1;451(1):91-6. Epub 2006 May 6.
- Wiley RG, Kline RH IV. Neuronal lesioning with axonally transported toxins. *J Neurosci Methods* 2000;103:73-82
- Wiley RG, Lappi DA. Suicide transport and immunolesioning 1994. Landes, Austin.
- Yamasaki C, Nishikawa K, Zeng XT, Katayama Y, Natori Y, Komatsu N, Oda T, Natori Y. Induction of cytokines by toxins that have an identical RNA N-glycosidase activity: Shiga toxin, ricin, and modeccin. *Biochim Biophys Acta.*2004 Mar 17;1671(1-3):44-50.
- Yan X, Hollis T, Svinth M, Day P, Monzingo AF, Milne GW, Robertus JD. Structure-based identification of a ricin inhibitor. *J Mol Biol.* 1997 Mar 14;266(5):1043-9.
- Yu L, Wan F, Dutta S, Welsh S, Liu Z, Freundt E, Baehrecke EH, Lenardo M. Autophagic programmed cell death by selective catalase degradation. *Proc Natl Acad Sci U S A.* 2006 Mar 28;103(13):4952-7.
- Zamboni M, Brigotti M, Rambelli F, Montanaro L, Sperti S. High-pressure-liquid-chromatographic and fluorimetric methods for the determination of adenine released from ribosomes by ricin and gelonin. *Biochem J.* 1989 May 1;259(3):639-43.
- Zarling JM, Moran PA, Haffar O, Sias J, Richman DD, Spina CA, Myers DE, Kuebelbeck V, Ledbetter JA, Uckun FM. Inhibition of HIV replication by pokeweed antiviral protein targeted to CD4+ cells by monoclonal antibodies. *Nature.* 1990 Sep 6;347(6288):92-5.
- Zhang C, Gong Y, Ma H, An C, Chen D, Chen ZL. Reactive oxygen species involved in trichosanthin-induced apoptosis of human choriocarcinoma cells. *Biochem J.* 2001 May 1;355(Pt 3):653-61.
- Zheng SS, Wai WL, Hin WY, Wu AR. Kinetics of IgE antibody response to trichosanthin alpha-momorcharin and beta-momorcharin in mice. *Chin Med J (Engl).* 1991 Apr;104(4):292-9.
- Zoubenko O, Uckun F, Hur Y, Chet I, Tumer N. Plant resistance to fungal infection induced by nontoxic pokeweed antiviral protein mutants. *Nat Biotechnol.* 1997 Oct;15(10):992-6.

## *Acknowledgements*

*Non est quod timeas ne operam perdidideris, si tibi didicisti.  
(Seneca)*

*The writing of this doctoral dissertation has been reached with the help, the guidance and the patience of many people.*

*Firstly, I am extremely grateful to my research guide, Prof. Andrea Bolognesi for his guidance, understanding, patience, knowledge and to encouraged me to grow as an experimentalist despite his busy schedules.*

*My sincere thanks also goes to Dr. Letizia Polito for her guidance through the methods, for the stimulating discussions, to be available to clarify my doubts and for her suggestions.*

*I would like to show my gratitude to Prof. Miguel Ferreras, Prof. Rosario Iglesias and Prof. Lucia Citores for their support and guidance during my living in Spain, for their helping not only for lab problems and for the innumerable coffee.*

*I would like also to thanks to my co-workers. I owe sincere thankfulness to Massimo, with whom I worked closely, especially for his patience and for his encouragement, helpful advice during these years and also for his humor. Many thanks also a Daniele and Lorenza for making the working days pleasure with their enthusiasm and for their patience in this stress period. Thanks also to all the people with whom I have been working during these years.*

*Finally, and most importantly, I would to thanks my parents, family and Francesco for their support, encouragement, quiet patience and unwavering love.*